UNIVERSITY OF MINNESOTA
INSTITUTE OF TECHNOLOGY
DEPARTMENT OF AERONAUTICAL ENGINEERING
ROSEMOUNT AERONAUTICAL LABORATORIES

This report may be released to OTS.

AN EXPERIMENTAL INVESTIGATION OF IMPACT AND SHOCK-WAVE BREAK-UP OF LIQUID DROPS

by
A. R. Hanson, E. G. [illegible]
and H. S. Adams

A final report to the U. S. Navy, Bureau of Aeronautics

Minneapolis 14, Minnesota
15 November 1955

APPROVED: John D. Akerman
Head of Department and Director of
Rosemount Aeronautical Laboratories

ACKNOWLEDGEMENTS

The authors wish to express special thanks to Mr. Arvid Grikis for his very able work in processing the large number of data negatives and preparing photographs for this report. Mr. Grikis was assisted by Lucile Reinke.

Thanks are also extended to F. Gage, J. Berzins, and R. Derksen of the Electronics Group under the supervision of Mr. Karl Chiswell.

This work has been supported by the U. S. Navy, Bureau of Aeronautics. The contract monitor has been Mr. L. M. Swanson, and it is a pleasure to acknowledge his continued interest and guidance.

Administrative matters relative to this contract have been handled by Professor John D. Akerman and Mr. F. J. Ross.

The typing and duplimat reproduction were capably carried out by the Secretarial Staff of the laboratory.

Finally, the authors wish to thank Dr. P. A. Pepper of Edo Corporation for valuable advice and a number of useful discussions.

TABLE OF CONTENTS

SUMMARY

This report describes an experimental investigation into the matter of evaluating sprays. Two particular aspects of the problem have been studied: 1) impact break-up of drops when the spray is sampled by means of coated slides, and 2) drop break-up associated with shock waves.

The first phase of the work made use of glass slides coated with highly viscous silicone oils to sample individual drops. An empirical equation has been established which specifies critical impact velocities for water drops whose diameters lie in the range 350-2270 microns. Extrapolation to smaller drops gives plausible values of critical velocities.

The second aspect of the problem was studied in a shock tube. New results have been obtained with water and methyl alcohol in the 100-700 micron range of drop diameters. Apparatus has been developed which is believed capable of studying shock break-up of considerably smaller drops, perhaps down to 25 microns in diameter.

LIST OF FIGURES

NOTATION

a_1 Velocity of sound in region 1

a Radius of sphere

C Constant in Rupe's equation

C_D Drag coefficient

C_p Specific heat at constant pressure

C_v Specific heat at constant volume

d Drop diameter

d_c Critical drop diameter

$\bar{E}$ Energy density of sound field

E Modulus of elasticity

e Eccentricity

$$E_{14} = \frac{(C_v T)_1}{(C_v T)_4}$$

f Frequency of sound

f_o Fundamental frequency of circular disc

f_1 First harmonic frequency of circular disc

G Curvature function

g Acceleration of gravity

h Thickness of disc

m Mass of drop

$\bar{F}$ Time-average force on a sphere

P_{41} Pressure ratio across diaphragm, p_4/p_1

P_{21} Pressure ratio across shock wave, p_2/p_1

R Radius of sphere

R_c Radius of sphere whose volume equals that of an oblate spheroid

R_1, R_2 Radii of curvature of drop surface in 2 principal planes

r Radius of disc

$U_{21} = \frac{u_2}{a_1}$

u Air velocity

u_c Critical air velocity

u_2 Air velocity between shock wave and contact surface

u_s Velocity of air particles induced by the sound

u_{rms} Root mean square of velocity

T Temperature

V_c Critical impact velocity of drop

v Velocity of drop

We Weber number

w_1 Shock wave speed

$W_{11} = \frac{w_1}{a_1}$

z Distance normal to wave-front

$\alpha_1 = \frac{\gamma_1 + 1}{\gamma_1 - 1}$

α_o, α_1 Constants for vibrator (Appendix B)

$\beta_1 = \frac{\gamma_1 - 1}{2\gamma_1}$

$\beta_4 = \frac{\gamma_4 - 1}{2\gamma_4}$

$\gamma_1 = \left(\frac{C_p}{C_v}\right)_1$

$\Gamma_{21} = \frac{\rho_2}{\rho_1}$

Γ Viscosity parameter

λ Wave-length of sound in air

μ_L Viscosity of drop liquid

ξ Displacement of air particles

ξ_o Displacement amplitude of air particles

ρ Density of disc

ρ_a Air density

ρ_L Density of sphere (drop)

ρ_1 Density of air in shock tube Region 1

ρ_2 Density of air behind shock wave

σ Surface tension of drop

σ Poisson's ratio (Appendix B)

I. IMPACT BREAK-UP - A COLLECTION PROBLEM

1. Background and Statement of Problem

a. General. In the field of liquid spray analysis one of the most important factors to be determined is the drop size distribution. This factor has been studied extensively both from the theoretical and experimental points of view. The determination of drop size distribution experimentally has been a problem for many years, and a number of methods have been devised. One of these is the collection of drops on slides or in cells for subsequent microscopic examination. Many other methods have been used but this one is of particular interest in the present work. A résumé of slide sampling and various other methods of spray analysis is given in Reference 1.

The collection method (on slides or in cells) has been used most widely because of its simplicity, directness, and relative ease of operation. Some of the problems involved are these: the discrimination against small drops (i.e., the small drops tend to follow the streamlines around the slide or cell); in the case of cells, the spreading action of the airstream on the collecting fluid; the tedious work involved in measuring the drops in the samples obtained; and the secondary break-up of drops when they strike the collecting surface.

The problem of discrimination against small drops can be overcome to a certain extent by reducing the width of the slide or cell, although complete collection occurs only when the slide or cell approaches the size of the drop. By shielding the slide or cell with a shutter, the action of the airstream on the surface of the collecting fluid can be minimized. Yet here again the presence of the shutter will disturb the flow ahead of the slide. Satisfactory sampling results when measurements are limited to those drops lying close to the stagnation point.

The work involved in measuring the size of drops can be reduced by photographing the samples and then using a semi-automatic scanning device, such as described by Rupe (ref. 2), for counting drops in each size group. If the bottom of the cell is coated with a suitable non-wetting agent, the drops will maintain their spherical shape when they

come to rest on the bottom of the cell. By the proper choice of immersion fluid the solubility of the drops can be ignored within the time required to make a microphotographic exposure.

Awareness of the problem of secondary break-up seems to be comparatively recent. Golitzine (ref. 3) recognized it and, by sampling the same spray at various speeds, decided that the velocities in which he was interested were too low for the drops to break upon impact with oil-coated slides. Most other investigators do not appear to have been concerned with impact break-up. This attitude may be partially justified by the circumstance that sampling was usually carried out at rather low velocities. Rupe (ref. 2) considered the problem in choosing the viscosity of the collecting fluid, and later made a detailed study of impact break-up in liquids of low viscosity.

b. Importance of Determining Critical Velocities of Single Drops. In the collection method of sampling sprays, care must be taken so that no secondary break-up occurs when the drops strike the collector. This break-up would be expected to depend mainly on the size of the drop, the velocity of impact, and the properties of the collector. Since a spray consists of many drops traveling at different velocities, it would be impossible to obtain any definite relationship between drop diameter and critical impact velocity by sampling a spray. A logical alternative, therefore, is to produce single drops and determine their critical velocities. The information so obtained can then be applied to the problem of determining the conditions for reliably sampling sprays.

c. Earlier Work on Critical Impact Velocity. Sahay (ref. 4) and Singh (ref. 5) observed the critical heights through which water drops of different sizes must fall in order to rupture when they strike oils of various viscosities. They noted that the critical height (velocity) of a given size drop decreased with increasing viscosity, reached a minimum at a viscosity of about 0.02 poise, and then increased in an approximately linear manner, as shown in Fig. 1. It is interesting to note that a minimum point is reached in the vicinity of the viscosity of water.

Sahay also plotted the critical height (velocity) vs. the reciprocal mass of the drop (Fig. 2) for collecting fluids of different viscosities, and found that as the mass increased the critical height decreased linearly. The viscosities of the liquids used are given in Table 1 below.

Table 1

Liquid No.	Viscosity
1	.1942 poise
2	.1738
3	.0562
4	.0324
5	.0182
6	.0105
7	.0082

Rupe (ref. 6) seems first to have realized that impact break-up could be a source of considerable error in the determination of drop size distribution. Rupe's interest was in drops smaller than roughly 1000 microns, whereas the smallest drop studied by Sahay and Singh was 2750 microns in diameter. In addition the impact velocities in Rupe's work were much higher. Because of the lack of pertinent information he performed a series of experiments with drops whose diameters ranged between 100 and 500 microns. He found that with kerosene as the collecting fluid the relationship between the critical velocity and the drop diameter is linear when plotted on log-log paper as in Fig. 3. The equation of this line is

$$V_c = \frac{C}{d} ,$$

where V_c is the critical velocity in meters/sec., d the diameter of the drop in microns, and C a constant equal to 1725.

d. Goal of Present Investigation. As the data obtained by Sahay, Singh, and Rupe indicate that the critical impact velocity even for small drops is comparatively low, a means of increasing this critical velocity must be obtained if sampling is to be successful in relatively fast

airstreams. The only property that can be varied conveniently appears to be the viscosity of the collecting fluid. The aim of this investigation has been to determine the critical impact velocities for drops using collecting liquids of much higher viscosity.

2. Experimental Technique and Apparatus

a. Historical Résumé. The first problem encountered in the determination of critical drop velocity is that of producing single drops the size of which can be controlled. Rupe (ref. 6) in his studies used a microburette patterned after the device invented by Lane (ref. 7). Rupe's microburette produced drops down to 75 microns in diameter.

In order to determine the velocity of a drop at the time of impact, an optical velometer was constructed. It is similar in principle to Rupe's and will be described in Section 2 b. Rupe varied the impact velocity of the drop by varying the distance from the collecting cell to the tip of the microburette. His collecting cell was 0.375-inch in diameter and 0.375-inch deep, being filled with kerosene having a kinematic viscosity of 2.32 centistokes and a specific gravity of .802 at 20°C.

Sahay's apparatus was quite simple. It consisted of a glass reservoir in which the water level was kept constant, and was equipped with a spout on the bottom to which capillary tubes of various sizes could be attached. This variety of sizes of capillary tubes enabled him to produce relatively large drops of controllable size. The drops were allowed to fall and strike an oil surface. The critical height was obtained by raising or lowering the reservoir to produce an impact velocity just sufficient to shatter the drop.

b. Description of Apparatus. Our version of the Lane microburette is shown in Figs. 4, 5, and 6. It consists basically of a 1/2-inch I.D. Plexiglas cylinder in which 0.007-inch I.D. hypodermic tube is axially mounted. The lower end of the hypodermic tube was turned down to a point, the upper end being connected through a short length of rubber tubing to the reservoir containing the drop liquid (water in this case). Air at an adjustable pressure could be forced to flow down the annular region between the Plexiglas cylinder and the hypodermic tube. This air in passing by

the tip of the hypodermic tube pulls a drop off when it reaches a certain size determined by the air velocity.

The reservoir (Fig. 7) is a sealable tank of approximately 1/2-pint capacity, which can be pressurized with a rubber bulb to force the liquid out of the tip of the hypodermic tube at the proper rate.

Water drops down to 200 microns in diameter were produced with this microburette, although the trajectories of drops smaller than 500 microns were quite erratic during initial tests. However, it was found that by coating the tip with a non-wetting agent* the trajectories were more nearly vertical. This held true down to approximately 300 microns in diameter, beyond which the trajectories again became erratic.

In use the microburette is placed in a small-scale wind tunnel (Figs. 4,5, and 6) where the drops can be accelerated to higher velocities. The contoured walls of this wind tunnel are made of wood, the other sides being of Plexiglas so that the drops could be observed forming and falling. Use of a dyed water made it easier to see when they struck the side of the tunnel. Naturally, if this were allowed to happen during the sampling, completely erroneous results would be obtained. The upper portion of the wind tunnel is a stilling chamber containing two fine mesh screens to aid in making the flow uniform from two compressed-air inlets. The bottom portion of the tunnel contracts to a constant area section 9-1/4 inches long and 1 x 1-inch inside dimensions. Static pressure taps were installed in each end of the tunnel so that the velocity of the air could be accurately set. A rough check on the air speed at the exit of the tunnel (with microburette removed) showed that velocities up to 250 ft./sec could be obtained. Accurate calibration of the wind tunnel was not necessary, because the actual velocities of the drops were measured with an optical velometer.

The optical velometer (Figs. 7 and 8) makes use of three parallel beams of light which project across the path of the drop diagonally at an angle of about 135° to the vertical. When the drop crosses these beams of light a small portion of each beam is refracted horizontally. These refracted rays are then picked up by a photoelectric tube and the resulting voltage pulses fed into an oscilloscope. The distance between the

*General Electric Dri-Film 9987

light beams is known, so the velocity of the droplet can be determined from the time interval between the pulses on the oscilloscope.

Several different light sources were used in an attempt to accentuate the signal produced by the refracted rays and thereby raise the signal-to-noise ratio. These light sources were a Cenco mercury vapor lamp, a ribbon filament microscope illuminator, and a General Electric BH6 mercury vapor lamp. The same light-tight housing was used for the first two (Fig. 7), whereas a special housing was constructed for the BH6 lamp, as shown in Figs. 9 and 10.

The amplitude of the signal on the oscilloscope trace was found to vary but little among the three different lamps. The ribbon filament microscope illuminator was finally adopted because of advantages in ease of operation and signal-to-noise ratio.

The light from the ribbon filament lamp is focused on a pin hole in a disc located in the focal plane of a collimating lens to produce a beam of parallel light. The latter is interrupted by an opaque film which has three parallel transparent lines. These lines are approximately 0.030-inch wide and 0.125-inch apart. The opaque film was made by placing three parallel wires on a sheet of photographic film and exposing to parallel light to obtain the desired density. One of these films is shown in Fig. 7.

The three parallel beams of light formed by this film are then passed through a 45° prism and directed across the path of the drops at an angle of 135° to the vertical. The first (top) beam is used to start the sweep of the oscilloscope, and the remaining two are used to determine the velocity of the drop.

Light refracted by the passage of a drop was sensed by Dumont Type 6292 photo-multiplier tube. The output of the latter was applied to the grid of a cathode follower whose heater current and plate voltages were supplied by batteries to eliminate noise. The output of the cathode follower was fed into a Dumont Type 304H oscilloscope equipped with a Land Polaroid camera. A typical photograph is shown in Fig. 11. An accurate audio frequency oscillator was used to determine the sweep time

of the oscilloscope which in turn leads to the time interval between the two signal pulses.

The collecting cells (Fig. 12) are 2 x 3-inch glass slides with 1/4-inch Flexiglas walls cemented around the edges. As recommended by Rupe (ref. 2), the bottoms of the cells were treated with GE Dri-Film 9987 to prevent the drops from flattening when they come to rest. The cells were filled to within 1/16-inch of the top of the walls with a Dow Corning "200" fluid whose kinematic viscosity is 12500 centistokes and whose surface tension is approximately 21.1 dynes/cm. A few tests were also made with a 30000 centistokes fluid of the same series. In use the collecting cell rests horizontally on a removable stand and is located approximately where the drops intercept the diagonal light beams.

To prevent the airstream from distorting the surface of the fluid in the collecting cell, a shutter with an opening slightly larger than the mouth of the tunnel was inserted between the tunnel and the collecting cell. This shutter (Fig. 12) is a simple blade type actuated by two solenoids. Blotter paper was attached to the top of the shutter to prevent intercepted drops from pooling and later falling into the collecting cell when the shutter is opened.

The microscope used for the examination of the samples is a Bausch and Lomb Series F with a mechanical stage and a graduated eye piece used for measuring drop diameters.

c. Procedure. The liquid reservoir is filled with water containing 1-1/2 per cent by weight of nigrosine dye. The microburette air is turned on and pressure applied to the liquid reservoir with the hand bulb so that one drop is forced out. The drop is collected with no accelerating air (i.e., no flow in the wind tunnel) so that the size can be determined. This is repeated until enough drops have been measured to show that a uniform size is being produced.

The accelerating tunnel air is then turned on slightly. Pressure is again applied to the liquid reservoir so that droplets are forced out of the tip at a slow rate (approximately 15 - 20 drops per minute). When the rate is established, the shutter is closed and a collection cell filled

with Dow Corning "200" fluid placed on the stand. The operator observes the tip through a hand microscope and when the drop is about to fall, opens the shutter. After the drop falls, he closes the shutter to prevent any more drops from falling into the collecting tray. The cell is then placed under a microscope to verify the size and to search for any smaller drops resulting from break-up. This is repeated several times for each setting of the accelerating air. If no break-up is observed, the velocity of the accelerating air is increased in steps and observations made at each setting until break-up is noted.

When the air pressure settings of the microburette and tunnel have been established for break-up, the dyed water is removed from the reservoir and replaced with clear water for the velocity determination. The tunnel pressure is then set somewhat lower than the break-up value and the drop size checked by collection to verify that the mean size is the same as with dyed liquid. Returning the tunnel pressure to the critical value defining break-up, the velocity was determined in the following way. The trace on the oscilloscope resulting from the passage of the drop across the three beams of light is photographed. A known frequency is then fed into the oscilloscope to determine the sweep speed of the trace. Measurement of the linear spacing of the signal pulses then leads to the time required for a drop to pass from one beam of light to the next. The distance between the beams is known, so the velocity of the drop can be calculated.

This complete procedure is repeated for various sizes of drops. The velocity is determined immediately after each break-up pressure setting has been established to minimize errors due to tip corrosion and contamination.

3. Analysis of Data

If it is assumed that each drop size has a unique critical impact velocity, then it should be possible to bracket this size experimentally. This was done in the present investigation by varying the setting of the tunnel air pressure so as to define two values of drop impact velocity. The lower value produced no break-up of the drops, the upper value resulted in all drops breaking, and the object being to make the difference as small

as possible. The resulting curve determined for drop diameters from 350 to 2270 microns is shown in Fig. 13. The empirical equation obtained for this curve is

$$V_c = 34.715 \ln \frac{2980}{d} \quad , \quad 350 \leq d \leq 2270 \qquad (1)$$

where V_c is the critical velocity of the drop in ft./sec. and d is the drop diameter in microns.

The evaporation of the drop before it is totally immersed in the collecting fluid is of some concern. A check was made simply by measuring the diameter of a drop at various times and comparing these values with those for a drop of equal initial diameter immersed in Stoddard's Solvent. A plot of the ratio of d, the diameter of the drop in the collecting fluid, to d_s the diameter of the drop in Stoddard's Solvent, vs. time is shown in Fig. 14. This figure indicates the trend of evaporation using 1000, 12500, and 30000 centistokes Dow Corning "200" fluids, when the original diameters of the drops are in the vicinity of 2000 microns.

An investigation was made to see if the collecting cell had any effect on the velocity of the drops. This was done by placing a slide slightly below the position where the drops pass through the light beams, measuring the velocity of the drop, and then comparing this value with that obtained when the slide was absent. It was found that the effect was less than experimental error and could therefore be neglected.

In order to determine the manner in which break-up occurred, high-speed motion pictures were taken from a position looking down on the collecting cell. The camera used is a Wollensak 16 mm. Fastax operated at approximately 3000 frames per second. Selected frames are shown in Fig. 16.

An interpretation of Fig. 16, based on the movie action, shows that immediately after impact ligaments are extended radially from the drop similar to patterns observed by Tsutsui (ref. 8). A short time later these ligaments are covered by more liquid from the main drop, after which the covering liquid recedes, exposing the ligaments again. Still later the ligaments separate and form small drops near the surface of the collecting liquid. This type of break-up, where small drops surround the

main drop at approximately the same level, was noted only in the case of drops larger than about 1000 microns.

Fig. 17 shows a movie sequence side view of a drop striking the collecting liquid. In this case the ligament is projected upward as well as outward, and then breaks up into secondary drops before falling to the collecting liquid. This type of break-up results in a line of smaller drops, likewise noted only for relatively large drops. The distortion of the surface of the collecting fluid caused by the tunnel airstream can be seen in Fig. 17.

Several tests were made with the 30000 centistokes liquid to see if further increase in the viscosity would affect the critical velocities. It was found that little or no increase in critical velocity resulted from the use of the more viscous collecting liquid.

Combining the results obtained by Sahay, Singh*, Rupe and this investigation as to the effect of the viscosity of the collecting fluid on the critical velocity, the curve shown in Fig. 15 results. There are no available values for critical velocity in the viscosity range of 100 - 10000 centistokes; however, it is logical to assume that the curve will have a shape approximately that shown by the broken line. The fact that the curve goes through a minimum can be justified by considering the extreme case of a sudden blast of air striking a water drop. The work reported in Section II indicates a critical break-up velocity of about 85 ft./sec. for a 600 micron water drop.

4. Conclusions

a. The critical impact velocity of a drop can be raised by increasing the viscosity of the collecting liquid. There appears, however, to be a limit to this trend, as indicated by the tests conducted with 30000 centistokes liquid.

---

*The work by Sahay was undertaken at Singh's suggestion, and the two investigations cover much the same ground. It is noted, however, that there is a lack of consistency between them on the values of surface tension and viscosity.

b. For the collecting liquids used in this investigation, the results are expressed by the equation

$$V_c = 34.715 \ln \frac{2980}{d} \quad , 350 \leq d \leq 2270 \quad ,$$

where V_c is the critical velocity in ft./sec. and d is the drop diameter in microns. This equation can be used to estimate values of V_c for $d < 350$; however, its use for $d > 2270$ is not warranted.

c. Evaporation of drops from the time they first meet the collecting surface until just submerged is negligible in the case of water drops captured in the Dow Corning silicone oils used in these tests.

All of the present work was carried out with water as the drop liquid. It is of considerable interest to know how curve of V_c vs. d would change for drops of other liquids. An experimental study conducted along the present lines could provide data on the effects of surface tension and viscosity of the drop liquid. Time and funds did not permit us to include such tests. It will merely be noted that from analogy to the break-up by air blasts one would expect that, for a given drop size, increasing surface tension or viscosity would raise the critical impact velocity. Before using viscous silicone oils for sampling drops of liquids other than water it would, of course, be necessary to check their miscibilities. For example, kerosene and gasolene are completely miscible with all of the Dow Corning "200" Fluids; whereas water and methyl alcohol are non-solvents. Other liquids (e.g., acetone, ethyl alcohol, and some of the higher alcohols) are immiscible in Dow Corning "200 Fluids whose kinematic viscosities are above 50 centistokes.

II. AIR BLAST BREAK-UP OF DROPS - A SHOCK TUBE STUDY

1. Background and Statement of Problem

a. General. The break-up of bulk liquid into sprays of individual drops has been a subject of particular interest and investigation ever since the advent of the internal combustion engine. During the period from roughly 1920 to 1940, a substantial amount of research was done in Europe and the United States on the atomization of fuel oil in Diesel engines. More recently the use of jet propulsion power units for air-

planes and ... rules has intensified the study of those factors which determine combustion efficiency. Among these factors, fuel atomization stands high in importance. There are, of course, areas of technology other than propulsion where knowledge of the physical basis of spray and aerosol formation is important. In fact, the detailed list would be rather lengthy, but two fields may be mentioned to illustrate the point. First, there is the field of chemical engineering, where extensive use of sprays is made in cooling operations and in chemical reactions between gas and liquid phases. A second example might be the insecticidal or fungicidal spraying operations used in agriculture.

b. Importance of Single-Drop Break-Up. In establishing the connection between atomization and single-drop break-up, it is perhaps helpful to outline quickly the main features of the disintegration of a liquid jet.

Consider, for example, a nozzle having a straight cylindrical orifice fed with liquid under pressure. Imagine further that the injection pressure can be controlled to make jet velocity an independent variable. This is essentially the experimental arrangement used by Haenlin (ref. 9). His results indicated four different types of jet disintegration: 1) break-up into drops solely under the influence of surface tension, 2) break-up with the influence of air friction, 3) break-up through wave formation, and 4) disruption or atomization. Types 1) and 2) have been treated theoretically by Rayleigh (ref. 10) and Weber (ref.11), and experimental results on drop diameter and break-up distance have confirmed their work fairly well. Type 3) agrees only qualitatively with Weber's theory, while that of Rayleigh does not apply. Type 4) is the most important of all in engineering applications; yet here the "theory" consists almost entirely of empirical equations in which the variables have been grouped by dimensional considerations.

In addition to the work referred to above, a large body of later experimental results has accummulated. The latter have had their origin in various tests aimed at shedding light on the basic mechanism of drop formation in sprays. The present consensus of opinion seems to affirm these three important stages in the atomization process. a) the develop-

ment of small surface disturbances which grow in amplitude, b) the action of air friction and pressure on free liquid surfaces causing the formation of drops and ligaments, and c) the subsequent splitting up of the ligaments and drops themselves by the relative air flow. These three stages most likely occur, regardless of whether the liquid jet enters still air at high speed, or whether a low-speed jet of liquid interacts with a fast air flow. It is the last of the three stages towards which the present study has been directed.

c. Earlier Work on Single-Drop Break-Up. It may be said, for the sake of simplicity, that there are two principal situations in which drops may break up. The first, which will be called the "steady" case, is where a drop is exposed to a more or less gradually increasing relative air velocity. Falling rain drops or a drop detached from an accelerating mass of liquid exemplify this case. The second, here called the "transient" case, exists when a drop is subjected suddenly to a change in relative air flow. This situation prevails when a drop is supported in a shock tube and exposed to the so-called "hot flow" region behind the principal shock wave.

Both the steady and transient cases have been investigated recently by Lane (ref. 12), who studied drops 500 to 5000 microns in diameter. The steady case he approximated by letting drops of known size fall into the entrance flare of a small vertical wind tunnel. By taking single flash photographs of different drops at various distances along the axis of the tunnel, the author was able to reconstruct the history of break-up of a typical drop. The photographs show that the influence of the air stream is to flatten the drop increasingly until, at a critical relative air speed, the drop is blown out downstream, like a bag attached to a heavy rim. The bag finally bursts, producing many fine drops; whereas the rim breaks up still later into much larger drops which comprise about three-quarters of the liquid in the original drop.

Transient break-up, as investigated by Lane (ref. 12), appears to take place in a manner quite different from that for the steady case. In this case there was no evidence of bag formation whatever. In contrast, the drops first became shaped like a plano-convex lens, with convex surface

facing the blast. This was followed by further deformation in which liquid from the edges of the drops appeared to be drawn downstream in a sheet and torn into ligaments which still later were broken into smaller drops.

The important rôle played by surface tension and viscosity in the atomization of liquids is well known, and a considerable amount of experimental work has been done to correlate these two physical properties with the performance of many types of spray devices. Yet, in the study of single-drop break-up, there appear to be substantial gaps in our knowledge of the effects of viscosity and surface tension. In his work on the steady case, Lane (ref. 12) investigated the effect of surface tension with various liquids covering the range 28 - 475 dynes/cm. Using glycerol, this same author found that only when the viscosity was very large did it have an effect on drop break-up. His results appear to indicate that even then viscosity only served to delay the break-up. Merrington and Richardson (ref. 13) performed some experiments with large falling drops whose diameters ranged from 1.8 to 10 mms. Their findings with respect to the influence of surface tension are not in accord with those of Lane, whereas in the matter of viscosity effects, their results were only qualitative. Hinze (ref.14) has treated the problem theoretically, with results agreeing only qualitatively with experiment.

Turning to the transient case, there appear to be no experimental data whatever on the effect of viscosity, although Lane (ref. 12) studied the influence of surface tension. Hinze's paper treats this case taking both properties into account.

The foregoing discussion has been rather general. Specific points will be entered into more thoroughly in Section 3c, where our results are related to the earlier work.

d. Goal of Present Investigation. The engineering importance of drops as small as 1 micron is generally recognized. Yet there are no data on the break-up of single drops below 500 microns. The present study was begun in an effort to supply experimental break-up data in the 100 - 1000 micron range. The effects of surface tension and viscosity were

to be investigated as thoroughly as time and funds would allow. Only the transient case was to be studied, for which purpose the shock tube appeared to offer the easiest avenue of approach.

2. Experimental Method and Apparatus

a. Historical Résumé. So far as the authors are aware, the only previous experimental work reported on the transient or blast break-up of drops is that of Lane referred to above. His apparatus made use of a "blast gun" to produce the transient pulse of air. Drops of known size were released from a burette located above the open end of the tube, and by letting the drops fall through light beams sensed by photo-cells, it was possible to fire the blast gun and take single flash photographs properly timed to show the stages of break-up.

Lane (ref. 12) chose the burette position such that the drop would cross the axis of the blast gun 5 cm. from the open end. The puncture of the diaphragm was timed to make the shock wave ahead of the air blast reach the drop just as the latter crossed the axis. Blast durations are stated (ref. 12) to have been approximately 4 milliseconds, with maximum blast velocities of about 330 ft./sec. Several blast velocities were measured by starting with smoke in the blast gun and taking high speed motion pictures of the emergent pulse of smoky air. In this way a curve was obtained showing blast velocity as a function of pressure in the compression chamber of the gun.

The work described above certainly represents an able and well-conceived attack on a difficult problem. However, there are a few aspects of the method which appear open to question. These are discussed more fully in Section 3c

b. Description of Shock Tube. Within the last ten years the shock tube has become a recognized tool in the field of fluid mechanics*. This development has necessarily raised our knowledge to the point where the main features of transient, compressible flows in one dimension are fairly well understood. Since the shock tube used in the present investigation is rather conventional it was possible to find sufficient information on design and operation in the literature (refs. 15 - 19).

---

*In a recent discussion with Dr. G.N. Patterson, Director of the Institute of Aerophysics of the University of Toronto, he pointed out that, whereas in 1946 there were only a few shock tubes in existence, there are now about 200 of them in Canada and the United States.

The shock tube is made up of sections of seamless brass tubing having a wall thickness of 1/4-inch and inside dimensions of 3 x 3 inches. Each section is fitted with flanges at either end, as shown in Fig. 18. The flanges are hard-soldered to the tube sections, then faced off perpendicular to the sides of the tube. Dowel pins provide accurate alignment, while one o-ring per joint seals against leaks in pressure or vacuum.

The assembled tube can be seen in Fig. 19. This view is from the open end of the expansion chamber. Trapezoidal plates raise the tube off the supporting rack, the latter being constructed of standard framing channel and can be adjusted for levelling purposes. Not clearly visible are oblique fore-and-aft braces which stabilize the frame against recoil when the shock tube is fired. A view from the test section, looking towards the compression chamber, is shown in Fig. 20, where some of the components are identified.

The overall length of the shock tube can be varied by adding sections. In this way a maximum length of 40 ft. can be reached. Furthermore, the assortment of sections is such that the test section can be positioned to expose, with overlap, any portion of the flow from within 1-1/2 inches of the diaphragm to the end of the expansion chamber. The total tube length shown in Fig. 19 is 29-1/2 feet.

A closer view of the test section is that of Fig. 21. The windows are 21 inches long and wide enough to expose the top and bottom inside walls of the tube. A backing plate with clamps allows the use of an 8 x 10-inch film-holder frame for shadowgraph pictures. To the left of the test section, extending through the top wall of the tube, is a pressure pickup which senses the passage of shock waves.

Rupture of the cellophane diaphragm separating the compression and expansion chambers is accomplished by a solenoid-operated plunger. This device can be seen in the "fired" position in Fig. 22. In use a strip of cellophane is held between the mating flanges which are clamped together with two "Vise-Grip" pliers. Figure 22 (left side) also shows one of three rollers which support the compression chamber and facilitate renewing the diaphram.

When the plans for the shock tube were being laid, it was considered advisable to group the main operating controls and gauges on a single panel. The arrangement worked out is shown in Fig. 23. The large gauge (top, left) measures pressure above atmospheric in the compression chamber, the range being 0 - 5000 mm.Hg. The two gauges on the right are absolute pressure gauges covering the range 0 - 800 mm Hg. in overlapping scales.

The latter gauges are for measuring pressures in the expansion chamber when it is evacuated. Six valves provide for controlled admission of compressed air, switching of gauges, and bleeding. The electrical sub-panel (center) consolidates control switches. From this position the various accessories can be turned on or off and the firing solenoid can be cocked and fired. Pilot lights are the dimming type, a useful feature when the room must be darkened for taking pictures. The last unit (bottom, center) provides electronic delay from 30 to 4500 microseconds and can be set within one microsecond in this range.

The way in which the shock tube, control panel, and accessories are interconnected is shown in Fig. 24. Since the basic timing signal originates in the pressure pickup when the shock wave travels over it, the location of the pickup must not be too close to the diaphragm. The underlying reason for this is the non-ideal manner in which the diaphragm bursts. The result is that the shock wave is originally curved and multiple, requiring time to reach full strength and become plane. Fortunately, this problem has received the attention of earlier workers, and our design was guided by their reports (ref. 15, 19).

Inasmuch as rather conventional operation of the shock tube was required, no elaborate measurements were made on the various flow quantities. In fact, to have done so would have necessitated a considerably larger investment in time and equipment. This work was, moreover, considered superfluous in view of existing information (refs. 15 - 19) on the performance of shock tubes comparable with ours in dimensions and operating conditions. Therefore, it was considered sufficient to check only those quantities within the capabilities of our instrumentation and which bear importantly on the drop break-up study. Probably the most important problem is that of accurate time delay to insure that the shock wave can be located precisely with respect to the drops. This means not only that the electronic delay unit must be stable and accurate; it also requires accurate measurement of the pressure ratio across the diaphragm, since this determines the speed of the shock wave. The two requirements were assessed together by taking several shadowgraph pictures of the shock wave, holding the delay and diaphragm pressure ratio P_{41} constant.

The results are shown in Fig. 25, where the numbers 52, 56, 57 refer to separate firings of the tube. The three photographs have been positioned so that the images of the upstream end of the test section window lie along a common line. Comparing the position of the shock waves, it is evident that location and repeatability are good. (The separation of the typical light and dark lines of the shadowgraph images results from the shock being somewhat off the axis of the light source.) The criss-crossed shocks following the main shock probably arise from a small mismatch at the first upstream coupling flange, and as such are much weaker than the primary shock wave.

A short discussion of the calculation of shock tube parameters is given in Appendix A.

c Camera and Light Sources. The arrangement of camera and light source can be seen from Fig. 26. The camera proper is from our Bausch and Lomb Type L photomicrography equipment and needed no modification. It is equipped with a 72 mm f/4.5 Bausch and Lomb Micro Tessar lens, which permits magnifications of approximately 3X to 10X. The light source shown is a modification of the General Electric unit (Type FT-130 Flash-tube). A closer view of the light source is shown in Fig. 27. The lens between the camera and the light source is a 14 in. f/6.3 Kodak Ektar. It was found later that this lens did not have any appreciable condensing effect and was therefore not used with the G. E. light.

The camera and light source are mounted on a carriage which permits motion along the full length of the test section window. A valuable feature of the Bausch and Lomb camera is the reflex viewer which consists of a tilting mirror and ground glass screen. Figure 20 shows the relationship between the camera-light assembly and the test section. The G. E. light proved unsuitable for shadowgraphs where the requirement for good definition is either parallel light or light from a source of small dimensions. Consequently, the spark source shown in Fig. 28 was used for shadowgraph pictures. This is one of several available in the laboratory and has a flash time of about 1.5 microseconds.

d. Acoustical Drop Holder. Although Lane did not state the reasons why he did not study the break-up of drops smaller than 500 microns, it is reasonable to believe that he stopped where he did because of instrumental difficulties. It is not likely that the production of smaller drops was the limitation, since the burette used was probably the same as that devised by Lane much earlier (ref. 7) and capable of producing uniform drops as small as 75 microns (ref. 6). The work described in Part I of this report demonstrated that as the drop diameter is decreased blow roughly 500 microns it is difficult to control their trajectories of fall. The region through which the drops must fall is, in the blast-gun arrangement of Lane, rather narrowly limited by the depth of field of the lenses as well as the widths of the light beams through which the drops had to fall.

Since the difficulties just mentioned stem mainly from the falling motion of the drops, it is natural to look for some way to hold them at rest*. The use of acoustic radiation pressure to support drops was brought to our attention by Bolt and Mirsky (ref. 20). For their work, the study of evaporation rates of volatile drops, they were able to use the sound field inside a commercially available unit, namely, a barium titanate piezoelectric cylinder**. The effects of radiation pressure in acoustics are not new, and the literature on the subject is rather extensive. In fact, the very application of supporting alcohol drops was demonstrated by Bücks and Müller (refs. 21, 22) in 1933, although the distances over which this action was effective appear to have been limited to 1 or 2 cm. The first systematic treatment of the theory relevant to this case seems to be that of King (ref. 23). A recent paper by Rudnick (ref. 24) reports

---

*The support of charged drops in an electric field, similar to the Millikan oil-drop experiment, was considered. Calculations showed that prohibitively high voltages would be required for drops of the sizes of interest. In addition no practicable way could be seen to produce charged drops of a given size and introduce them into the shock tube in a controlled manner.

**Manufactured by Brush Electronics Company, Cleveland, Ohio.

measurements of the force exerted on spheres by sonic radiation pressures.

Barium titanate is a ceramic material which can be formed into plates, cylinders, discs, and other shapes, and then made piezoelectric by polarization in an electric field. Nearly all of the commercial elements have several modes of vibration whose resonant frequencies lie in the ultrasonic region. After experimentation with various shapes, the vibrator shown in Fig. 29 was developed. The driving element is a barium titanate cylinder, 2.00 inches long, 2.00 inches O.D., and of 0.188 inch wall thickness. Outer and inner surfaces have plated silver electrodes. To one end of this cylinder a flat duraluminum diaphragm has been rigidly cemented. The particular mode of vibration used is a lengthwise extension and contraction excited at a nominal frequency of 50 Kc. Power is fed through leads which attach to corrugated phosphor-bronze strips, the outer one of which is visible in the photograph. The leads of an iron-constantan thermocouple can be seen entering the open bottom of the barium titanate cylinder, the junction of the two wires being taped to the inner electrode surface. An occasional check on the temperature is necessary since heating occurs during operation and surface temperatures in excess of about 170°F will cause depolarization of the ceramic.

In normal use the cylinder is held inside the knurled brass base which is provided with a machined phenolic plug for electrical insulation. The purpose of the internal threads cut in this base may be seen in Fig. 30. The flanged part at the right bolts to the bottom of the shock tube test-section, and the mating threads allow the vibrator diaphragm to be brought flush with the inside lower wall of the test section. Actually the diaphragm surface is only approximately flush because some adjustment is required to establish maximum amplitude of the stationary sound field.

During the bench testing of the vibrator it was found that the stability with which drops were held was much enhanced by a small concavity in the reflector. This feature was accordingly included in the design of the reflector plugs shown in Fig. 31. The short plug mounts flush with the top inside wall of the test section, while the longer plug extends about 1 inch below the wall. Some of the tests with water

drops required the stronger sound field existing in the smaller space between the vibrator and the longer plug.

Additional discussion of the mechanism of support of drops by radiation pressure is given in Appendix B, where there are also further remarks on vibrator design. It will suffice here to illustrate the capabilities of the acoustical drop holder in its present form. Figure 32 shows four pictures taken with the vibrator set up on the bench. The reflector is a concave lens cemented to a steel disc, the latter being attached to a micrometer head for accurate adjustment of the spacing between vibrator and reflector. In operation, a drop of liquid is placed on the vibrator diaphragm and the exciting frequency tuned to resonance, whereupon the liquid is thrown upwards in a spray of fine drops*. The coagulating action (refs. 25- 28) of the sound field on the drops causes them to unite into single drops spaced one-half wavelength apart. The pictures of Fig. 32 show some of the stages in this action. High speed movies were also taken in an effort to see the details of this coagulating process. Frame speeds up to 700 per second were obtained with a Fastax 16 mm. camera using an extended lens barrel to give 3X magnification. The resulting movies showed that the first effect of the sound is to stratify the fine drops into layers separated by a half wavelength. Within each layer the individual drops revolve rapidly around a larger central drop, the latter being formed early in the stratification phase. The final stages of the coagulation process occur when an entire layer of tiny drops has been combined into one central drop with several satellite drops rotating around it. The satellites are then observed to collide and unite with the central drop until a single drop hangs alone in the sound field.

Operation of the acoustical drop holder in the test section of the shock tube is shown in Figs. 33 and 34. Nine drops of methyl alcohol can be seen in Fig. 33. Extending through a small central hole in the reflector plugs (top wall of the test section) is the needle of a hypodermic syringe (cf. Fig. 20) used to release larger drops 2 or 3 mm. in diameter which land on the diaphragm. Fig. 34 illustrates the use of

---

*By slide sampling and microscope examination these drops were found to have diameters lying roughly in the 5 - 25 micron range.

the long reflector plug to produce the stronger sound field required to hold relatively larger water drops.

3. Analysis of Experimental Data

a. Test Procedure. The existence of a critical value for the amplitude of a step-wise air blast to hit and just break a drop is intuitively logical. It implies that the present problem becomes solved when the curve of u_c vs. d_c has been found, where u_c is the critical velocity for a drop whose diameter is d_c. Consequently there are two ways which suggest themselves more or less immediately of carrying out the experiments. These are discussed in the following two paragraphs.

First, if drops of any given size could be introduced into the sound field and held stably, the value of u_c could be found by a series of firings of the shock tube in which the diaphragm pressure ratio P_{41} was varied over a small range. This small range of P_{41} would produce a corresponding one in u_2, the air velocity between the shock wave and the contact surface. In this way a pair of close values of P_{41} (and of u_2), would be found such that the smaller value would deform but not break the drop, while the larger value would rupture the drop into two or more fragments. Thus the interpolated value of u_2 could be taken as the appropriate value of u_c for that particular diameter d_c. The foregoing approach was actually considered, and several methods of producing drops of uniform size were tried. It would serve no purpose here to report these trials in detail. Suffice it to say that they were found to be inadequate on two counts: the drops were either not sufficiently uniform in size or, what is more serious, they could not be produced with low enough velocities to be captured by the sound field.

The second approach would maintain P_{41} (and u_2) constant and vary the drop diameter between successive firings of the shock tube. Thus, the two close values of d could be found, the larger value for the drop that just breaks and the smaller value for the drop that deforms yet survives. This method would seem beset by the same difficulty as the first, namely, that of producing drops of a given size. Actually such an objection is valid against the method as described. However, a happy circumstance is the manner in which the acoustical drop holder performs. As mentioned earlier, and as is evident in Figs. 32, 33, and 34, the coagulation of

fine drops in the sound field produces an assortment of sizes. Generally the diameters decrease with increasing distance from the vibrator although this is not always the case. By proper control of the power and frequency of the driving signal fed to the vibrator it is possible to vary the amount of liquid sprayed up, which in turn changes the size range of the suspended drops. Further, since the field of the camera and light was sufficient to include as many as eight drops in a single photograph, the break-up of drops covering a considerable size range can be determined from one firing of the shock tube.

The second method just described was found to be practicable. In some cases it was necessary to take many pictures at a given value of P_{41} in order to find the two close values of d which would define the point u_c, d_c on the break-up curve. Nevertheless, the total number of pictures required was not prohibitive, as later discussion of the data will show. In fact, some points on the curve were found with as few as 8 shots or 16 pictures.

Additional control over drop size can be achieved by letting evaporation proceed until the desired range of sizes is reached. This was actually done in the case of water drops where the long reflector plug produced a stronger sound field capable of holding an assortment of drops for 15 or 20 minutes, during which time some would evaporate completely. Where the short plug reflector was used - and this was the case for most of the work - the sound field, for reasons not fully understood, usually lacked the power to hold drops stably for more than a minute or two. However, even this short time was sufficient to take the required pictures.

Although it is possible to determine the size of the drops by measuring the diameters of their images on the ground glass screen of the camera, this procedure is not conducive to speed or accuracy. Instead, a separate photograph was taken of the drops in the sound field before firing the shock tube. This first photograph could be taken quickly by the simple expedient of placing the film against the inside surface of the ground glass screen. The metal clips holding the ground glass also accommodated the 5 x 7-inch cut film, the only trick being

to fasten a piece of double-faced Scotch tape to the [illegible] to prevent the film from sagging out of the focal plane [illegible] the reflex mirror upwards after taking the first picture [illegible] the camera for the time-delay photograph of the drops after the passage of the shock wave. Figure 35* shows a typical pair of photographs from which original size and subsequent break-up can be obtained.

Contrast Process Ortho cut film in the 5 x 7 inch size was used almost exclusively. A combination of good resolving power and moderate speed suit this film to the present work. Since some light was essential to the adjustment of the acoustical drop holder, an orthochromatic film was highly desirable.

It is clear that the viscosity of a drop will resist distortion from a spherical shape. The result of this is that photographs of the break-up of drops must be delayed sufficiently that they can be seen either to break or merely to oscillate. Verification of the rupture or survival of a given size of drop was done by a series of pictures and with delays from 500 to 4200 microseconds.

Two liquids were used, water and methyl alcohol. Their surface tensions, viscosities, and densities at 20°C (68°F) are as follows (ref. 29).

	Surface Tension (dynes/cm.)	Viscosity (centipoises)	Density (gm/cu.cm.)
Water	72.75	1.005	1.00
Methyl Alcohol	22.6	0.596	0.80

Methyl alcohol was investigated first since it had been found to respond more readily than water to the spraying and coagulating action of the sound field. All of the alcohol tests were made using the short reflector plug. Working next with water, aided by the experience gained in the alcohol tests, it was found that drops roughly 200 - 400 micron in

---

*Unless stated otherwise, time delays noted on the break-up pictures are figured from the time the shock wave reaches the vertical centerline of the drops. The streaks on the reflex picture (a) are caused by some scratches on the tilting mirror.

diameter could be held in the sound field fairly well using the short reflector plug. On the other hand, drops outside this range could be held satisfactorily only when the longer reflector plug was used.

b. Drop Break-up Results. Several hundred photographs, showing the break-up of over a thousand individual drops, were taken during this investigation. These photographs reveal many interesting details of the break-up process. Yet in spite of differences in detail there are basic similarities in the break-up of all the drops studied. These common features are shown in Fig. 36. When the air velocity u_2 is considerably above the critical value u_c, break-up is as shown in (a). It is worth noting that the work of Lane led him to conclude that this is only way break-up occurs in the transient or blast case. On the other hand, all of our results indicate that at values of u_2 slightly exceeding u_c break-up proceeds in the stages shown in (b). This is the "bag" mode of break-up found by Lane but specifically stated by him to occur only in steady cases. The sequence of events shown in Fig. 36 is made up of single photographs of different drops whose initial diameters, however, were nearly the same.

Although the manner of drop break-up was observed to be basically one of bag formation, there are one or two additional features which are rather interesting. Figure 37, for example, reveals that with some drops the bag develops a reentrant portion near its middle, somewhat suggestive of the stamen of a flower. This "stamen" increases in length with time, and as can be seen in Figs. 38, 39, and 40, stands more or less alone as the rim and remaining portion of the bag are carried downstream. Incidentially, the upper two drops in Fig. 38 and the uppermost drop in Fig. 39 are noticeably deformed but not broken or "bagged". Fig. 43 is an enlargement of a portion of Fig. 37(b).

A second feature of interest is shown in Figs. 41 and 42. Here may be seen new details in the structure of the bags, especially the unbroken ones. Small dark spots surrounded by concentric rings are noteworthy; but whether they are the beginnings of points of rupture of the bag is still a matter of conjecture. A somewhat similar effect has been noticed by York (ref. 30) in the case of conical spray films, where small heavy-

rimmed holes are observed and believed to initiate break-up of the film. Figure 44 shows in greater enlargement some of the detail of Figs. 41(b) and 42(b).

The determination of the break-up curve of u_c vs. d_c for water and methyl alcohol was carried out by taking several hundred pairs of photographs of the type just discussed. Drop diameters fell in the range of 300 - 700 microns, for which the critical air velocities u_c were between 60 and 240 ft./sec. The results are shown on the graph of Fig. 45, where also the points of Lane (ref. 12) have been plotted. Curve A has been drawn to fit our experimental points as well as those of Reference 13. Curve B goes through our values for methyl alcohol, while Curve D has been drawn through the values of Reference 12 for the same liquid. A considerable divergence of B and D is evident. Curve C is the one recommended by Lane (ref. 12) to fit his water points. It is based on a theoretical relationship between the transient and steady cases. More will be said of these curves in the discussion of results in the next section.

In order to illustrate the way in which the photographs were evaluated, the bar charts of Figs. 46 and 47 have been prepared. It can be seen from these that the gap between the smallest drop broken and the largest drop not broken is quite small. The "doubtful" bars embrace those drops where the quality of the photographs did not permit a decision as to break-up. The uncertainty which these doubtful cases introduce into the values of d_c is generally not more than a few per cent. The values plotted in Fig. 45 are those given at the bottom of Figs. 46 and 47.

c. Discussion. In analyzing his results, Lane (ref. 12) started with the empirical equation found for the "steady" case,

$$(u - v)^2 d_c = 612,$$

where v is the velocity of the deformed drop just prior to break-up. The quantities u and d_c are as defined earlier, but the units are now meters/sec. for the velocities and mms. for d_c. When ft./sec. and microns are used, as in this report, the equation becomes

$$(u - v)^2 d_c = 6.59 \times 10^6 \qquad (2)$$

Equation (2), being for break-up by steady airstreams, is not applicable to the transient case. In order to apply Eq. (2) to the transient case, Lane makes use of a theoretical result of Taylor (ref. 3)* which states that, for a given drop diameter and liquid, the break-up velocities for the two cases are connected by the relation,

$$\frac{(u - v)_{\text{transient}}}{(u - v)_{\text{steady}}} = \frac{1}{\sqrt{2}} = 0.71 \qquad (3)$$

Lane suggests that Eqs. (2) and (3) combine to give,

$$(u - v)^2 d_c = (0.71)\ (6.59 \times 10^6) = 4.68 \times 10^6, \qquad (4)$$

as the relation covering the transient case. Equation (4) has been plotted as Curve C of Fig. 45.

The form of the preceding equations appears first to have been given by Triebnigg (ref. 32). Break-up was assumed by Triebnigg to occur when the surface tension pressure was equalled or exceeded by an average air pressure corresponding to the total drag of a spherical drop. That is,

$$\text{Average Pressure} = \frac{\text{Total Drag}}{\text{Frontal Area}^{**}} \geq \text{Surface Tension Pressure},$$

which leads to

$$\rho_a (u - v)^2 C_D \geq \frac{8\sigma}{d} \quad , \qquad (5)$$

where ρ_a is the air density, v the velocity of the drop just before break-up, and σ the surface tension of the drop. For water and air under standard conditions, and using the value $C_D = 0.4$ (ref. 33) Eq. (5) becomes

$$(u - v)^2 d_c = 12.9 \times 10^6 \quad , \qquad (6)$$

which is to be compared with Eq. (2). Photographs show that a drop becomes greatly distorted during the short period preceding actual rupture; so a sphere drag coefficient is probably too low. For comparison, the drag coefficient of a disc normal to the flow in the proper Reynolds number range is roughly $C_D = 1.2$ (ref. 33) leading to the equation,

$$(u - v)^2 d_c = 4.3 \times 10^6 \qquad (7)$$

*The authors have been unable to obtain a copy of this report.

**"Frontal area" here means the projected area. $\frac{\pi d^2}{4}$

The frontal area used in Eq. (7) is that of a disc whose diameter is twice that of the original drop. This estimate is supported by measurements of the diameter of flattened drops reported by Lane (ref. 12).

In the equations above, the velocity v of the drop has been retained. This is practicable and perhaps necessary in the steady case. However, the measurement of v in the transient case is difficult, because it involves small displacements and short times which are not easy to obtain. This fact stands out when it is realized that the entire break-up process takes roughly a millisecond or less, during which time the drop is radically altered in shape and finally broken. Moreover, there does not appear to be any basic physical reason why correlations of break-up with u_c itself should not be valid. The fact that the experimental results confirm the existence of a unique pair of values u_c, d_c lends plausibility to this view. Therefore in what follows it will be assumed that, for given liquid properties, the velocity behind the shock determines break-up. The report by Lane (ref. 12) makes no mention of measuring v in the transient case, and his curves of drop diameter vs. critical velocity show that v is neglected. Consequently we have done the same in plotting u_c vs. d_c.

At first sight it might appear that to neglect v is to oversimplify the problem. This may, in fact, be true with drops of great viscosity where the resistance to deformation may delay the break-up process to the point where v becomes nearly equal to u. Nevertheless the exact role of viscosity remains obscure, and it does not appear possible to decide the point at this time. On the other hand, results with liquids of relatively low viscosity (e.g., water or methyl alcohol) suggest that the conditions for break-up are determined by drop diameter, surface tension, and initial velocity of the air blast.

This latter point of view has been adopted by Hinze (refs. 14, 34) whose theory assumes that drop break-up takes place when the dynamic pressure of the air at the stagnation point of the drop exceeds the surface tension pressure by a certain factor. It is known (ref. 35) that when a liquid surface is curved the pressure is greater on the concave side than on the convex side. The pressure difference depends on the surface tension and the curvature, and is given by the relation

$$\Delta P = \sigma \left(\frac{1}{R_1} + \frac{1}{R_2} \right) , \tag{8}$$

where R_1 and R_2 are the radii of curvature of the surface in two orthogonal planes, the so-called principal planes. ΔP is usually spoken of as the "surface tension pressure". In the case of a sphere of radius R,

$$\Delta P = \frac{2\sigma}{R} . \tag{9}$$

When a drop is first touched by the flow behind the shock, the overpressure at the stagnation point is $1/2\ \rho_2 u_2^2$. The ratio of the two pressures is

$$\frac{\text{Dynamic Pressure of Air}}{\text{Surface Tension Pressure}} = \frac{\rho_2 u_2^2 R}{4\sigma} . \tag{10}$$

Hinze makes use of the Weber number We defined as just four times the ratio of Eq. (10), or

$$We = \frac{\rho_2 u_2^2 R}{\sigma} \tag{11}$$

The theory of Hinze allows small deviations from spherical shape, and relies on an experimentally determined value of the critical Weber number to define the condition leading to break-up. Limiting cases of low and high viscosity are considered in the following way:

Examples:

Low Viscosity	High Viscosity
Water, $\Gamma = 7.0 \times 10^{-3}$	Glycerol, $\Gamma = 570$
Methyl Alcohol, $\Gamma = 3.9 \times 10^{-4}$	Heavy Oils, $\Gamma \approx 9000$

The viscosity parameter has the definition,

$$\Gamma = \frac{\mu_L^2}{\sigma R \rho_L}$$

where μ_L is the viscosity of the drop and ρ_L is its density. According to Hinze, then the break-up relation follows from Eq. (11) when

$$\frac{\rho_2 u_2^2 R}{\sigma} = (We)_{crit.} \quad , \tag{12}$$

from which

$$u_c^2 d_c = \frac{2\sigma(We)_{crit.}}{\rho_2} \quad , \tag{13}$$

using the earlier notation.

Hinze's treatment does not give $(We)_{crit.}$, which must come from experiment. Values of u_c, d_c from the present experiments are tabulated below, together with the computed values of $(We)_{crit.}$

Table 2

Liquid	u_c (Ft/Sec.)	d_c (Microns)	σ (Dynes/cm.)	ρ_2 (Slugs/cu.Ft.) x 10^4	$(We)_{crit.}$
Distilled Water	84.3	600	72.75	25.59	3.60
" "	109.5	410	72.75	26.13	4.23
" "	157.3	270	72.75	27.24	6.00
" "	238.5	120	72.75	29.18	6.55
Methyl Alcohol	60.0	625	22.6	25.11	5.98
" "	84.3	330	22.6	25.59	6.34
" "	109.5	230	22.6	26.13	7.62
" "	157.3	118	22.6	27.24	8.41

Arithmetic averages of the above values of $(We)_{crit.}$ give

$(We)_{crit.} = 5.1$ (for distilled water)

$(We)_{crit.} = 7.09$ (for methyl alcohol).

where the value for distilled water does not agree very well with $(We)_{crit.}$ = 13.1 reported by Hinze (ref. 14). A least-squares determination of the best fit of the data points leads to these equations of break-up:

$$u_c^2 d_c = 6.21 \times 10^6 \qquad \text{(for distilled water)} \qquad (14)$$

$$u_c^2 d_c = 2.71 \times 10^6 \qquad \text{(for methyl alcohol)} \qquad (15)$$

Equations (14) and (15) have been plotted in the graphs of Figs. 48 and 49 and are extrapolated below 100 microns to indicate trends down to 10 micron diameters.

Considering the role of surface tension and density, Eq. (13) predicts that, for the same size of drop, the values of u_c for water and methyl alcohol should be in the ratio,

$$\frac{(u_c)_{\text{distilled water}}}{(u_c)_{\text{methyl alcohol}}} = \left[\frac{\sigma_{\text{distilled water}}}{\sigma_{\text{methyl alcohol}}}\right]^{1/2} = 1.79, \qquad (16)$$

where the values of surface tension are 72.75 dynes/cm. for water and 22.6 dynes/cm for methyl alcohol. That the 1/2-power variation with surface tension is not borne out by the present results is evident from Table 3 below*. No explanation is offered for this divergence, although it is believed to be real and not merely experimental error. If the exponent is 1/3 instead of 1/2 the agreement is better, since $(72.75/22.6)^{1/3} = 1.48$.

Table 3

d_c (Microns)	u_c (Ft./Sec.)		$\frac{(u_c)_{\text{Dist. Water}}}{(u_c)_{\text{Methyl Alcohol}}}$
	Distilled Water	Methyl Alcohol	
600	83.0	60.8	1.365
300	112	75.5	1.483
250	156	101	1.544
120	246	157	1.567
			Average: 1.49

*Values u_c, d_c read from Curves A and B of Fig. 45.

The results reported here allow no conclusion about the influence of viscosity upon break-up. Some tests reported by Lane (ref. 12) suggest that viscosity, except when very large as in the case of glycerol, merely acts to delay break-up. It seems clear that a quantitative investigation of the effect of viscosity is needed. The values tabulated in handbooks show that it is possible to select liquids which have nearly the same surface tension but greatly different viscosities. By choosing such liquids the separate effects of the two parameters may be investigated.

It remains to consider the errors in these experiments. First, there is the error in u_c. This is directly related to the errors in the diaphragm pressure ration P_{41} in the shock tube and the temperatures of the air in the two chambers. The accuracy with which the pressure p_4 and p_1 were determined such that the ratio, $P_{41} = p_4/p_1$, was known to within about 1 per cent, which produces a theoretical error in u_2 of slightly less than 1 per cent. The basic work of verifying the shock tube equations has already been done (refs. 15 - 19). It appears that the most accurate determinations of u_2 have been made indirectly by measuring the shock speed w_1. The results agree well with theory, particularly for the low pressure ratios used in this investigation. A maximum error of $\pm$ 3 per cent in u_2 seems reasonable.

The second important error is that associated with d_c. Mention has already been made, in connection with the bar graphs of Figs. 46 and 47, of the error in determining d_c from the break-up photographs. The initial size of a drop, as measured on the first photograph of each pair, can be determined with an error of no more than $\pm$ 3 per cent, and generally the error will be considerably smaller. The precision of determining d_c is believed to be approximately $\pm$ 5 per cent of the mean value.

The above discussion of errors has not touched the question of how the sound field which supports the drops may influence the results. An accurate analysis has not been possible because neither time nor equipment have permitted measurements of the sound field. Nevertheless, some rough estimates have been made which are believed to indicate the correct order of magnitude of the effects. Some of the photographs (e.g., Fig. 38) show that the drops can be flattened by the sound field. That such

flattening can be made very small by proper adjustment of the sound generator is attested by the photographs of Fig. 38. Deviations from spherical shape become smaller with decreasing drop diameter and, in fact, most photographs show less than 3 per cent difference between the maximum and minimum dimensions of deformed drops. The detailed structure of the sound field is not known and its determination by theory or experiment would be a problem more properly handled by specialists. Our experiments have shown, however, that the drops can be rather easily blown out of the sound field by small drafts. This simple observation show that the drag force on the drop in the direction of u_2 is much greater than the horizontal component of the radiation pressure force.

Since the ultrasonic vibrations of the air particles are approximately at right angles to u_2, there is a question whether the maximum vibrational velocities can, through vector addition with u_2, significantly change the effect of air pressure on the drop. A rough calculation, which is believed to give a generous value for the vibrational velocity, is carried out in Appendix B. The maximum effect is to increase the root mean square value of u by about 3 ft./sec. This variation is believed negligible compared with u_2 = 60 ft./sec.

Possible interaction between the shock wave and the sound field was anticipated as a second order effect. One way in which such interaction might manifest itself would be to cause a warping of the shock front. This is an effect which one might expect to be more prominent the weaker the shock wave, and should be detectable by a schlieren system. Time and equipment did not permit us to pursue this phase.

The use of the long reflector plug (see Fig. 34) was a necessity to increase the strength of the sound field so as to hold the smallest and largest water drops stably. Water drops in the 200 - 400 micron range were held satisfactorily with the short reflector plug, as were methyl alcohol drops of all sizes investigated. The extension of the long plug into the test section will cause some disturbance to the shock wave and the flow behind it. Time did not allow the taking of shadowgraph pictures of this effect. Generally, however, the drops nearest d_c in size were arranged to be close to the middle of the space between vibrator and plug, where the flow behind the shock should be least disturbed. Certainly, in

future work, means should be found to strengthen the sound field without using the long plug.

Lastly, there is the influence of drop deformation by the sound field on break-up. Consider two identical drops and suppose that one is deformed (e.g., flattened into spheroidal shape) while the other remains spherical. The question raised is this: Will the drops have appreciably different values of critical velocity u_c? An attempt is made in Appendix C to estimate the effect of drop deformation on break-up by evaluating the right-hand side of Eq. (8) for a deformed drop. The drop is assumed to be an ellipsoid of revolution about the minor axis. It is shown that for given values of ρ_2 and u_2 the stagnation-point Weber number is smaller than in the case of a spherical drop of the same volume. Although some of our photographs (e.g., Fig. 37) indicate considerable flattening, the majority show a ratio of maximum to minimum drop diameter of less than 1.08. Under the assumption that the critical Weber numbers are identical for the deformed and spherical drops, the critical velocities obey the relation,

$$(u_c)_{def.} = G^{1/2}(u_c)_{sph.}$$

as a first approximation using ρ_2 = constant and where G is a function of the curvature at the stagnation point. For a diameter ratio of 0.866, $G^{1/2} = 0.948$, and

$$(u_c)_{def.} = 0.948 \quad (u_c)_{sph.}$$

4. Conclusions

The following conclusions have been reached:

a. The critical or break-up curves for water and methyl alcohol, over the 100 - 700 micron range of drop diameters, are defined by the following empirical equations:

$$u_c^2 d_c = 6.21 \times 10^6 \qquad \text{(distilled water)} \qquad (14)$$

$$u_c^2 d_c = 2.71 \times 10^6 \qquad \text{(methyl alcohol)} \qquad (15)$$

Plotting the experimental points on log-log paper resulted in a straight

line for both the water data and methyl alcohol data. The resulting equations are

$$u_c^{1.495} d_c = 4.61 \times 10^5 \qquad \text{(distilled water)} \qquad (17)$$

and

$$u_c^{1.706} d_c = 6.65 \times 10^5 \qquad \text{(methyl alcohol)} \qquad (18)$$

b. Break-up of a drop by the formation of a bag occurs in the transient flow behind the shock wave. This conclusion is at variance with that of Lane who states that bag formation does not take place in transient air flows. It is shown that the mode of break-up limited by Lane to the transient case actually takes place when the blast velocity exceeds the critical value by an appreciable amount.

c. The mere passage of a drop through a normal shock wave, or a normal shock running over a drop, will not of itself cause break-up. It is the relative velocity between drop and air on the high-density side of the shock wave which, if sustained long enough, will shatter drops above critical size.

d. Some of the present photographs show considerable surface detail in the structure of the bag. A pattern of concentric rings surrounding a central point suggests that initial rupture of the bag may occur at such regions. Moreover, a bag can rupture under the effect of several such openings developing simultaneously.

e. Based on work with water and methyl alcohol, the dependence of u_c (assuming constant drop diameter) on surface tension is approximately $u_c \propto \sigma^{1/3}$. This is to be contrasted with the 1/2-power variation found by Lane. The present investigation is not complete enough to refute his results. Further study of the effect of surface tension for drops below 500 microns should be carried out.

f. No conclusions regarding the effect of drop viscosity are possible from these results. There remains a complete lack of quantitative experimental data on this important point. Further work should be attempted to fill this gap in our knowledge.

g. The application of ultrasonic radiation pressure to holding

liquid drops in a shock tube has been demonstrated. The effect of the sound field on the break up results appears to be negligible. The use of the method is not restricted to liquid drops, but can favorably be used, with proper optical instrumentation, to study the flow around small, solid spheres and other shapes.

h. The present apparatus can be used to obtain approximate drag coefficients of deformed drops up to the point of rupture. Drop trajectory calculations seen often in the literature make use of values of C_D based on wind tunnel tests of solid spheres or discs. It is possible that better values could come from shock tube tests, although little has been done here to establish the accuracy of the method.

APPENDIX A

Shock Tube Flow Equations

The development of the shock tube flow equations has been covered quite completely in Reference 17 and will not be repeated here. It was found, however, that the available curves could not be read accurately for the low pressure ratios used in this work. Accordingly new curves were calculated and plotted to cover the appropriate range. The quantities of interest are the following: shock wave speed w_1, air velocity u_2 behind the shock wave, pressure ratio across the shock wave P_{21}, pressure ratio across the diaphragm P_{41}, and air density ρ_2 behind the shock wave. (See shock tube states in Fig. 24.)

The equations for relating the initial pressure ratio P_{41} across the diaphragm to the other quantities mentioned are the following:

$$\frac{1}{P_{41}} = P_{14} = \frac{P_1}{P_4} = \frac{1}{P_{21}} \left[1 - (P_{21}-1) \sqrt{\frac{\beta_4 E_1}{\alpha_1 P_{21}+1}} \right]^{1/\beta_4} \tag{19}$$

$$u_{21} = \frac{u_2}{a_1} = \frac{P_{21}-1}{\gamma_1 \sqrt{\beta_1(\alpha_1 P_{21}+1)}} \tag{20}$$

$$W_1 = \frac{w_1}{a_1} = \left[\beta_1(\alpha_1 P_{21}+1)\right]^{1/2} \tag{21}$$

$$\Gamma_{21} = \frac{\rho_2}{\rho_1} = \frac{1+\alpha_1 P_{21}}{\alpha_1 + P_{21}} \tag{22}$$

Where

$$P_{21} = \frac{P_2}{P_1}$$

$$\beta_1 = B_4 = \frac{\gamma_4 - 1}{2\gamma_4}$$

$$\alpha_1 = \frac{\gamma_1 + 1}{\gamma_1 - 1}$$

$$\gamma_1 = \gamma_4 = \left(\frac{C_p}{C_v}\right)_1$$

a_1 = Velocity of sound in Region I

C_p = Specific heat at constant pressure

C_v = Specific heat at constant volume

$E_{14} = \frac{(C_v T)_1}{(C_v T)_4}$

Considering air on both sides of the diaphragm, the following values apply.

$a_1 = 5.95$ $\qquad$ $\rho_1 = 2.377 \times$ Slugs/Cu.Ft.

$\beta_4 = \beta_1 = 0.144$ $\qquad$ $E_{14} = 1$

$\gamma_1 = \gamma_4 = 1.404$ $\qquad$ $T_1 = T_4$ $\quad$°C

To find the dimensional quantities, P_{41}, Γ_{21}, W_{11} and U_{21} as functions of P_{21}, the latter was varied in increments of 0.1. The results have been plotted in Figures 50 and 51. These curves were used to determine the actual flow parameters for the conditions prevailing in the present shock tube work.

APPENDIX B

[illegible] FIELD AND VIBRATOR DESIGN

1. Acoustic Radiation Pressure

The force on a sphere arising from the acoustic radiation pressure of a sound field has been worked out theoretically by King (ref. 23), who considered the cases of plane progressive and stationary waves. For the latter case, which is approximately anplicable to the present situation, King found that the time-average of the force on a sphere of radius a is

$$\bar{P} = 4\pi^2 \, (a^3/\lambda) \sin \left(4\pi \frac{z}{\lambda}\right) \cdot F \, (\rho_1/\rho_L) \cdot \bar{E} \qquad (23)$$

where

λ = wavelength of sound in air

z = distance normal to wave-fron

$$F(\rho_1/\rho_L) = \frac{1 + 2/3 \, (1 - \rho_1/\rho_L)}{2 + \rho_1/\rho_L}$$

ρ_1 = density of air

ρ_L = density of sphere (or drop)

$\bar{E}$ = energy density of sound field.

The energy density $\bar{E}$ may be found from the relation,

$$\bar{E} = \frac{\rho_1 (2\pi f \xi_o)^2}{2} = 2\pi^2 \rho_1 f^2 \xi_o^2 \qquad (24)$$

where f is the frequency of the sound and ξ_o is the displacement amplitude of the air particles.

For the two liquids used in the present work, the density ratios are the following:

Water	Methyl Alcohol
$\rho_1/\rho_L = 0.00123$	$\rho_1/\rho_L = 0.00152$

These values show that the condition $\rho_1/\rho L \ll 1$, is adequately met, so that the density function is closely $F(\rho l/\rho L) = 5/6$, reducing Eq. (23) to

$$\bar{P} = \frac{10}{3} \pi^2 \, (a^3/\lambda) \sin (4\pi \, 2/\lambda) \cdot \bar{E} \qquad (25)$$

Equation (24) has been verified experimentally in some recent work by Rudnick (ref. 24).

Since the purpose of the calculations which follow is to illustrate in a qualitative way the order of magnitude of the radiation pressure force on drops, it will be satisfactory to assume a value for ξ_o. The work of St. Clair (refs. 25, 26) reports values of $\xi_o \approx 50$ microns at f = 10 kc. A value $\xi_o = 25$ microns at f = 50 kc ($\lambda = 0.695$ cm.) will be assumed for the present calculations of $\bar{E}$ and $\bar{P}$. Using $\rho_1 = 1.228 \times 10^{-3}$ gm/cu. cm. (2.38×10^{-3} slug/cu. ft.) and the values of f and ξ_o just mentioned, Eq. (24) gives $\bar{E} = 379$ ergs/cu.cm. This value of $\bar{E}$ applied to a 1000 micron drop (a = 500 microns) reduces Eq. (25) to

$$\bar{P} = 2.24 \sin (4\pi 2/\lambda) \tag{26}$$

which, along with the displacement ξ, has been plotted as a function of z in Fig. 52. It can be seen there that $\bar{P}$ varies sinusoidally at a frequency twice that of ξ. In the arrangement to support drops against gravity there are evidently 1/8-wave length intervals along the z axis wherein it is possible for a drop to rest in stable equilibrium.

The exact position at which a drop will rest stably may be found by equating $\bar{P}$ to the weight of the drop. That is

$$\bar{P} = \frac{10}{3} (\pi a^3/\lambda) \bar{E} \sin (4\pi z_o/\lambda) = mg = \frac{4}{3} \pi a^3 \rho_L g ,$$

where m is the mass of drop and g the acceleration of gravity. The preceding equation leads to

$$\sin (4\pi z_o/\lambda) = \frac{2 \rho_L g \lambda}{5\pi \bar{E}}$$

which can be solved for z_o to give

$$z_o = (\lambda/4\pi) \sin^{-1} \frac{(2\rho_L g \lambda)}{5\pi \bar{E}} \tag{27}$$

Considering water drops ($\rho_L = 1.00$ gm/cu.cm.) and a frequency of 50 Kc ($\lambda = 0.695$ cm), Eq. (27) becomes

$$z_o = 0.0553 \sin^{-1} (86.7/\bar{E}) \qquad (28)$$

Examination of Fig. 52 shows that the positions of stable drop support are specified by the relation

$$z = (2n + 1) \frac{\lambda}{4} - z_o \qquad (29)$$

where $n = 0, 1, 2, \ldots$, and z_o is given by Eq. (28), where the range of z_o is $0 \leq z_o \leq \lambda/8$. A plot of z_o vs. $\bar{E}$, as calculated from Eq. (28), is shown in Fig. 53. It is worth noting that z_o is independent of drop diameter within the general limitation of King's theory that $(2\pi a/\lambda) \ll 1$. This does not mean that stable support of drops is impossible under other conditions. In fact, the largest drop in Fig. 32(a) has a radius a = 0.15 cm, leading to $(2\pi a/\lambda) = 1.4$. However, the quantitative use of King's theory is not valid for drops so large.

Two typical drops are shown in Fig. 52. The value of $\bar{E}$ is that calculated for 50 Kc. and ℓ_o = 25 microns. If the sound energy were decreased the drops would fall to lower positions until $z_o = \lambda/8$, which is actually an unstable position corresponding to $\bar{E}$ = 86.7 ergs/cu.cm.

2. Vibrator Design

As mentioned earlier, the barium titanate cylinders have three modes of vibrations: radial, thickness, and lengthwise (i.e., along the axis of the cylinder). It was found that the radial mode, which occurs at f = 30 Kc for the cylinder in question, would rather quickly break the cement bond* between the cylinder and the dural diaphragm. The thickness mode is excited at much higher frequencies around 530 Kc, and it would be difficult to couple energy into the diaphragm with this mode.

Lengthwise expansion and contraction was found to excite the dural diaphragm to circular modes of vibration of sufficient amplitude to support drops in the manner already described. The problem of matching the fundamental or some harmonic frequency of the diaphragm to the driving frequency of the barium titanate cylinder is, of course, basic to obtaining optimum sound output.

*A number of adhesives were tried with varying success. The one finally adopted is an epoxy resin called "A-6" by its manufacturer, Armstrong Products Co., Warsaw, Indiana.

A [illegible] may operate in the [illegible] circular or radial [illegible] determined by test tones or vibration and sound. Preliminary [illegible] a diaphragm of 0.082-inch dural sheet cemented to one end of the cylinder showed that the lengthwise mode excited the diaphragm to vibrate with one nodal circle similar to the first circular mode of [illegible] For such modes of vibration the frequency of a clamped-edge disc is

$$f_n = \frac{\lambda_n^2 h}{r^2} \left[\frac{386E}{\rho(1-\sigma^2)} \right]^{1/2} \qquad (30)$$

where

f_0 = fundamental frequency

f_1 = first harmonic frequency

λ_0 = .467

λ_1 = 1.626

h = thickness of disc, inches

r = radius of disc measured from center of inner clamping edge, inches

E = Modulus of elasticity, lbs. (F)/sq. in.

ρ = density, lb. (M)/ cu. in.

σ = Poisson's ratio

Considering 24 S I dural ($E = 10.5 \times 10^6$ lbs. (F)/ sq. in., $\sigma = 0.355$, $\rho = .100$ lb. (M)/cu. in.) and a cylinder for which r = 0.812 inch, Eq. (30) gives

$$f_0 = [illegible] \times 10^4 h_0 \qquad (31)$$

and

$$f_1 = 59.6 \times 10^4 h_1 \qquad (32)$$

Letting f_0 and f_1 equal 50 Kc in Eqs. (31) and (32) and solving for the thicknesses results in $h_0 = 0.328$-inch and $h_1 = 0.084$-inch.

The thicknesses just mentioned neglect any loading effect of the diaphragm on the frequency of the cylinder. Although our search of the literature on this effect was not exhaustive, it does not appear to have been analyzed in a manner producing useful design formulas. In view of this situation it was surmised that an experimental determination of the optimum thickness could be made by cementing an overly thick diaphragm to the cylinder and then cutting it down in small increments. Such a procedure was actually tried, but it did not produce consistent results. In the case of one cylinder it developed internal cracks caused by lathe machining, while in other cases the adhesive bond between diaphragm and cylinder became faulty. It is possible that future improvement in the bonding will make the method successful.

As a result of tests with a number of cylinders, each having a somewhat different diaphragm thickness, two values of thickness, namely, 0.086-inch and 0.125-inch , were found best from the standpoint of holding drops. The calculated disc frequencies f_o corresponding to these thicknesses are 51.2 Kc and 74.5 Kc, respectively.

St. Clair (ref. 36) has described a different type of sound generator working in the 10 - 30 Kc range. The arrangement is essentially that of a dynamic loudspeaker in which the usual voice coil has been replaced by a free-free bar of circular cross-section. The bar has a machined driving ring which extends into the flux gap of the magnet structure, the latter having been modified by the addition of an exciting coil. Power fed into the exciting coil induces a sinusoidal current in the driving ring which excites longitudinal vibrations in the bar. The sound fields produced by this generator are reported by St. Clair to be strong enough to support lead shot.

We have made some tests on a 20 Kc vibrator patterned after St. Clair's design. The performance was not nearly as satisfactory as the vibrator using the barium titanate cylinder. However, this may arise from defficiencies in our design and does not necessarily mean that the St. Clair generator is basically unsuited for the present application. There appear to be two important differences in our versions of the two types of vibrators, namely, frequency and the radiation pattern. At the

present time we are not prepared to analyze these factors adequately.

3. Effect of Sound Field on u

Consider the idealized case where the uniform flow behind the shock wave interacts with a plane stationary sound field. The displacement of air particles by the sound waves can be written

$$\xi = \xi_0 \sin (2\pi z/\lambda) \sin (2\pi a_1 t/\lambda) \tag{33}$$

At a particular point z_o the amplitude factor is $\xi_0 \sin (2\pi z_o/\lambda)$, and for large energy densities a drop will be held very close to a displacement loop (maximum ξ) where $\sin (2\pi z_o/\lambda) \cong 1$. Then

$$\xi = \xi_0 \sin (2\pi a_1 t/\lambda) \tag{34}$$

and the velocity induced by the sound will be

$$u_s = \dot{\xi} = \xi_0 (2\pi f) \cos (2\pi a_1 t/\lambda) \tag{35}$$

Inasmuch as the Weber number has been taken as a criterion for break-up it is of interest to find the square of the total velocity u of the air relative to a drop fixed at z_o. Vector addition of the steady and fluctuating velocity components leads to

$$u^2 = u_2^2 + u_s^2 = u_2^2 + (2\pi f \xi_0)^2 \cos^2 (2\pi f t) . \tag{36}$$

Granting that the dynamic pressure acting for a certain time* leads to break-up, it is of interest to calculate the average value of u^2, namely,

$$\overline{u^2} = \overline{u_2^2 + (4\pi^2 f^2 \xi_0^2) \cos^2 (2\pi f t)}. \tag{37}$$

*For the drop sizes investigated, this time is considerably greater than one period T of the sound. The present example takes f = 50 Kc, for which T = 20 microseconds.

The standard definition of a time-average,

$$(\overline{}) = \frac{1}{T} \int_0^T (\ )\, dt \ ,$$

applied to Eq. (37) leads to

$$\bar{u}^2 = \frac{1}{2} \int_0^T u_2^2 \, dt + \frac{4\pi^2 f^2 \xi_o^2}{T} \int_0^T \cos^2(2\pi f t) \, dt. \qquad (38)$$

Integrating Eq. (38), and noting that u_2 = constant for a given value of P_{41}, gives

$$\bar{u}^2 = u_2^2 + 2\pi^2 f^2 \xi_o^2 \ . \qquad (39)$$

When f = 50 Kc and ξ_o = 25 microns (0.821×10^{-4} ft.) Eq. (39) becomes simply

$$\bar{u}^2 = u_2^2 + 332 \qquad (40)$$

or, in terms of the root mean square,

$$u_{rms} = (\bar{u}^2)^{1/2} = u_2^2 + 332)^{1/2} \ . \qquad (41)$$

The following table illustrates the relative magnitudes of u_{rms} and u_2.

Table 5

u_2 (ft./sec.)	u_{rms}
60	62.7
84.3	86.3
157.3	158.2
238.5	239.0

In view of the assumption made for the sound field, it is believed that the values tabulated above overestimate u_{rms}. In any case, these

values would apply only during the short time after the passage of the shock wave that the drop is near the axis of the sound field. Experience with the drop holder indicates that roughly 2 mm. or more from the axis it is no longer possible to support drops. A drop whose critical velocity is 60 ft./sec., for example, will move about 10 mm. before breaking. Consequently it seems probable that most of the time that a drop is deforming it will be acted upon by essentially u_2, the contribution of u_s being negligible.

If it is assumed, as did Hinze, that break-up is determined by the Weber number at the stagnation point, then the effect of deformation may be calculated from Eq. (8) and the definition of Weber number. Thus, if R_1 and R_2 are the principal radii of curvature at the stagnation point on a deformed drop,

$$(We)_{def.} = \frac{2 \rho_2 u_c^2}{\sigma\left(\frac{1}{R_1} + \frac{1}{R_2}\right)} \tag{42}$$

This relation, with Eq. (11), gives the ratio,

$$\frac{(We)_{sph.}}{(We)_{def.}} = \frac{R}{2}\left(\frac{1}{R_1} + \frac{1}{R_2}\right) , \tag{43}$$

where R is the radius of a spherical drop volume equal to that of the deformed drop. When no deformation is present, $R_1 = R_2 = R$, and Eq. (43) reduces to unity.

Under the present assumption a deformed drop will break up if its stagnation-point Weber number equals the critical Weber number for a spherical drop of equal volume. That is

$$\left[(We)_{def.}\right]_{crit.} = \left[(We)_{sph.}\right]_{crit.} ,$$

which implies

$$\frac{(\rho_2 u_c^2)_{def.}}{\frac{\sigma}{2}\left(\frac{1}{R_1} + \frac{1}{R_2}\right)} = \frac{(\rho_2 u_c^2)_{sph.} R_c}{\sigma} \tag{43}$$

Equation (43) can be rewritten

$$\frac{(\rho_2 u_c^2)_{def.}}{(\rho_2 u_c^2)_{sph.}} = C, \tag{44}$$

where the curvature function G is defined as

$$G = \frac{R}{2}\left(\frac{1}{R_1} + \frac{1}{R_2}\right) \qquad (45)$$

Actually ρ_c is a function of u_c, but as a first approximation let $(\rho_c)_{def.} = (\rho_c)_{sph.}$ Then from Eq. (44),

$$(u_c)_{def.} = G^{1/2}\,(u_c)_{sph.} \qquad (46)$$

Using the value of $(u_c)_{def.}$ from Eq. (46) and the shock tube curves in Appendix A a corresponding value $(\rho_c)^{(1)}_{def.}$ can be found. A second approximation $(u_c)^{(1)}_{def.}$ can then be calculated from Eq. (44), where now

$$\frac{(u_c^{(1)})^2_{def.}}{(\rho_2 u_c^2)_{sph.}} = G,$$

from which

$$(u_c^{(1)})_{def.} = G^{1/2}\left[\frac{(\rho_2)_{sph.}}{(\rho_2)^{(1)}_{def.}}\right]^{1/2}(u_c)_{sph.} \qquad (47)$$

The nature of the calculation probably does not warrant higher approximation than the first, as a later example will show.

In order to obtain numerical values for the function G it is necessary to make some assumptions regarding the shape of the deformed drop. The vertical drop profiles of Fig. 37 are approximately elliptical, and visual observation from above the drops showed them to be closely circular in the horizontal plane. Accordingly the assumed drop surface will be that of an oblate spheroid defined by the equation

$$\frac{x^2 + y^2}{a^2} + \frac{z^2}{b^2} = 1,$$

where x is measured in the direction of w_2, and [illegible] spheroids along the axis of the suspended drops. Let R_1 be the radius of curvature in the x, y-plane and R_2 that in the x, z-plane. The trace of the surface in the x, y-plane is the circle, $x^2 + y^2 = a^2$, so $R_1 = a$. In the x, z-plane the trace is the ellipse.

$$\frac{x^2}{a^2} + \frac{z^2}{b^2} = 1 ,$$

whose radius of curvature at the stagnation point (x = -a, y = 0, z = 0) is $R_2 = b^2/a$. Substituting the values for R_1 and R_2 in Eq. (45) gives

$$G = \frac{R_c}{2} \left(\frac{1}{a} + \frac{a}{b^2} \right) \tag{48}$$

as the curvature function.

The volume of the oblate spheroid is $4/3\ \pi\ a^2 b$ and must equal the volume of a sphere of radius R_c, which leads to the condition $a^2 b = R_c^3$. Making use of this, Eq. (48) can be written

$$G = \frac{R_c^6 + a^6}{2aR_c^5} \tag{49}$$

In terms of the eccentricity of the ellipse, $e^2 = 1 - (b/a)^2$, Eq. (49) becomes

$$G = \frac{2 - e^2}{2(1 - e^2)^{5/6}} \tag{50}$$

The graph of Eq. (50) has been plotted as Curve A in Fig. 54.

For the case when the long axis of the oblate spheroid drop is normal to the air flow, $R_1 = R_2 = a^2/b$. The equation for G becomes

$$G = R_c^4/a^4 , \tag{51}$$

or in terms of eccentricity,

$$G = (1 - e^2)^{2/3} \tag{52}$$

A plot of Eq. (46) is shown as Curve B in Fig. 54.

As a numerical example to illustrate the magnitude involved, assume a value for eccentricity of e = 0.50. This corresponds to b/a = 0.866, which is actually smaller than that observed on the drops used in the data of Figs. 45, 48, and 49. From Curve A of Fig. 54, G = 0.898 when e = 0.50, and $G^{1/2}$ = 0.948. Consequently Eq. (46) predicts that

$$(u_c)_{def.} = 0.948\ (u_c)_{sph.} ,$$

or about 5 per cent decrease in critical velocity due to the assumed deformation.

The photographs of Fig. 37 (a) show that large drops (much larger than the critical size) under certain conditions of the sound field, can be considerably deformed. The lowest drop, for example, gives a measured ratio, b/a = 0.6, for which e = 0.80. In this case G = 0.625, and

$$(u_c)_{def.} = 0.791\ (u_c)_{sph.} ,$$

or about a 20 per cent decrease in u_c caused by deformation.

1. Fiszdon, J. W. and Miesse, C.C.: Injection of Liquids into Gases with Special Reference to Combustion Systems. Report by Battelle Memorial Institute, December 1951.

2. Rupe, Jack H.: A Technique for the Investigation of Spray Characteristics of Constant Flow Nozzles Part I. Paper presented at Conference on Fuel Sprays, University of Michigan, 30 March 1949.

3. Golitzine, N.: Method for Measuring the Size of Water Droplets in Clouds, Fogs, and Sprays. Note 6, National Aeronautical Establishment, Ottawa, Canada, 1951.

4. Sahay, B. K.: Rupture of Water Drops over Liquid Surfaces. Indian Journal of Physics, Vo. 18, 1944, pp. 306 - 310.

5. Singh, B. N.: Eine Beobachtung beim Heraufallen von Wassertropfen auf Oloberflachen. Zeits f. Physik, Vol. 136, 1953, pp. 105 - 107.

6. Rupe, Jack H.: Critical Impact Velocities of Water Droplets as a Problem in Injector Spray Sampling. Jet Propulsion Laboratory, California Institute of Technology, Progress Report No. 4-80, 1950.

7. Lane, W. R.: A Microburette for Producing Small Liquid Drops of Known Size. Journal of Scientific Instruments, Vol. 24, 1947, pp. 98 - 101.

8. Tsutsui, Toshimasa: Rupture Phenomena of Liquid Drops. Tokyo Institute of Physical and Chemical Research, Vol. 16, 1931, pp. 109 - 124.

9. Haenlein, H.: Ueber den Zerfall eines Flussigkeitsstrahles. Forschung aug dem Gebiete des Ingenierwesens, Vol. 2, No. 4, 1931 pp. 139 - 149. (Available in English translation as NACA TM 659.)

10. Rayleigh, Lord: On the Instability of Jets. Proc. Lond. Math. Soc., Vol. 10, 1878, ppg. 4 - 13.

11. Weber, C.: Zum Zerfall eines Flussigkeitsstrahles. Zeits. Ang.Math. Mech., Vol. 11, 1931, pp. 136 - 154.

12. Lane, W. R.: Shatter of Drops in Streams of Air, Ind. Engr. Chem., Vol. 43, No. 6, 1951, pp. 1312 - 1317.

13. Merrington, A. C., and Richardson, E. G.: The Break-up of Liquid Jets. Proc. Phys. Soc., Vol. 59, 1947, pp. 1 - 13.

14. Hinze, J. O.: Critical Speeds and Sizes of Liquid Globules. Applied Scientific Research, Vol. A1, 1949, pp. 273 - 288.

15. Payman, W. and Shepherd, W. C. F.: Explosion Waves and Shock Waves VI. The Distrubance Produced by Bursting Diaphragms with Compressed Air. Proc. Roy. Soc. (London), Vol. A186, 1946, pp. 293 - 321.

16. Bleakney, W., Weimer, D. K., and Fletcher, C. H.: The Shock Tube: A Facility for Investigations in Fluid Dynamics. Rev. Sci. Instr., Vol. 20, 1949, pp. 807 - 815.

17. Glass, I.I., Martin, W., and Patterson, G. N.: A Theoretical and Experimental Study of the Shock Tube, Institute of Aerophysics, University of Toronto, UTIA Report No. 2, 1953.

18. Lobb, R. K.: On the Length of a Shock Tube. Institute of Aerophysics, University of Toronto, UTIA Report No. 4, 1950.

19. Geiger, F. W., and Mautz, C. W.: The Shock Tube as an Instrument for the Investigation of Transonic and Supersonic Flow Patterns. University of Michigan, Engineering Research Institute Report on Project M720-4, June 1949. (With an Addendum by R. N. Hollyer, Jr.)

20. Bolt, J. A. and Mirsky, W.: Apparatus for Suspending Small Droplets in Space. Paper presented at Conference on Atomization, Sprays and Droplets, Northwestern University, September 1953.

21. Bücks, K. and Müller, H.: Über einige Beobachtungen an schwingenden Piexoquarzen und ihrem Schallfeld, Zeits. Physik, Vol. 84, 1933. pp. 75 - 86.

22. Bergmann, L.: Ultrasonics. John Wiley and Sons, Inc., New York, 1938. pp. 42 - 43

23. King, L. V.: On the Acoustic Radiation Pressure on Spheres. Proc. Roy. Soc. (London), Vol. A147, 1934, pp. 212 - 240.

24. Rudnick, I.: Measurements of the Acoustic Radiation Pressure on a Sphere in a Standing Wave Field. Paper presented at May 1951 meeting of Acoustical Society of America, Washington, D. C.

25. St. Clair, H. W.: Agglomeration of Smoke, Fog, or Dust Particles by Sonic Waves. Ind. Eng. Chem., Vol. 41, 1949, pp. 2434 - 2438.

26. St. Clair, H. W., Spendlove, M. J., and Potter, E. V.: Flocculation of Aerosols by Intense High-Frequency Sound. U.S. Department of Interior, Bureau of Mines Report of Investigations 4218, March 1948.

27. Soller, K.: The Mechanism of the Formation of Fog by Ultrasonic Waves. Trans. Faraday Soc., Vol. 32, 1936, pp. 1532 - 1536.

28. Wood, R. W., and Loomis, A. L.: The Physical and Biological Effects of High-Frequency Sound-Waves of Great Intensity. Phil. Mag., Vol. 4, 7th Series (1927), pp. 417 - 436.

29. Hodgman, C. D. and Holmes, H. N.: Handbook of Chemistry and Physics. Twenty-fourth Edition, Chemical Rubber Publishing Co., 1940.

30. York, J. L: Provate Communication. Cited in Reference 1.

31. Taylor, Sir Geoffrey: Ministry of Supply, Paper AC 10647/Phys C69 (1939).

32. Triebnigg, H: Der Einblase und Einspritzvorgang bei Diselmaschinen. Springer, Vienna, 1925.

33. Vennard, J. K.: Elementary Fluid Mechanics. John Wiley and Sons, New York, 1940, pp. 309.

34. Hinze, J. O.: Forced Deformation of Viscous Liquid Globules. Applied Scientific Research, Vol. A1, 1949, pp. 263 - 272.

35. Adams, N. K.: The Physics and Chemistry of Surfaces. Oxford University Press, 3rd Edition, 1941, pp. 8, 9.

36. St. Clair, H. W.: An Electromagnetic Sound Generator for Producing High Frequency Sound Waves. Rev. Sci. Inst., Vol. 12, 1940, pp. 250 - 256.

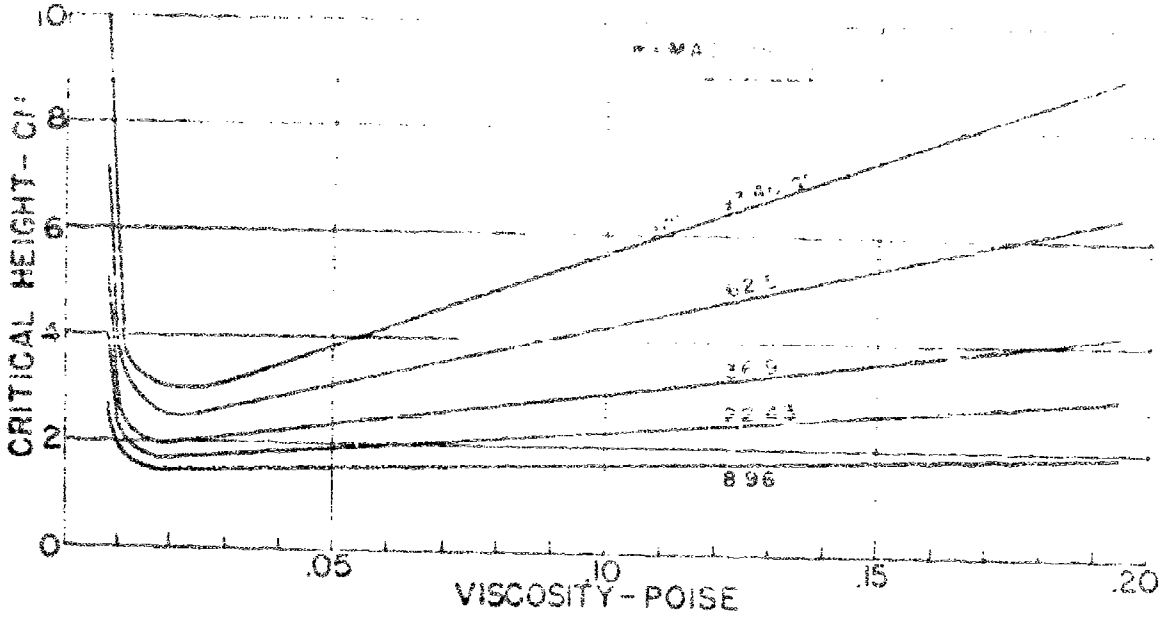

FIGURE 1. CRITICAL HEIGHT VS VISCOSITY (SMITH, REF. 1)

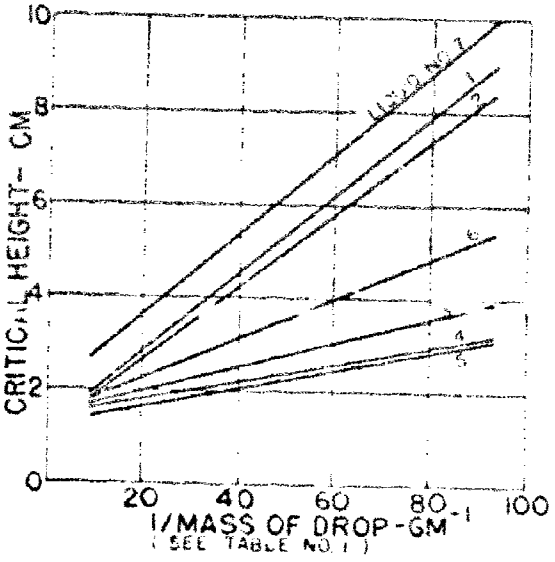

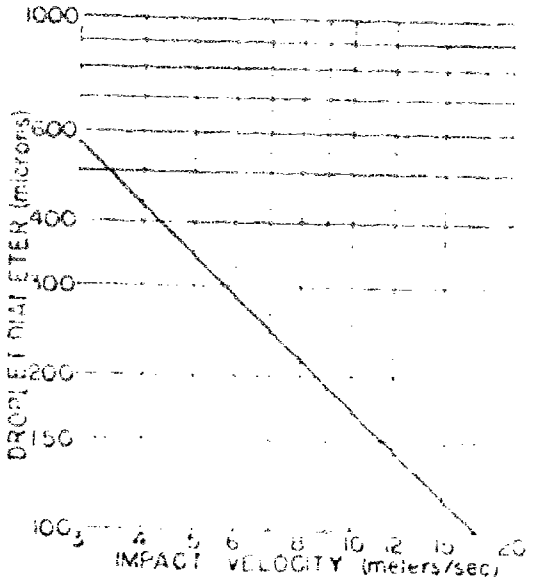

FIGURE 2. CRITICAL HEIGHT VS RECIPROCAL OF DROP MASS (SMITH, REF. 1)

FIGURE 3. [illegible] (SMITH, REF. 1)

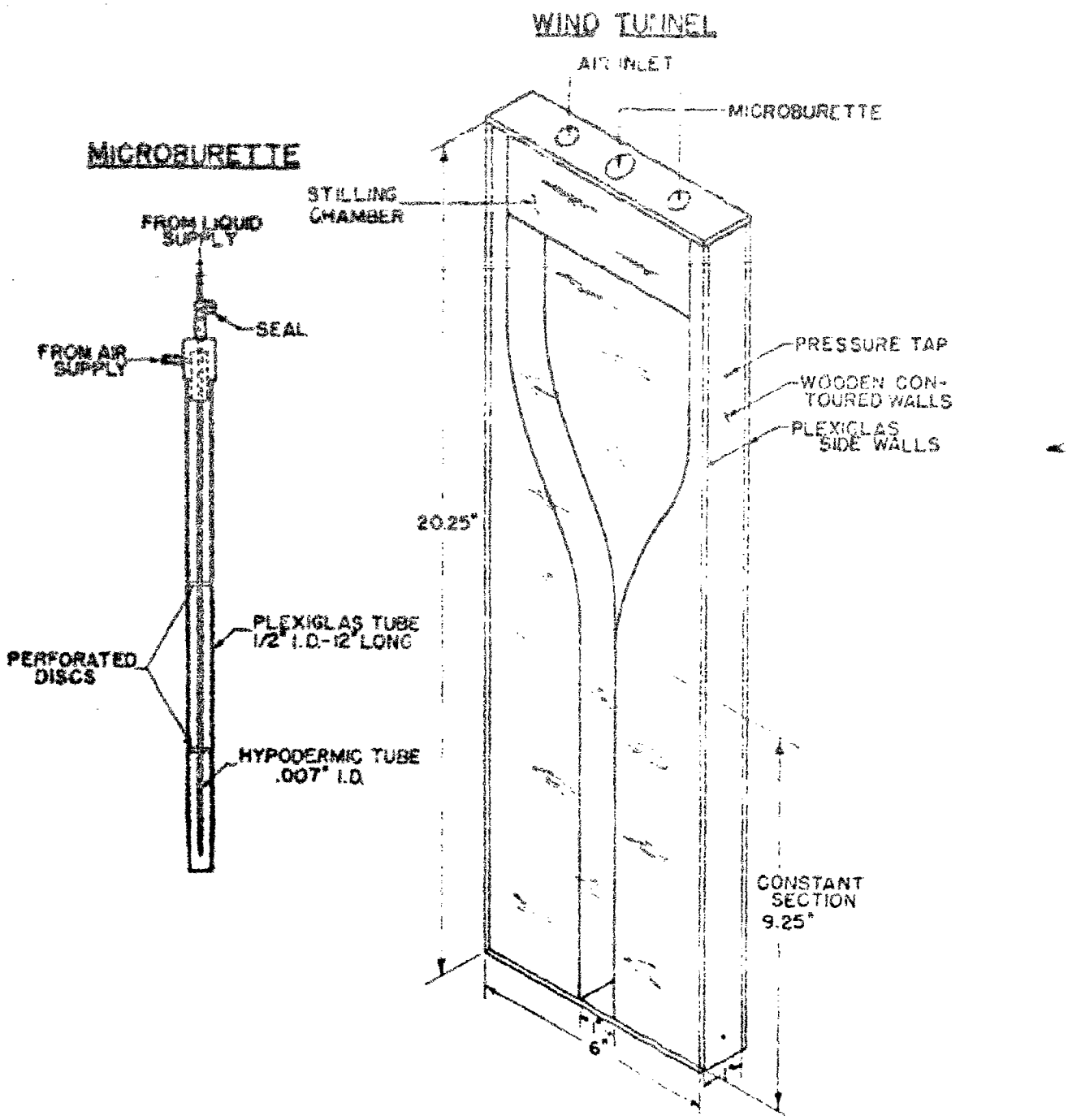

FIGURE 4. SCHEMATIC DIAGRAM OF MICROBURETTE AND WIND TUNNEL

INCHES

FIGURE 7. OVERALL VIEW OF TEST APPARATUS

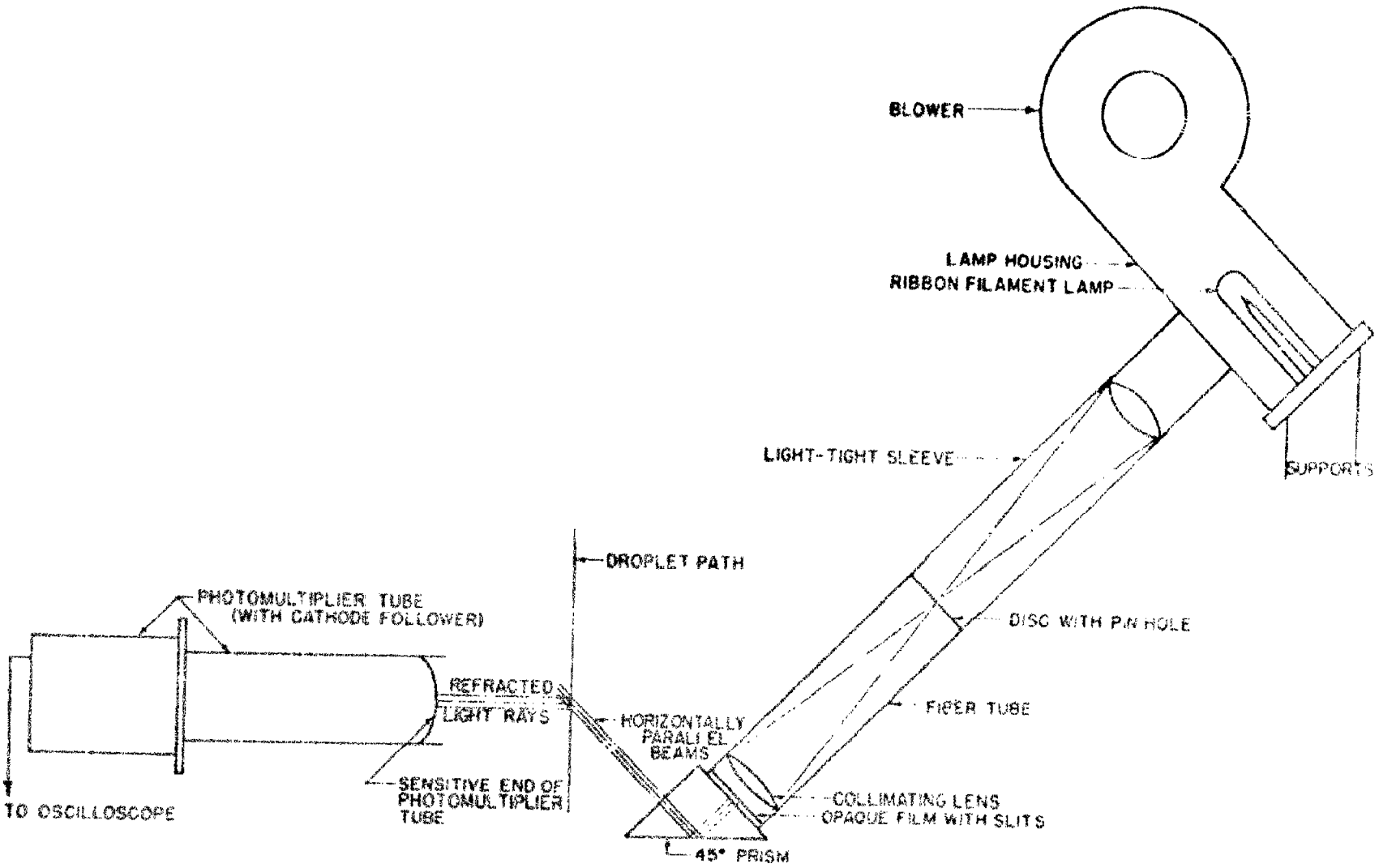

FIGURE 8. SCHEMATIC DRAWING OF OPTICAL VELOCIMETER

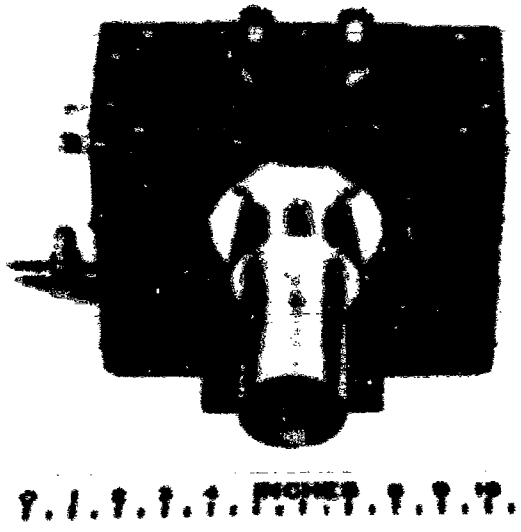

FIGURE 9. FRONT VIEW OF BH6 LAMP HOUSING

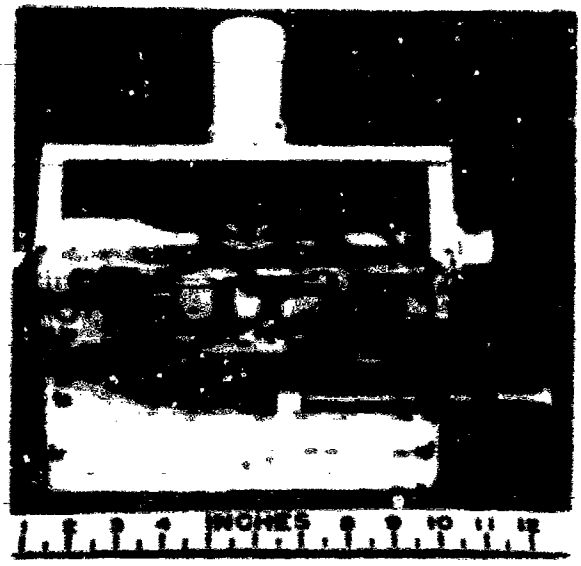

FIGURE 10. BACK VIEW OF BH6 LAMP HOUSING WITH TOP AND BACK REMOVED

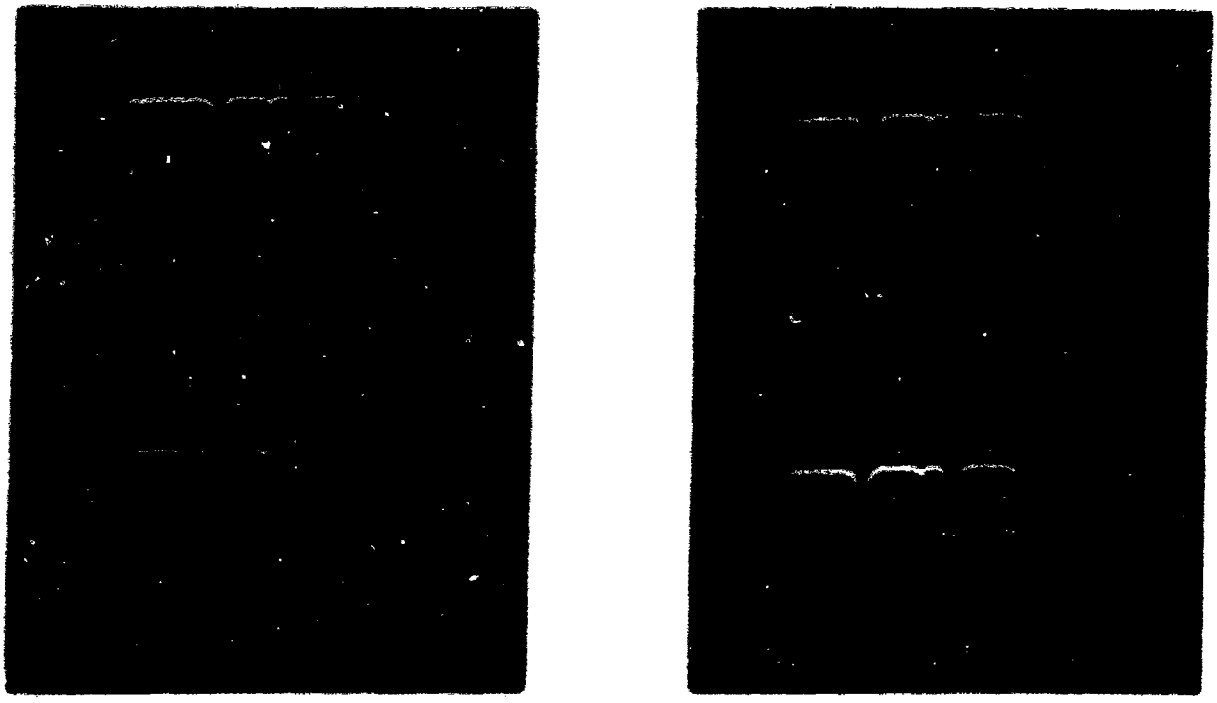

FIGURE 11. TYPICAL OSCILLOSCOPE TRACES USED IN DROPLET VELOCITY DETERMINATION

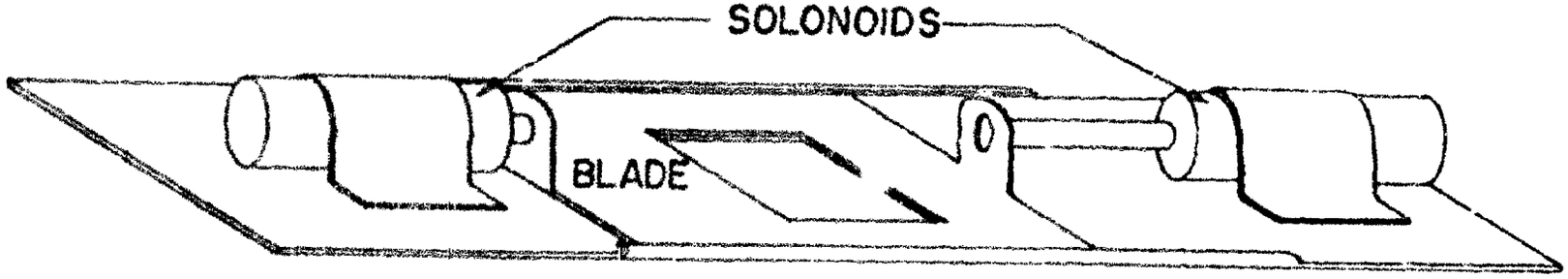

SHUTTER

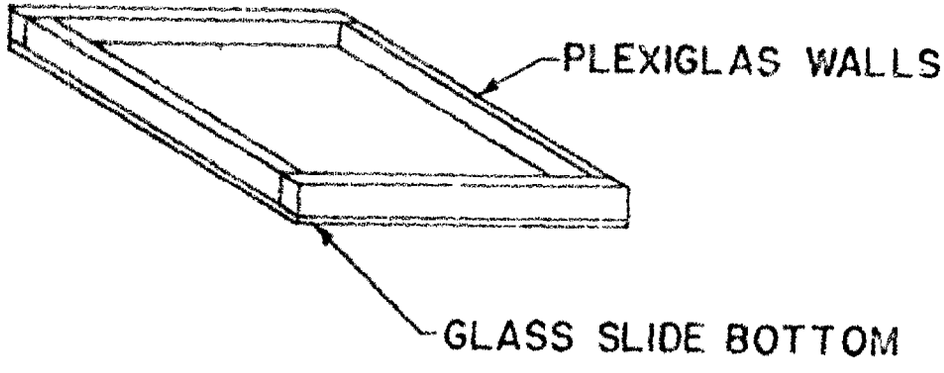

COLLECTING CELL

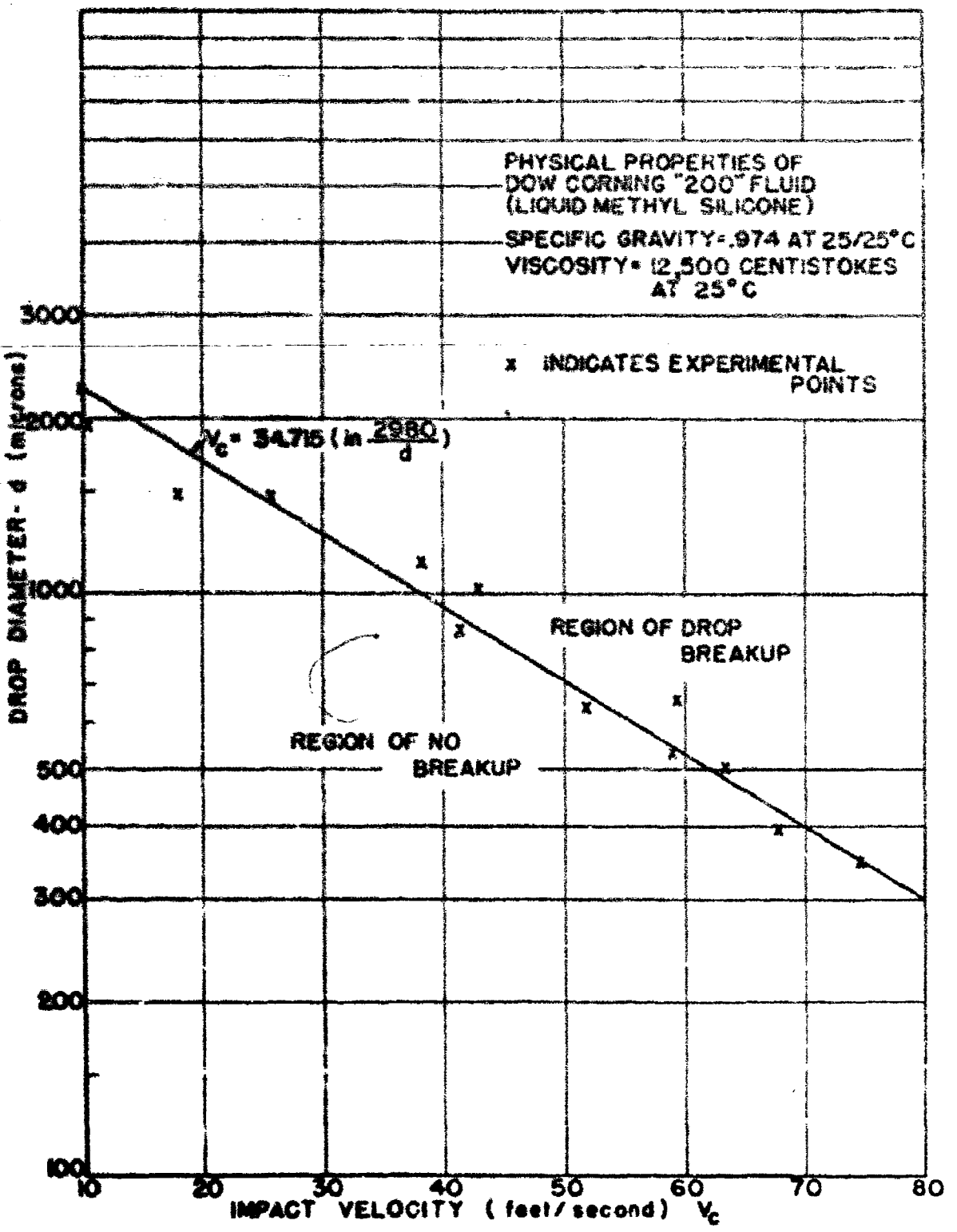

FIGURE 13. CRITICAL IMPACT VELOCITIES OF WATER DROPS STRIKING AIR-OIL INTERFACE

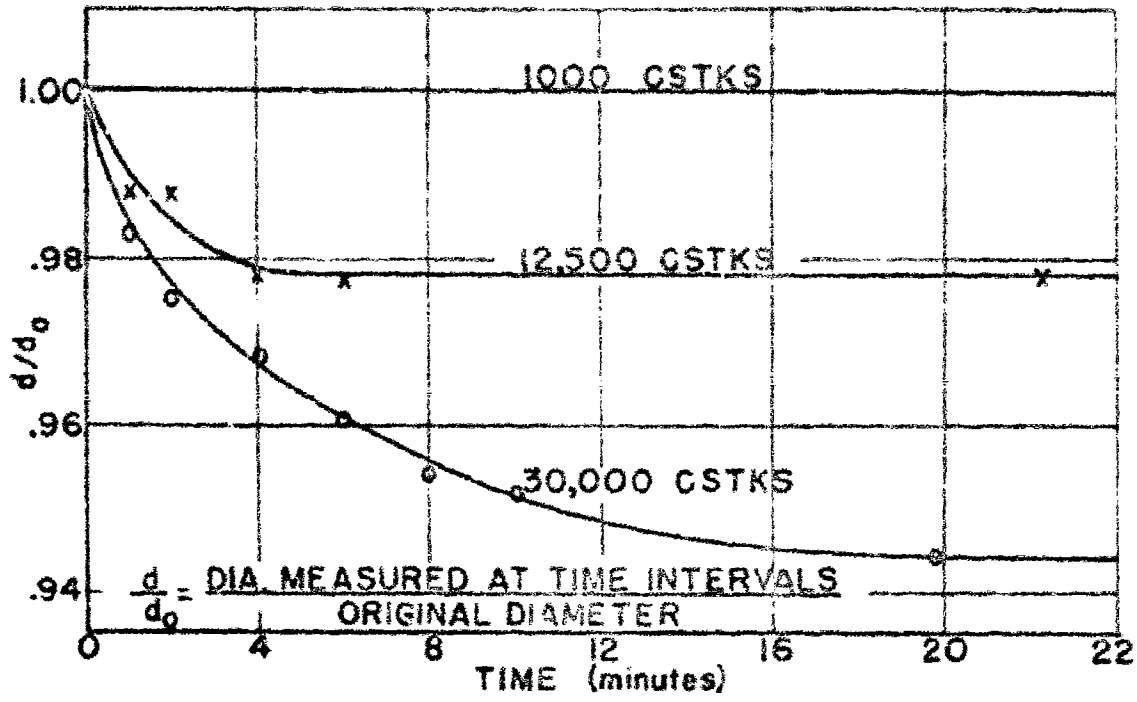

FIGURE 14. EVAPORATION OF WATER DROP WHILE PENETRATING AIR-OIL INTERFACE

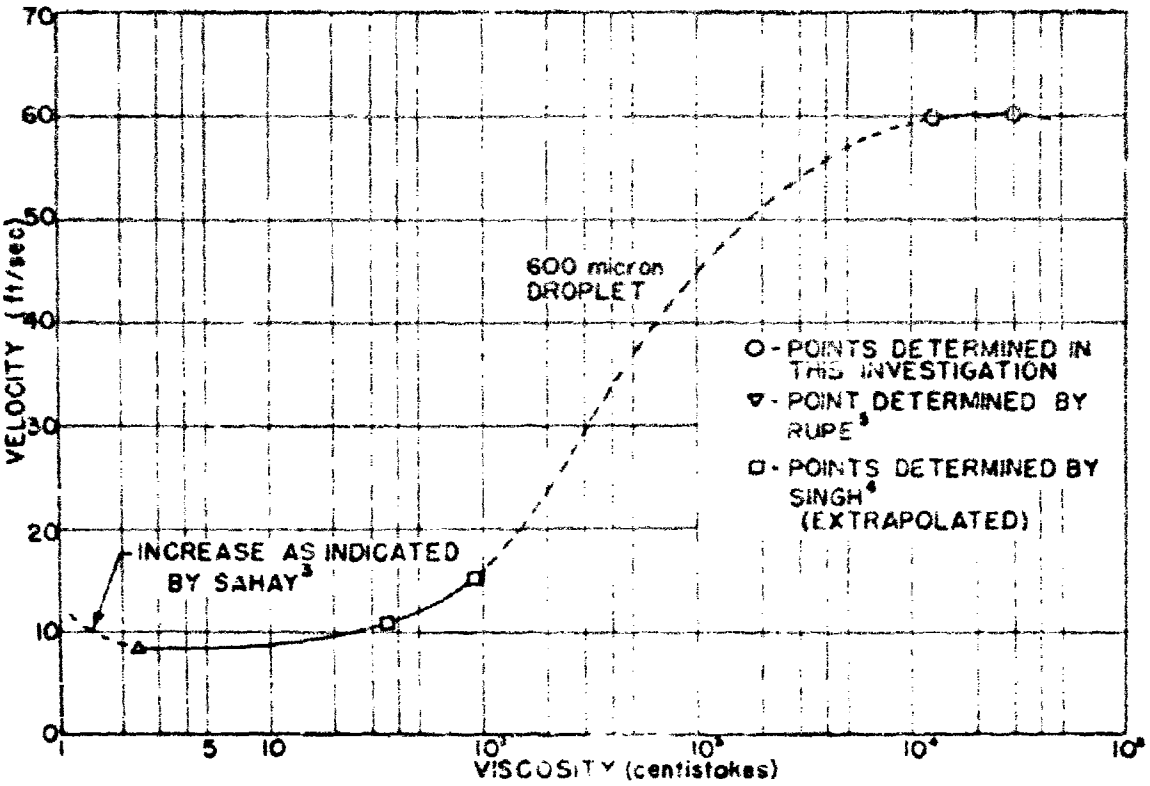

FIGURE 15. CRITICAL VELOCITY OF WATER DROP VS VISCOSITY OF COLLECTING FLUID

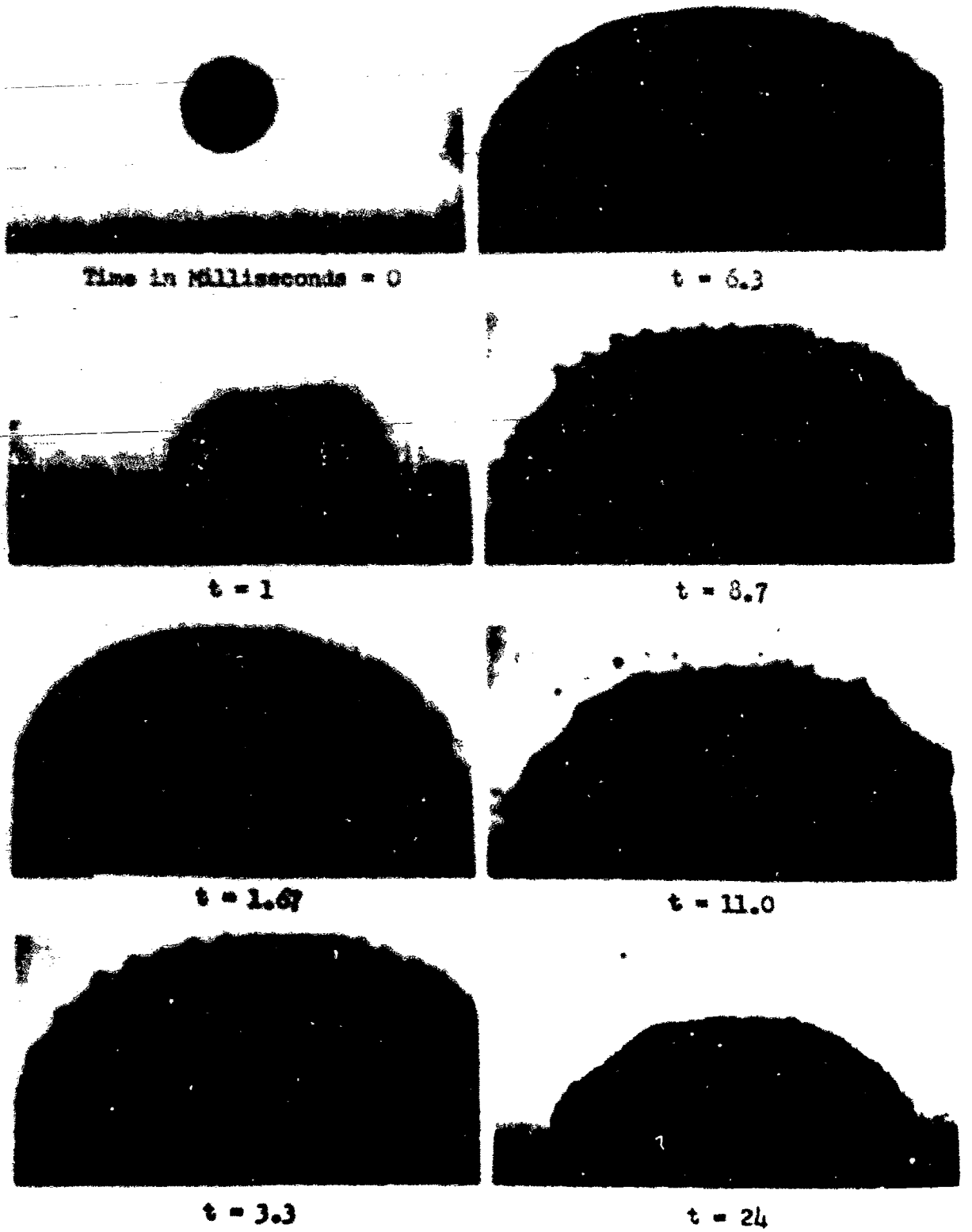

Drop Diameter = 2000 Microns; Drop Velocity = 20 ft/sec.
Oil - 12500 Centistokes Dow Corning "200" Fluid

FIGURE 16. TOP VIEW OF WATER DROP STRIKING AIR-OIL INTERFACE (3000 Frames/Sec.)

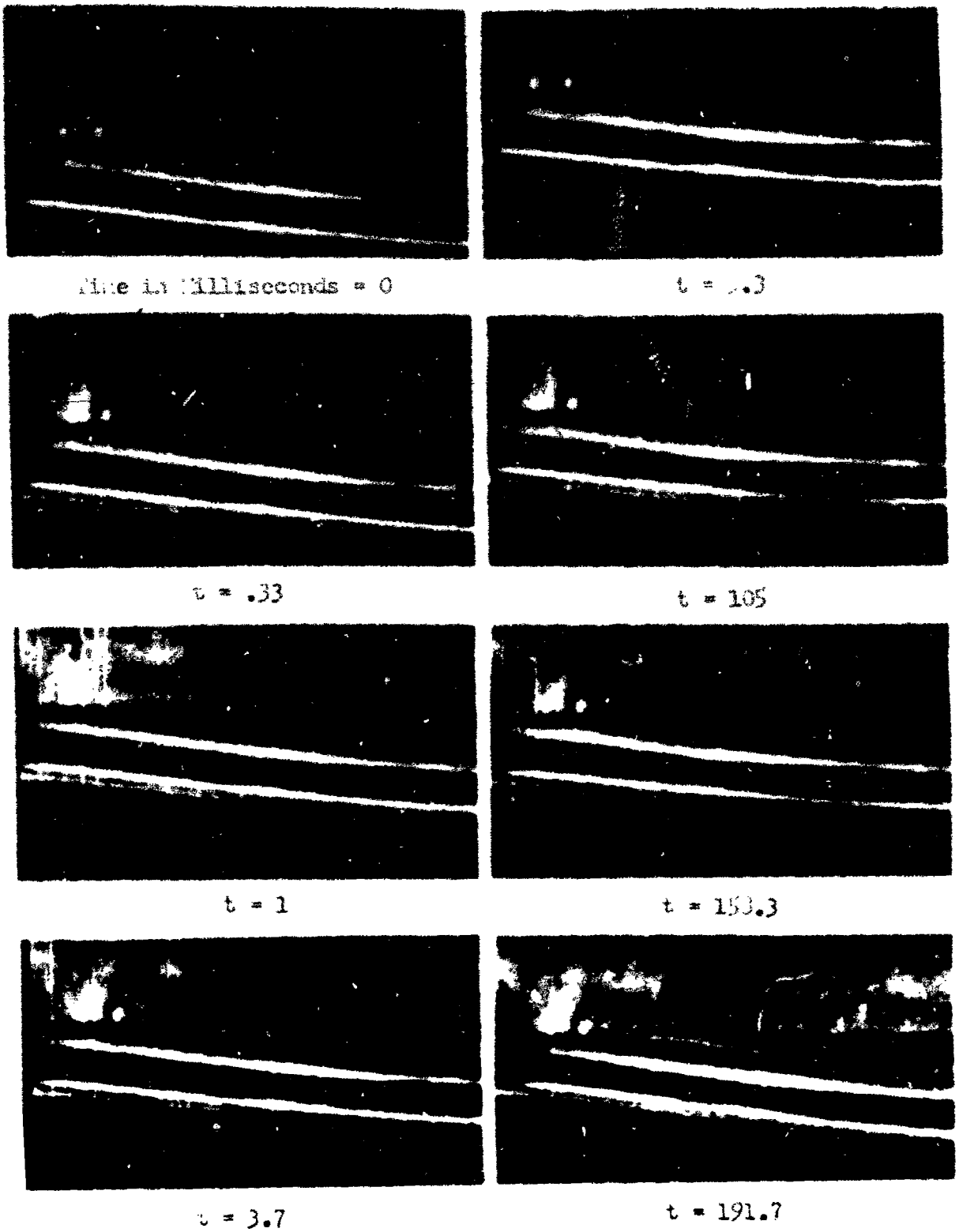

Drop Diameter = 1000 Microns; Drop Velocity = 25 Ft/Sec.
Oil = 12500 Centistokes Dow Corning "200" Fluid

FIGURE 17. SIDE VIEW OF WATER DROP STRIKING AIR - OIL INTERFACE (3000 Frames/Sec.)

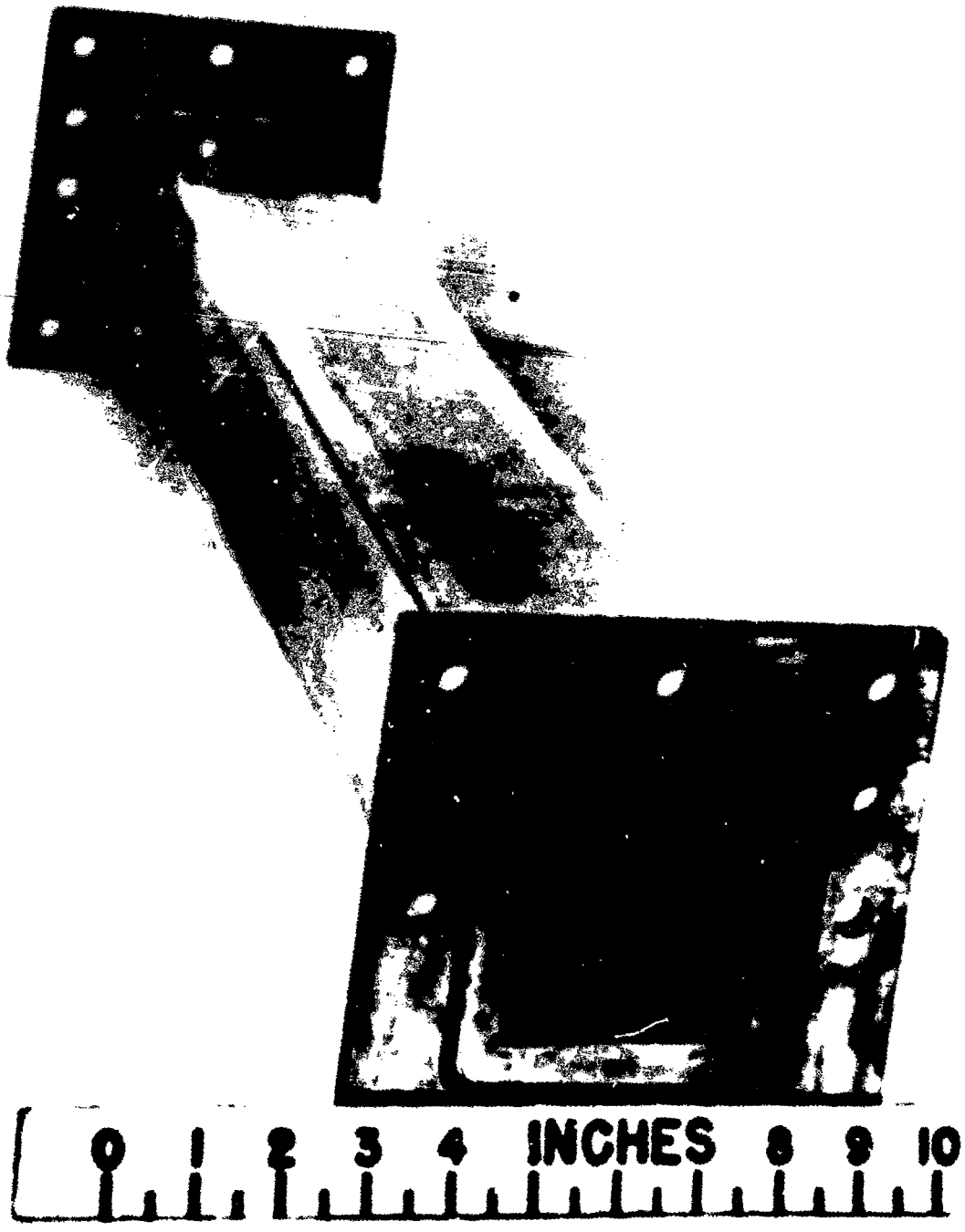

FIGURE 13. SHOCK TUBE SECTION

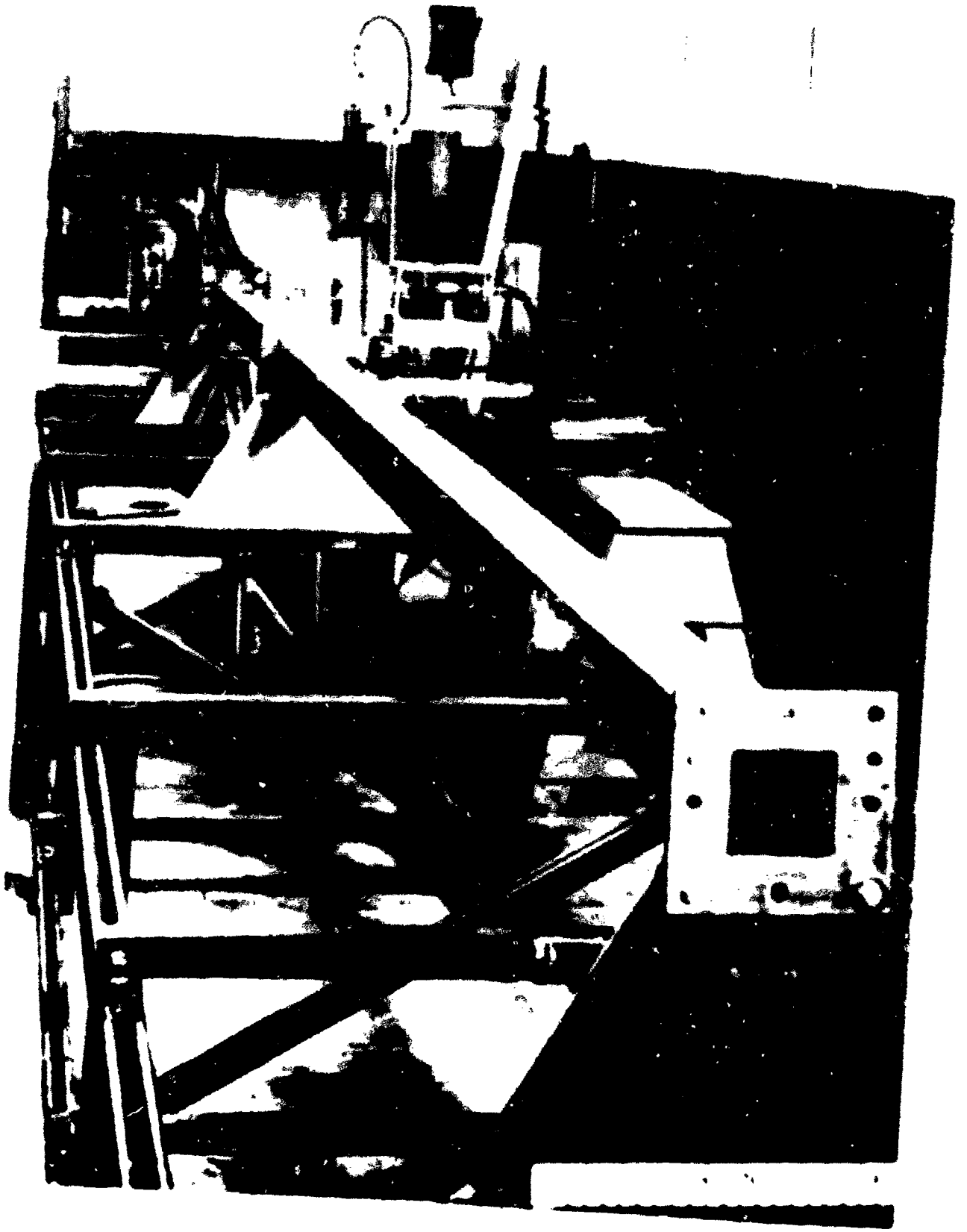

FIGURE 19. SHOCK TUBE ASSEMBLY

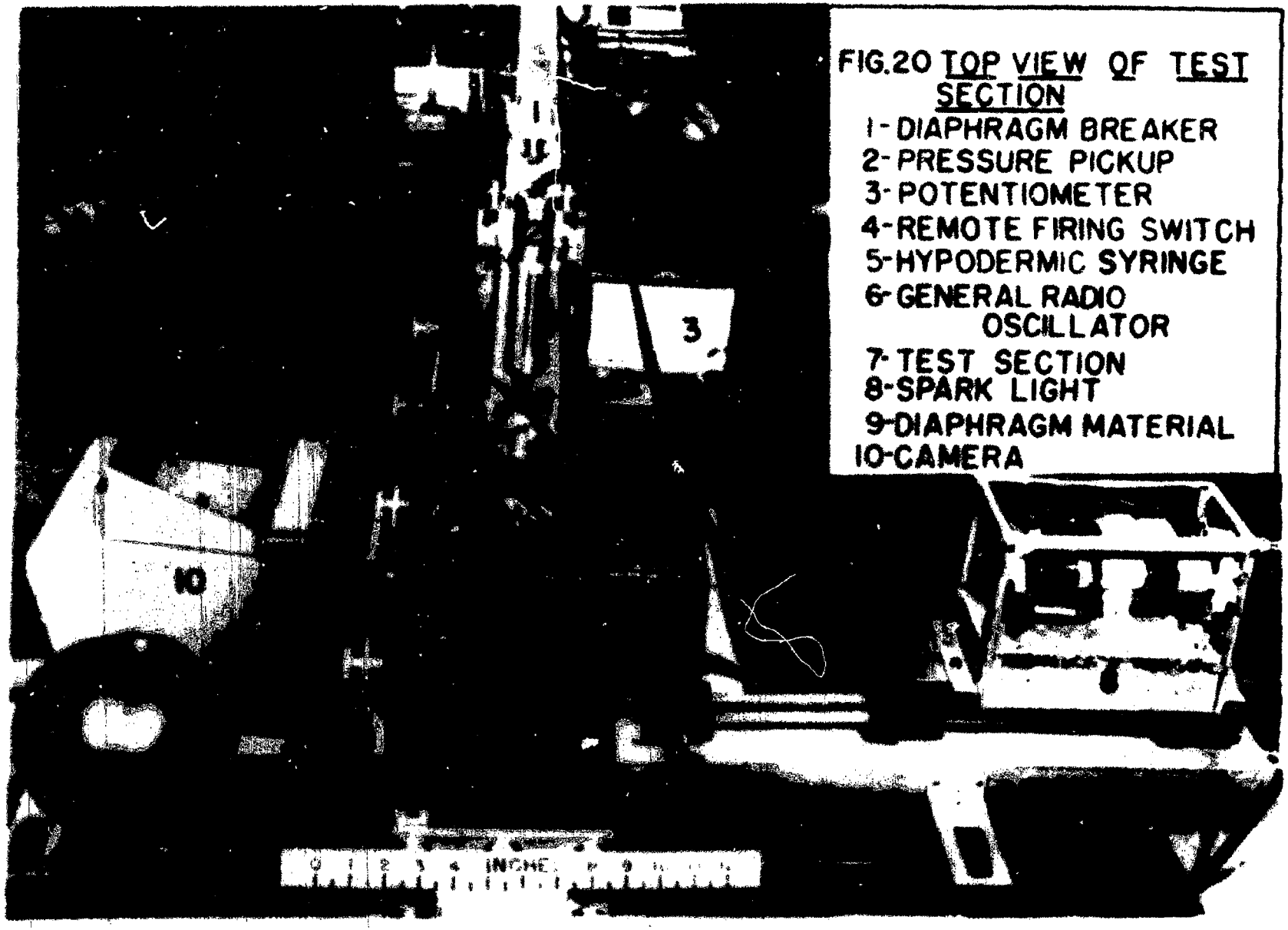

FIG.20 TOP VIEW OF TEST SECTION

1- DIAPHRAGM BREAKER
2- PRESSURE PICKUP
3- POTENTIOMETER
4- REMOTE FIRING SWITCH
5- HYPODERMIC SYRINGE
6- GENERAL RADIO OSCILLATOR
7- TEST SECTION
8- SPARK LIGHT
9- DIAPHRAGM MATERIAL
10- CAMERA

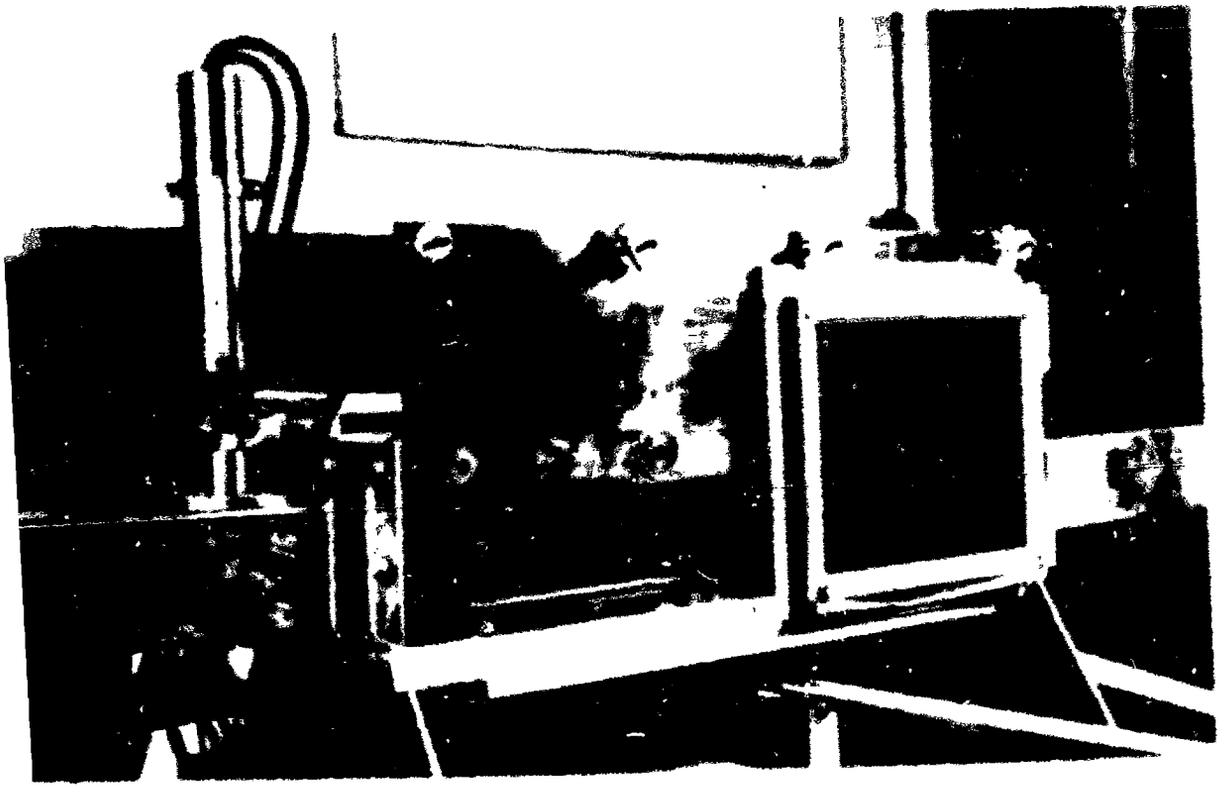

FIGURE 21. SIDE VIEW OF TEST SECTION

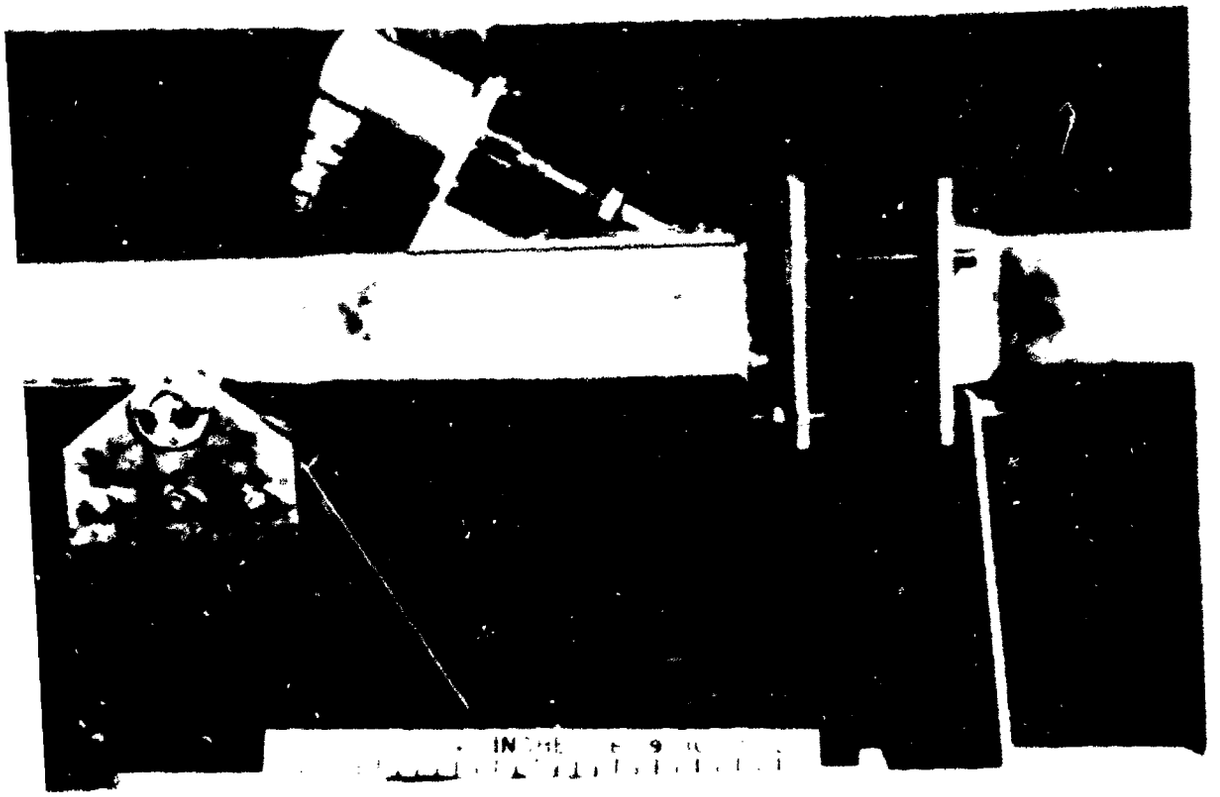

FIGURE 22. [illegible]

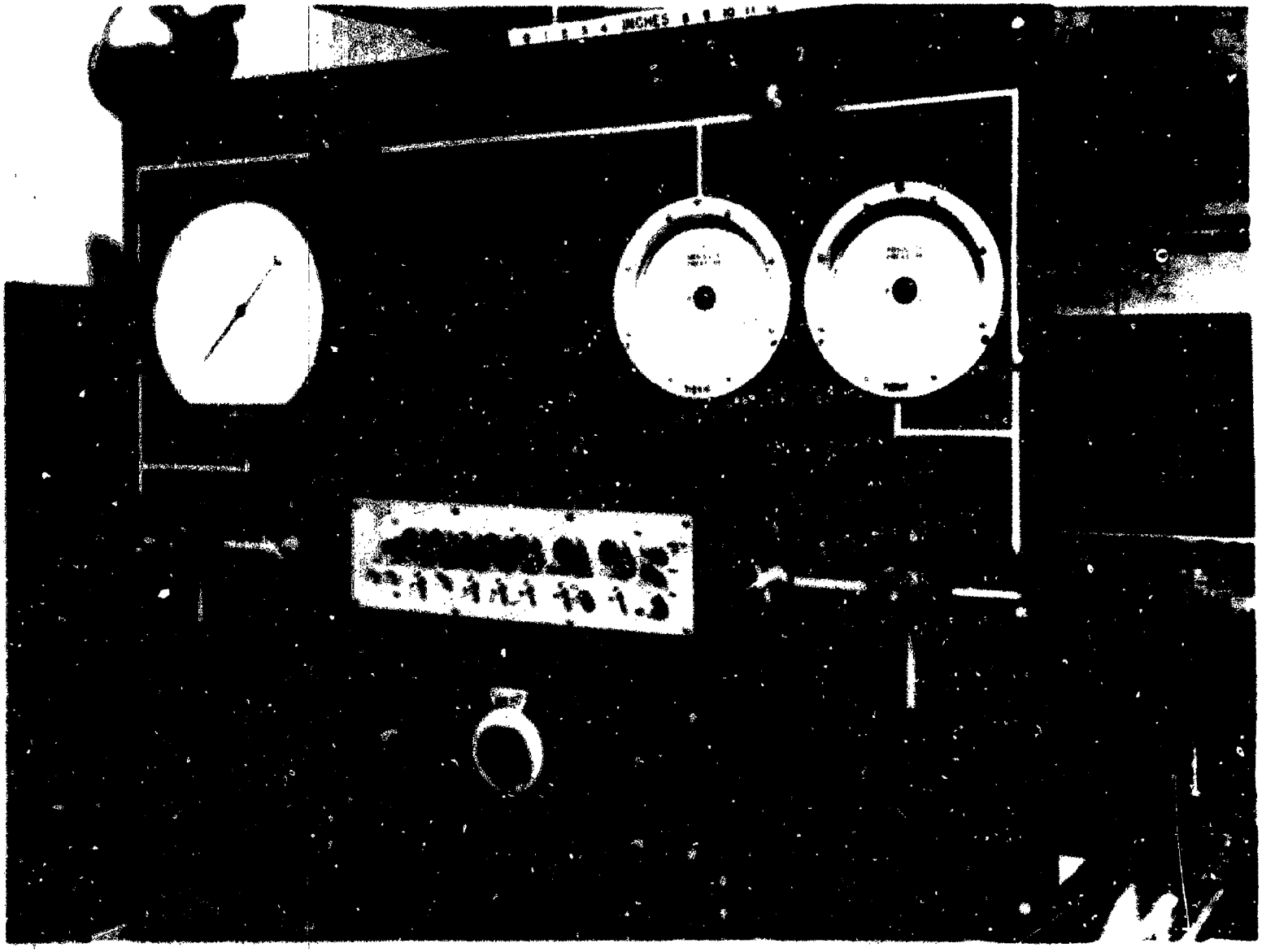

FIGURE 23. CONTROL PANEL

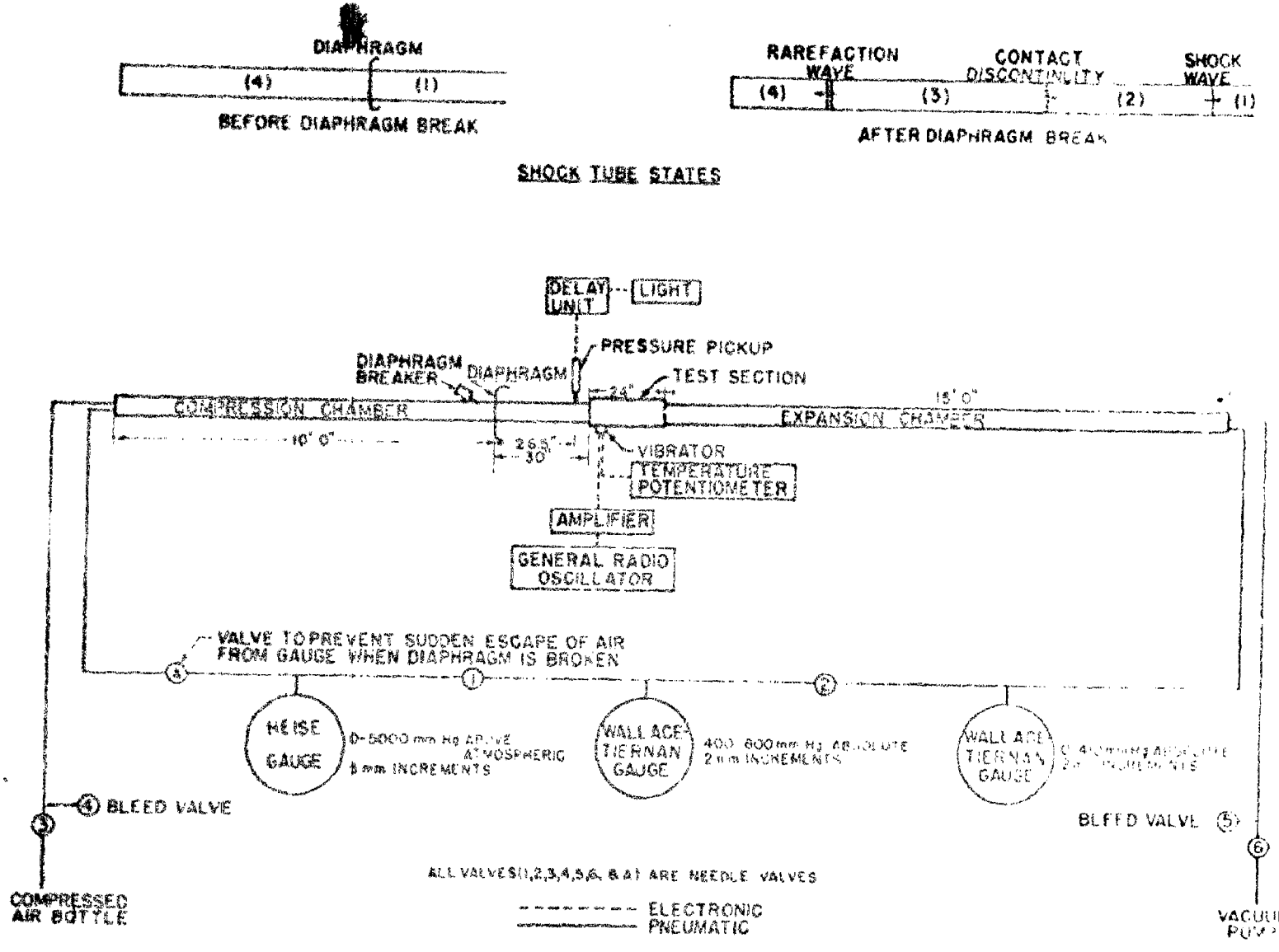

FIGURE 24. FUNCTIONAL DIAGRAM OF SHOCK TUBE AND ASSOCIATED EQUIPMENT

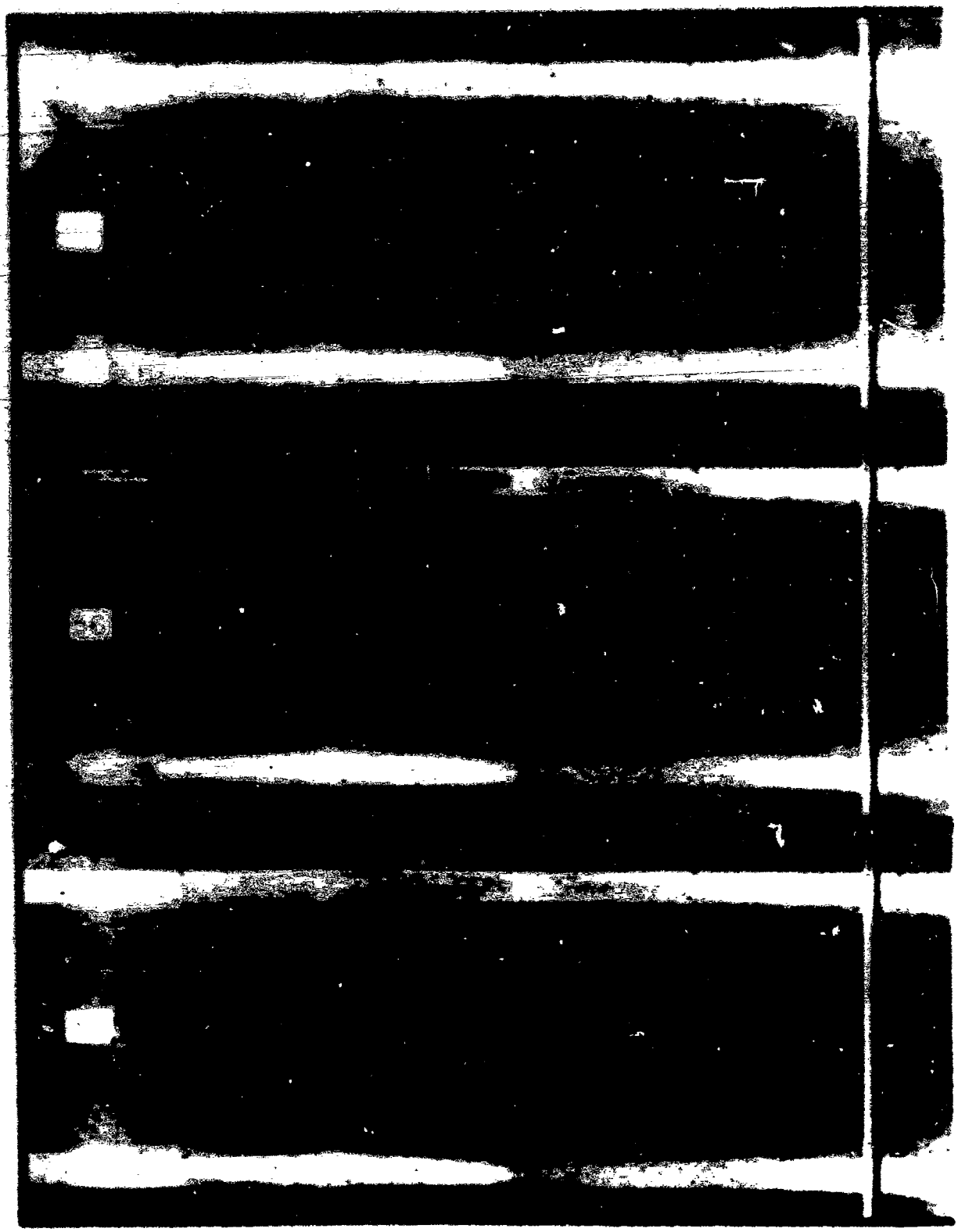

Delay = 750 μsec; P_{41} = 2

FIGURE 25. SHADOWGRAPH PICTURES OF SHOCK WAVES

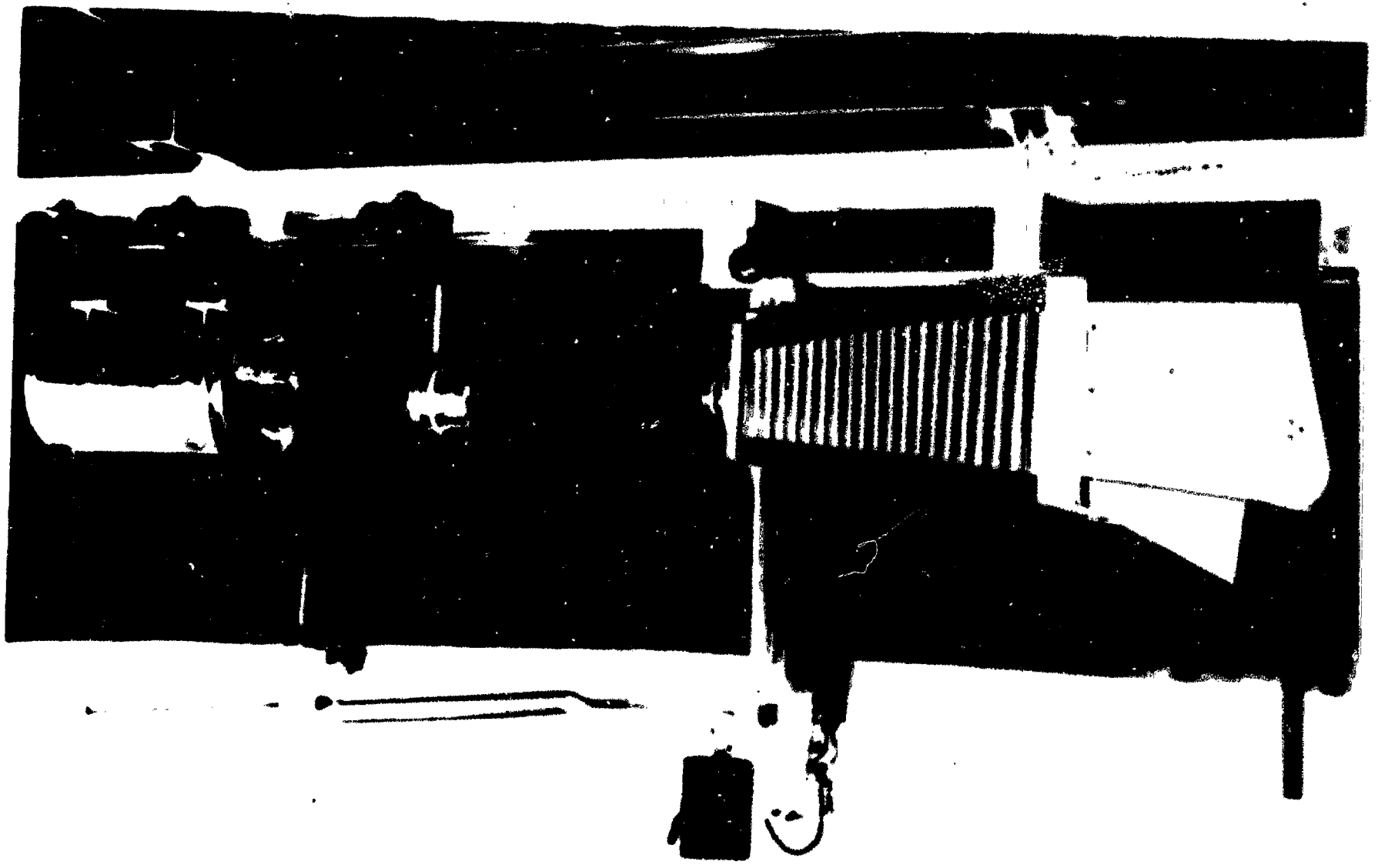

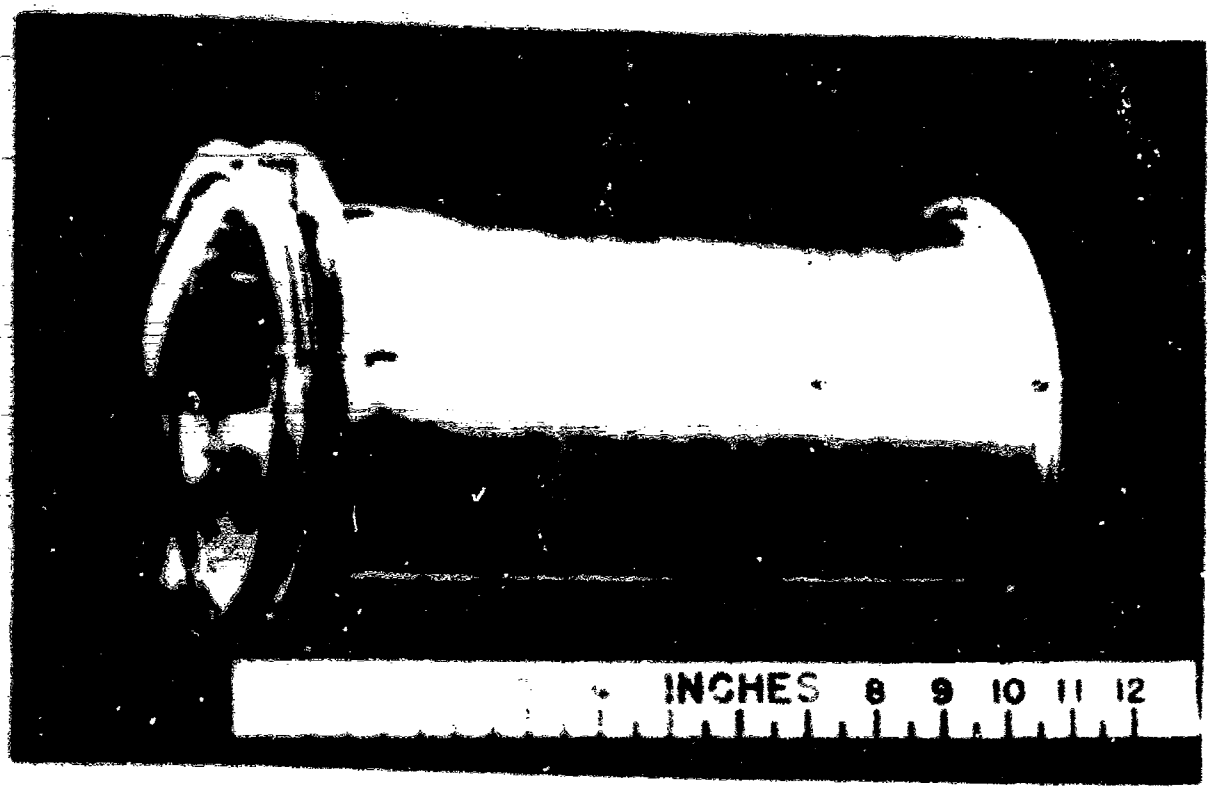

FIGURE 27. GENERAL ELECTRIC FLASH TUBE

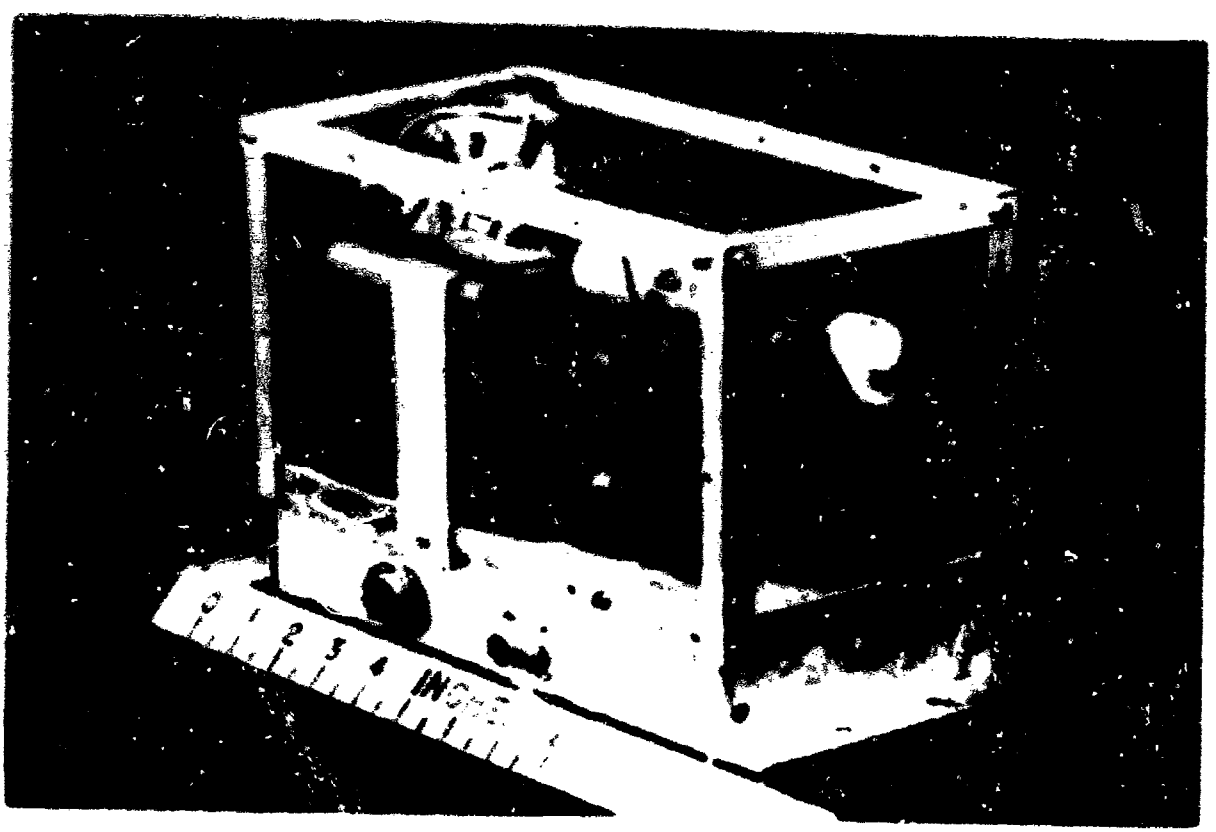

FIGURE 28. SPARK LIGHT SOURCE

FIGURE 29. ULTRASONIC VIBRATOR AND BASE

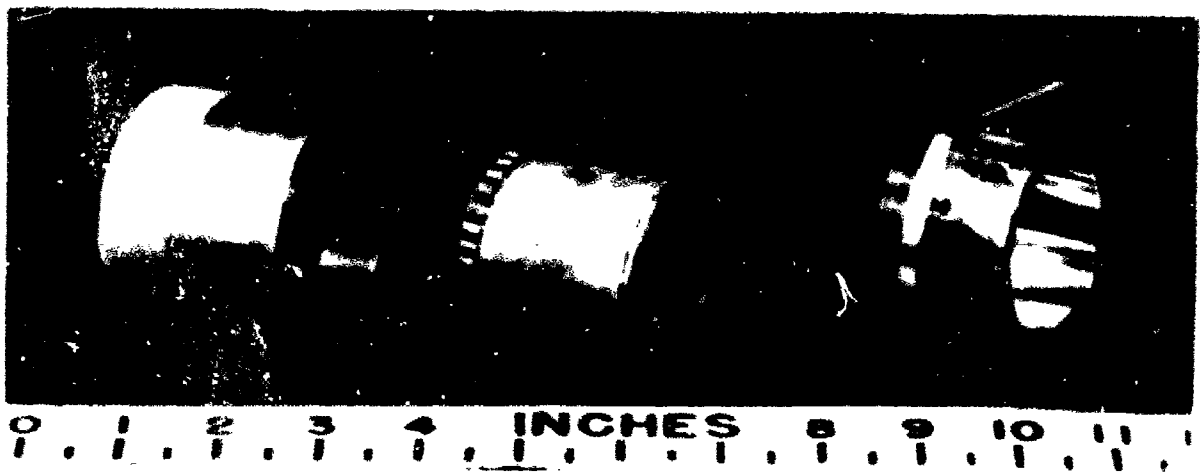

FIGURE 30. ULTRASONIC VIBRATOR AND COMPLETE HOUSING

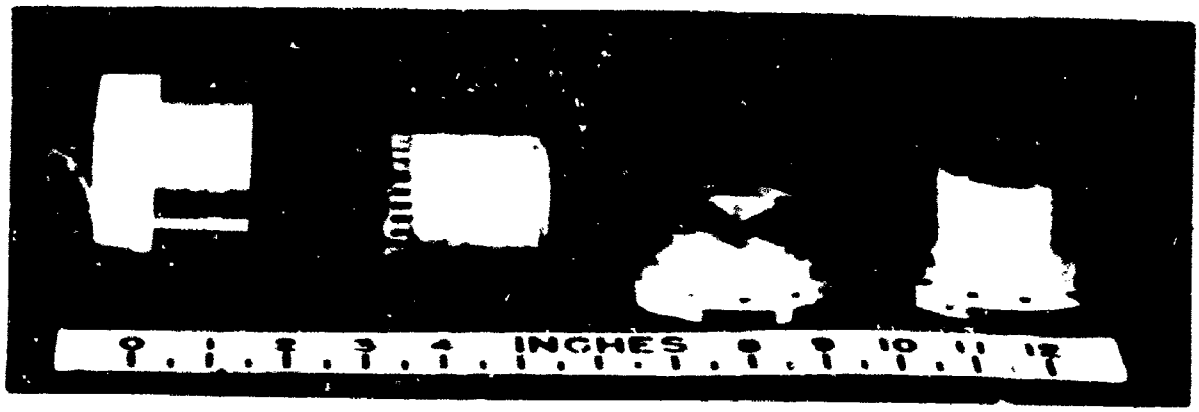

FIGURE 31. ULTRASONIC VIBRATOR AND REFLECTOR PLUGS

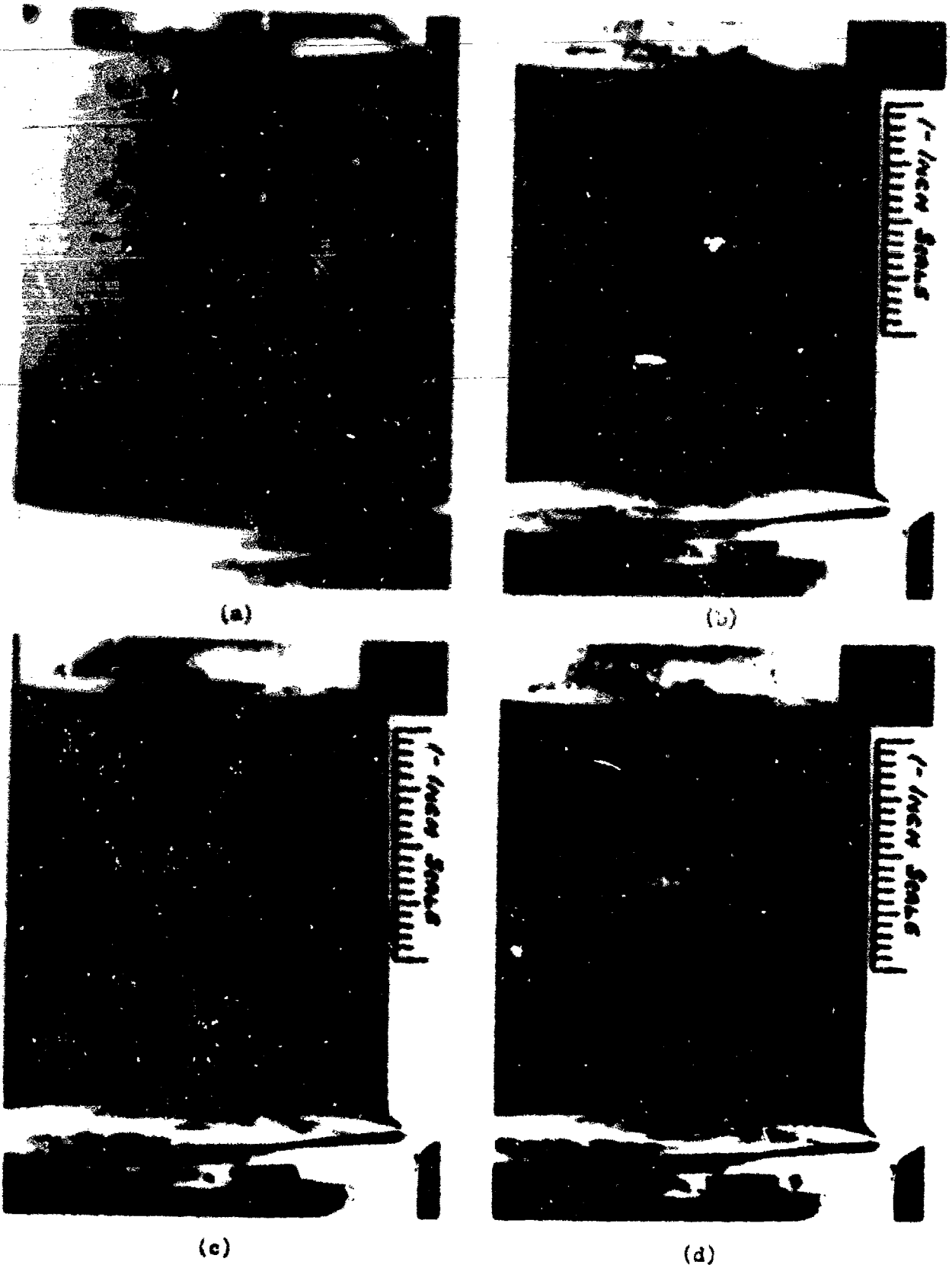

FIGURE 32. [illegible] SETUP SHOWING DROPS SUPPORTED IN [illegible] FIELD

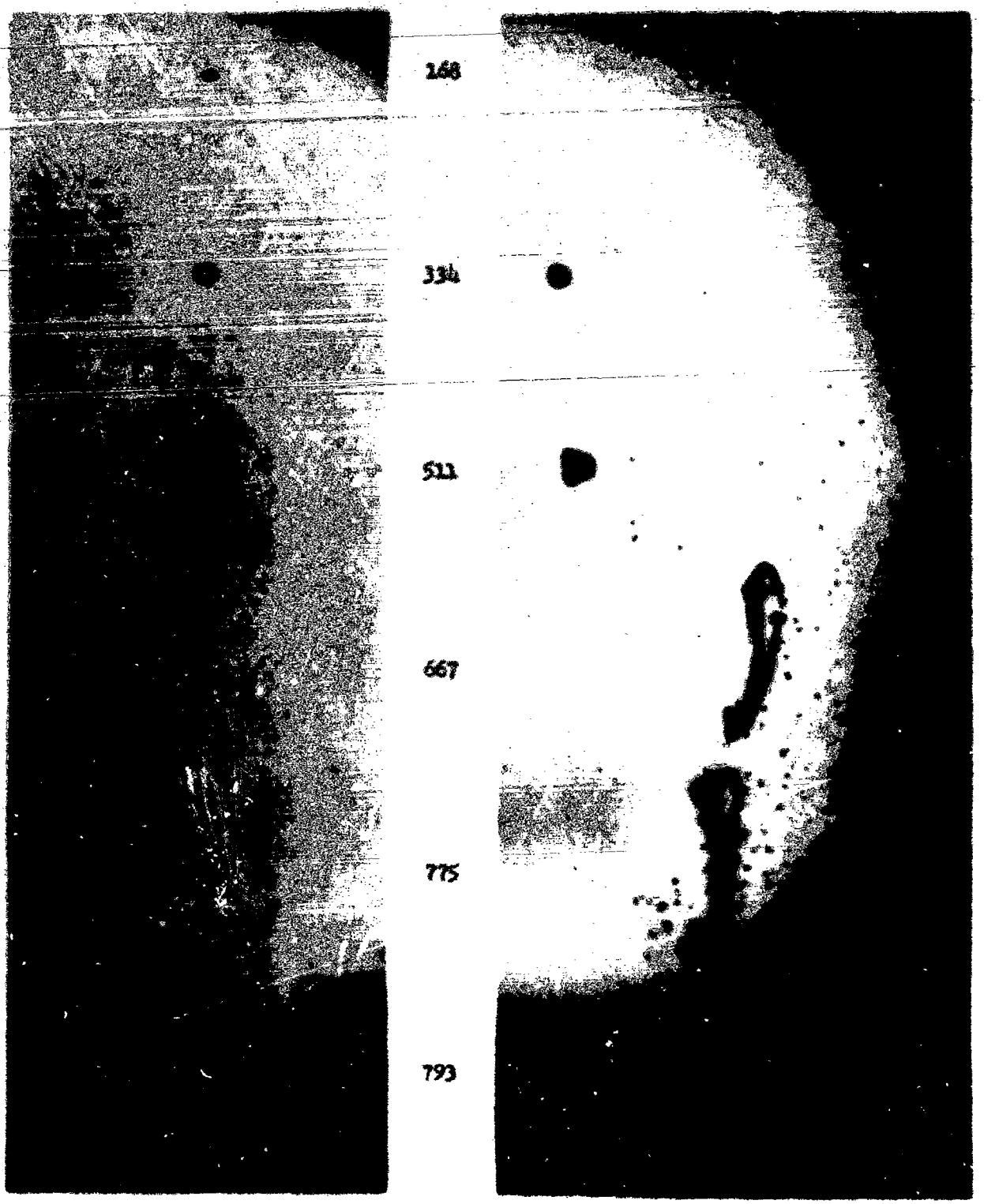

(a) Reflex photograph before firing shock tube.

(b) Normal photographs after firing shock tube. Delay, 3.20 msecs.

Air Velocity = 60 ft./sec.; Liquid - Methyl Alcohol
Run No. 276

FIGURE 35. TYPICAL PAIR OF PHOTOGRAPHS SHOWING ORIGINAL DROP SIZES AND SUBSEQUENT BREAK-UP.

(a)

Time (μsec): 0 20 7. 1C

Run No.: 96 1-60

Initial Drop Diameter = 3[illegible] Microns; Air Velocity, u_2 = 22[illegible] Ft./sec.
Liquid - Ethyl Alcohol

(b)

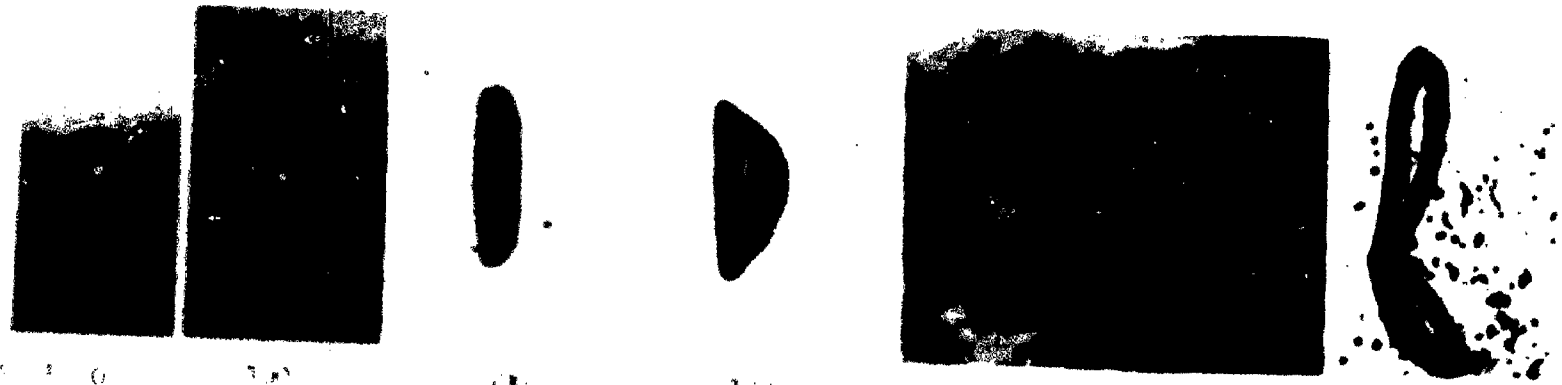

Time (μsec): 0 [illegible] [illegible] 1[illegible]

Run No.: 230 235 236 259

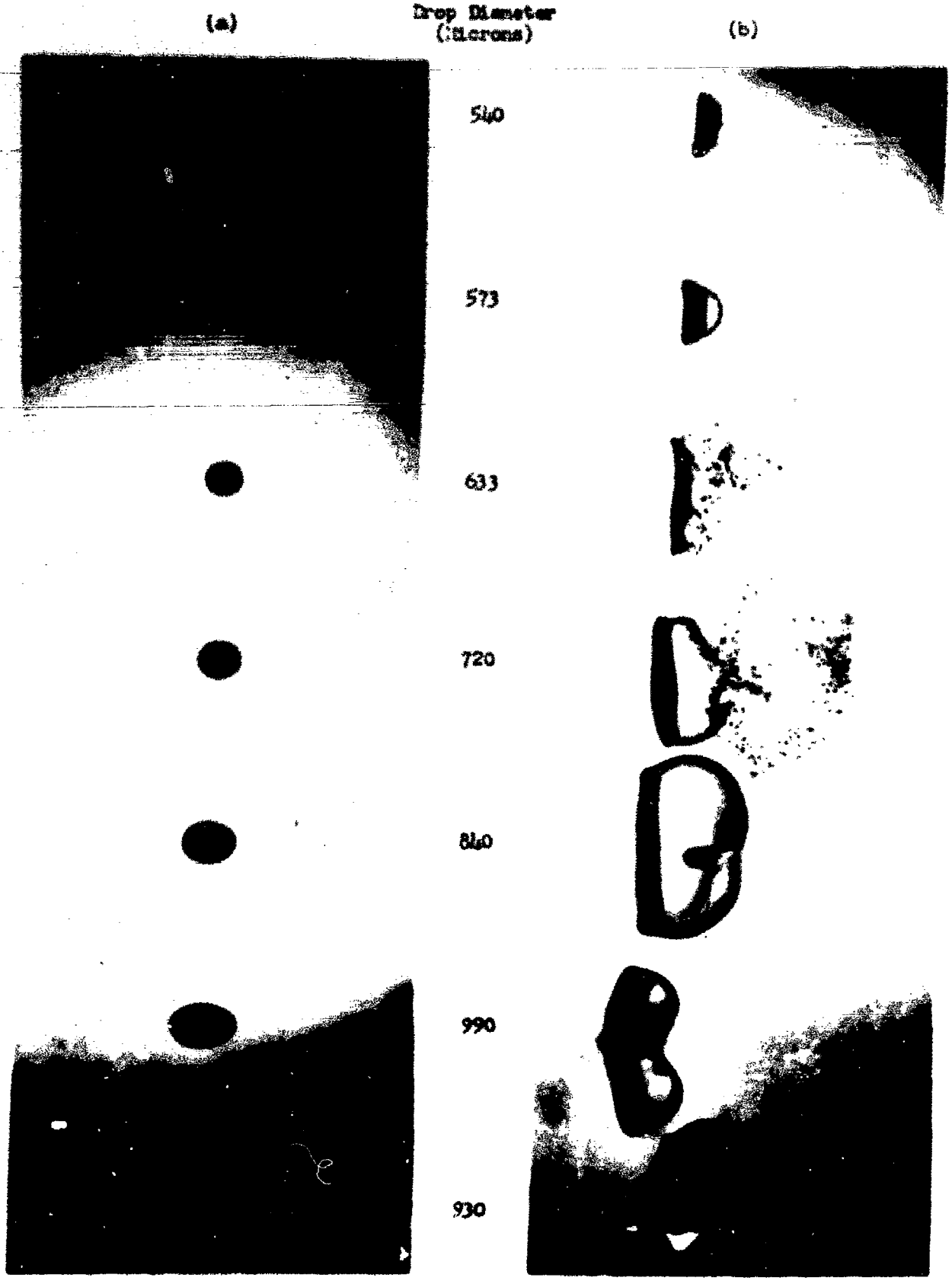

Air Velocity, u_2 = 84.3 ft./sec.; Delay (b) = 1500 μsecs;
Liquid - Water; Run No. 453

FIGURE 37. DROP BREAK-UP

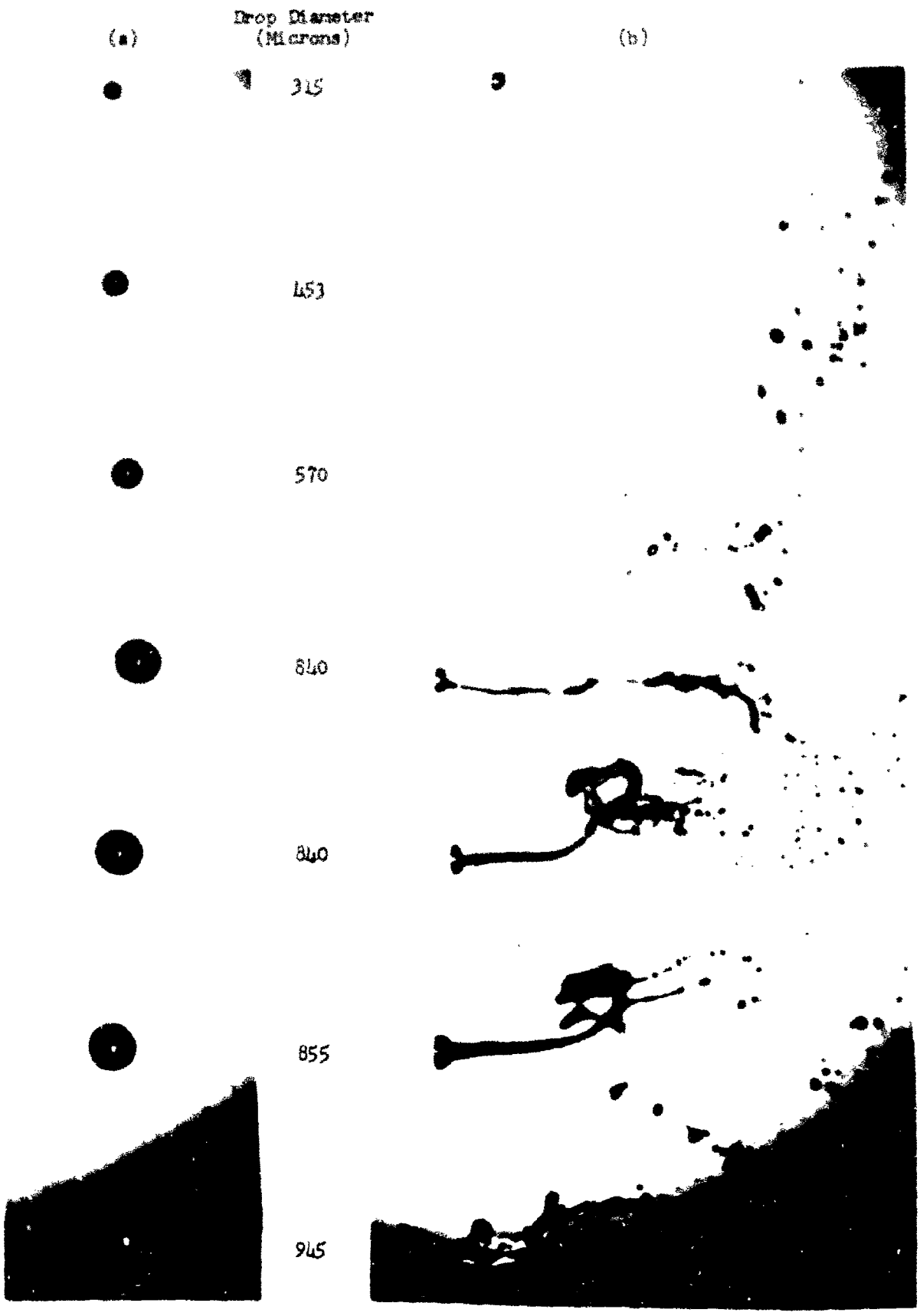

Air Velocity, u_2 = 109.5 ft./sec.; Delay (b) = 1500 μsecs;
Liquid - Water; Run No. 434

FIGURE 38. DROP BREAK-UP

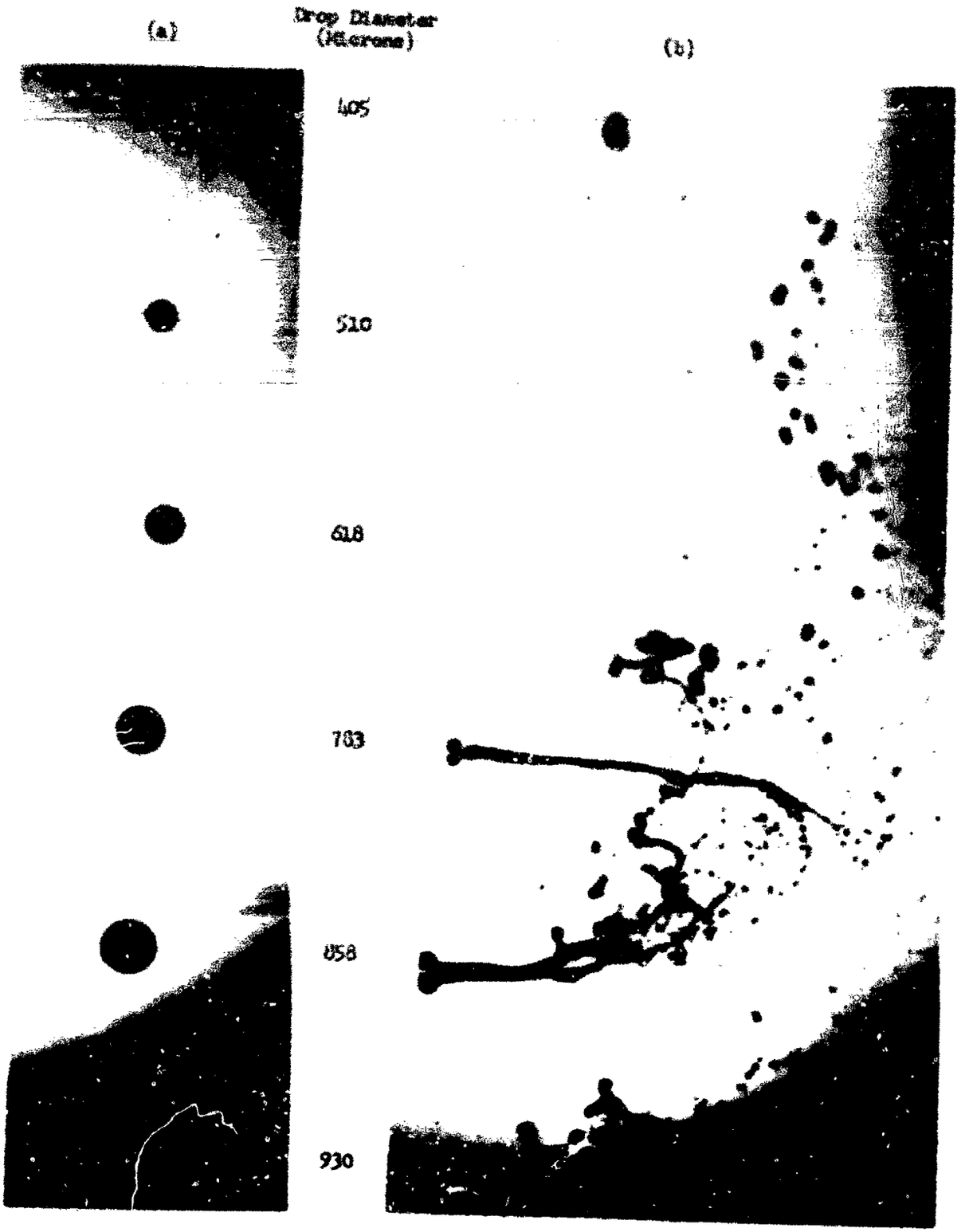

Air Velocity, u_2 = 109.5 ft./sec.; Delay (b) - 1500 μsecs;
Liquid - Water; Run No. 436

FIGURE 39. DROP BREAK-UP

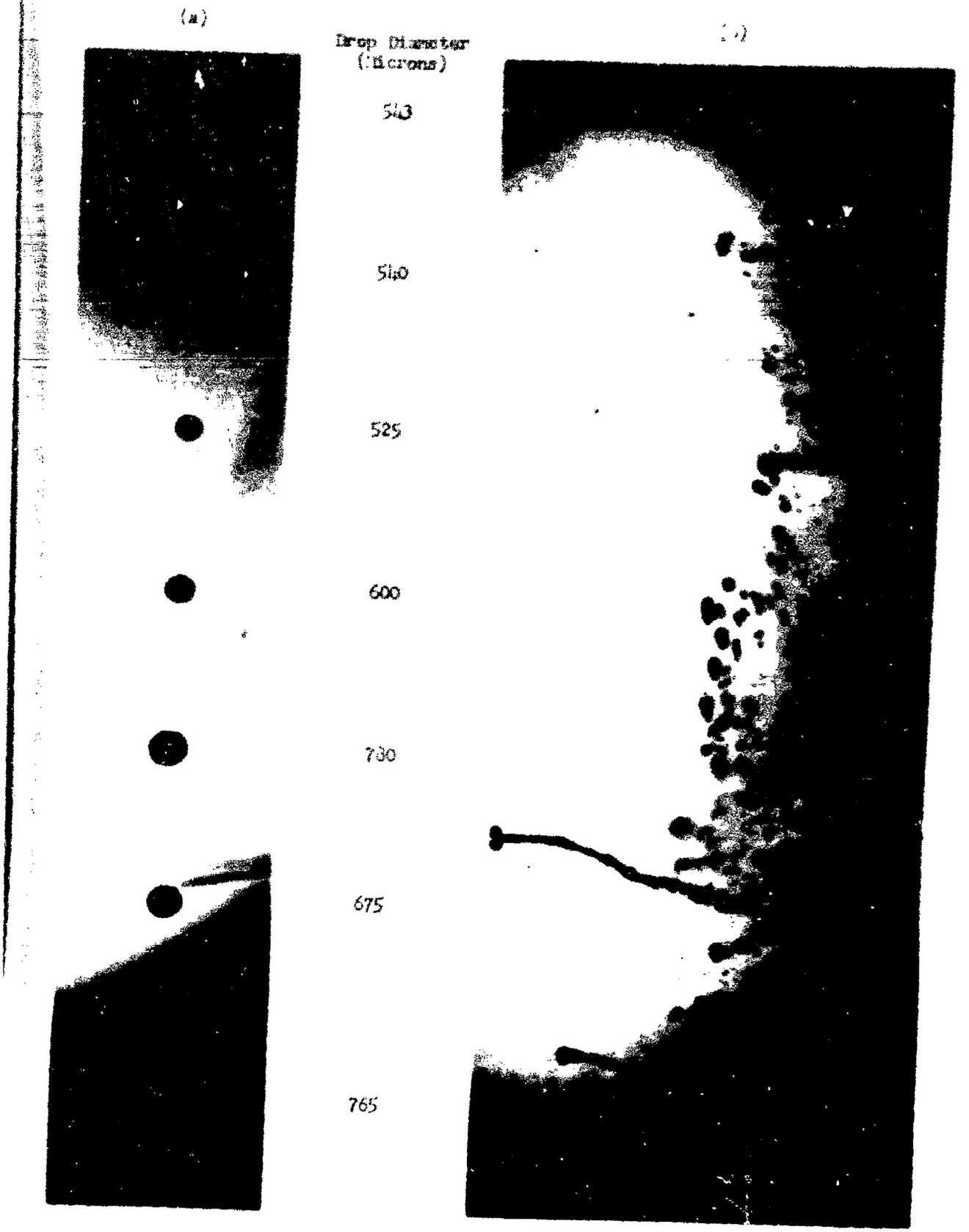

Air Velocity, u_2 = 109.5 ft./sec.; Delay (δ) = 1500 μsecs;
Liquid - Water; Run No. 433

FIGURE 40. [illegible]

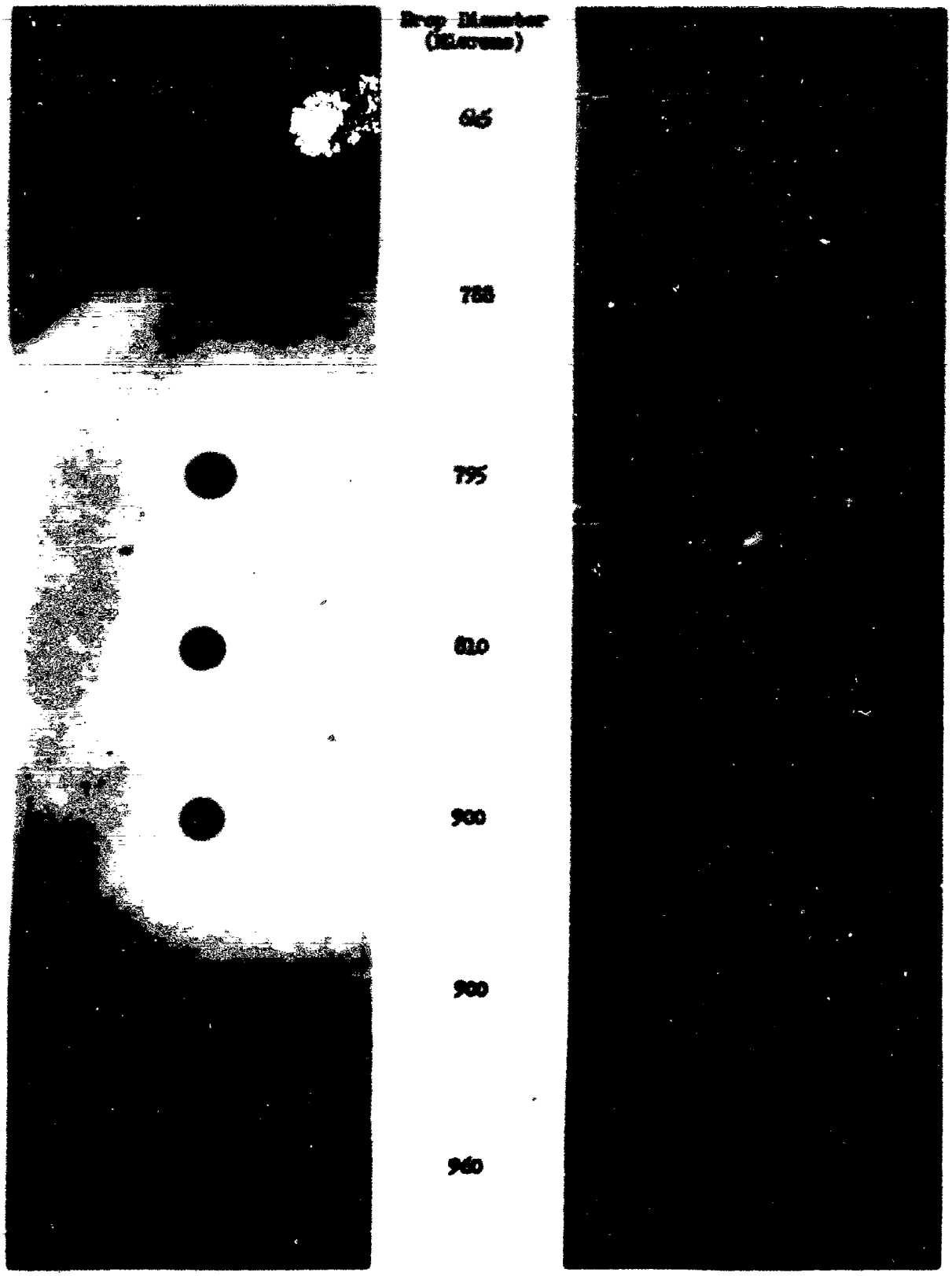

(a) (b)

Air Velocity, u_g = 209.5 ft./sec.; Delay (b) = 1500 μsecs;
Liquid - Water; Run No. 440

FIGURE 41. DROP BREAK-UP

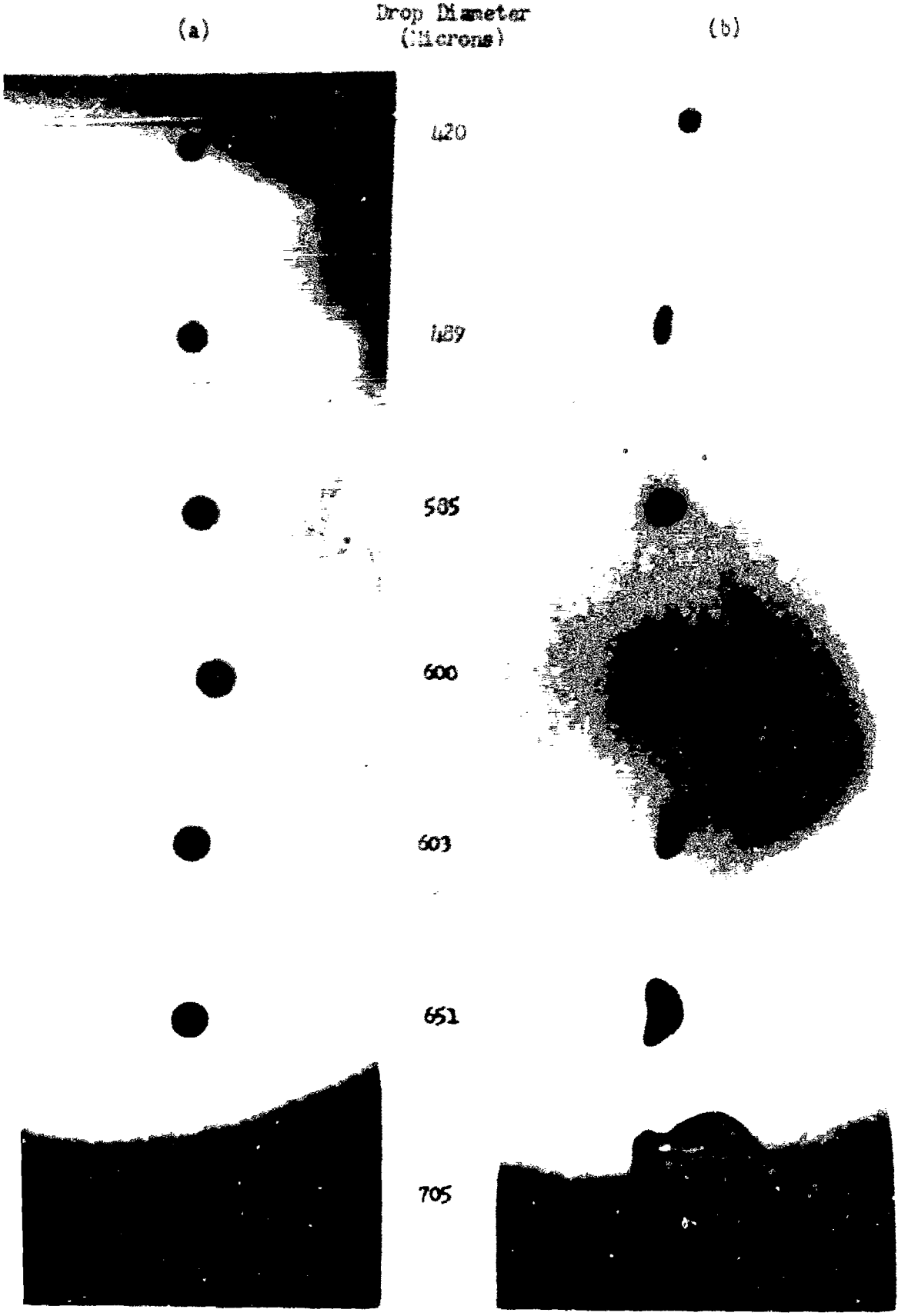

Air Velocity, u_2 = 109.5 ft./sec.; Delay (b), 1500 μsecs;
Liquid, Water; Run No. 439

FIGURE 42. DROP BREAK-UP

T 6821

Enlargement of a portion of Figure 37 (b)

FIGURE 43. PHOTOMAPS SHOWING STRUCTURE OF DROPS

(a) Enlargement of a portion of Figure 1 (b)

(b) Enlargement of a portion of Figure 2 (b)

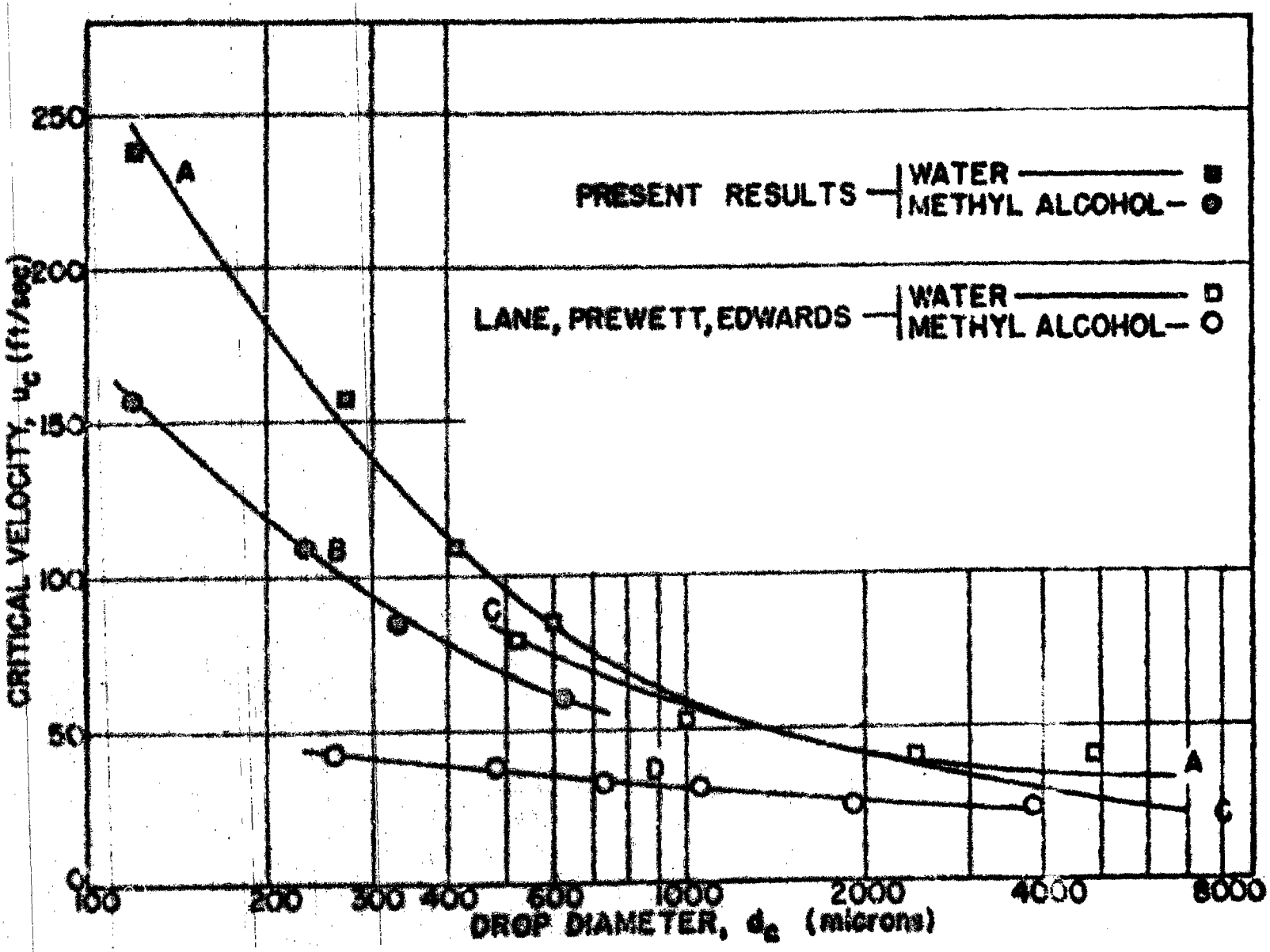

FIGURE 45. CRITICAL VELOCITY VS. DROP DIAMETER

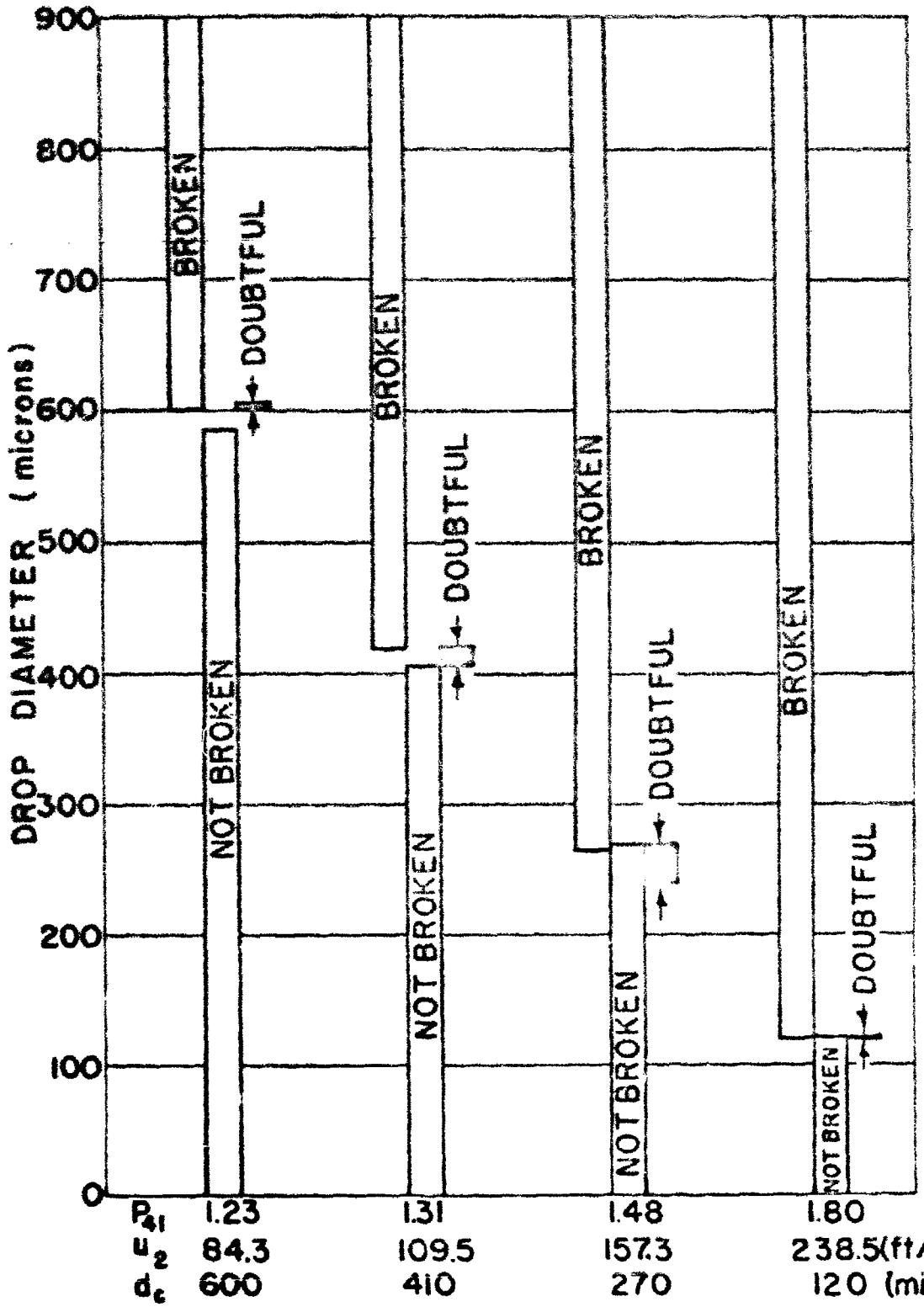

FIGURE 46. B-R CHART ILLUSTRATING DETERMINATION OF CRITICAL DROP DIAMETER (MICRON)

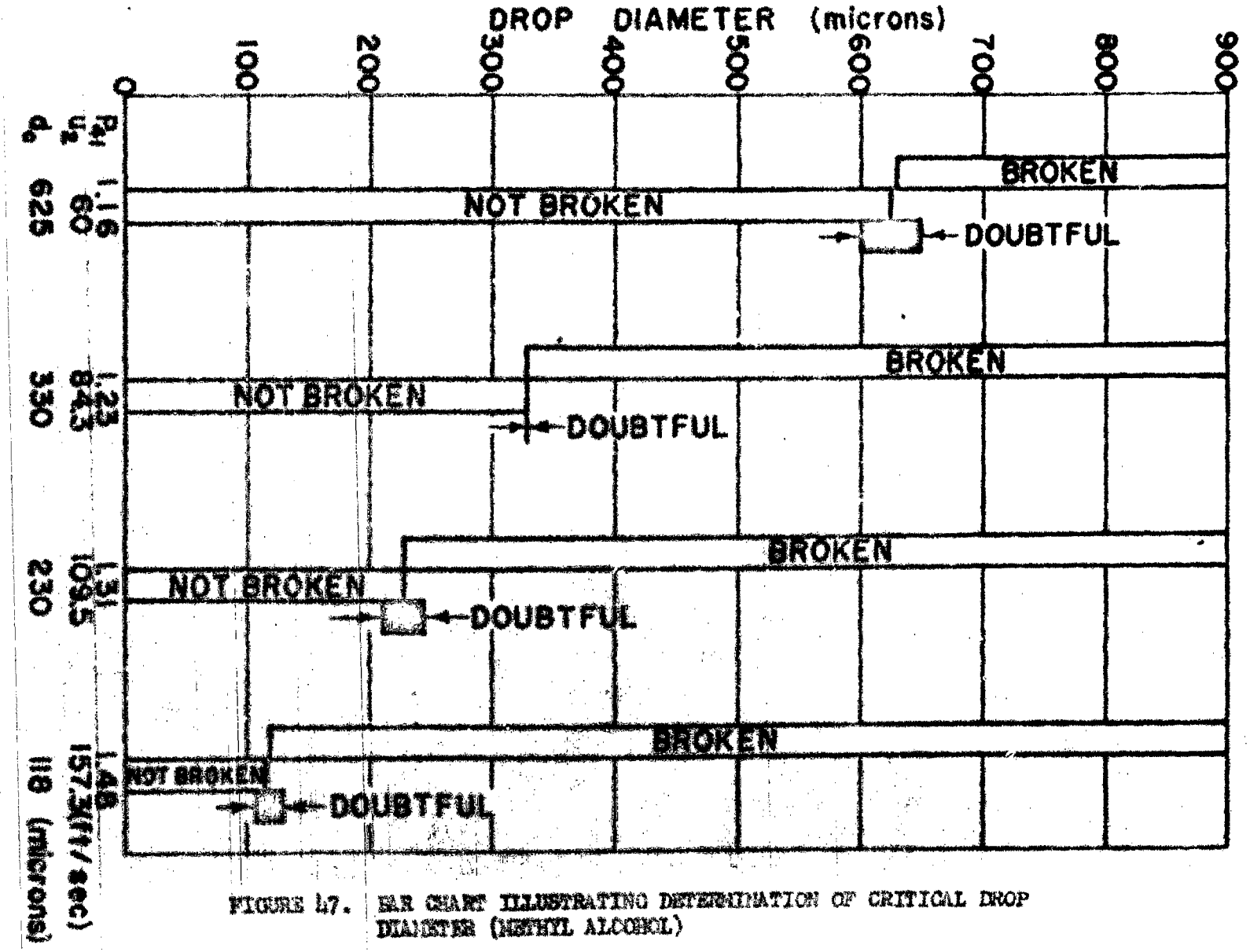

FIGURE 47. BAR CHART ILLUSTRATING DETERMINATION OF CRITICAL DROP DIAMETER (METHYL ALCOHOL)

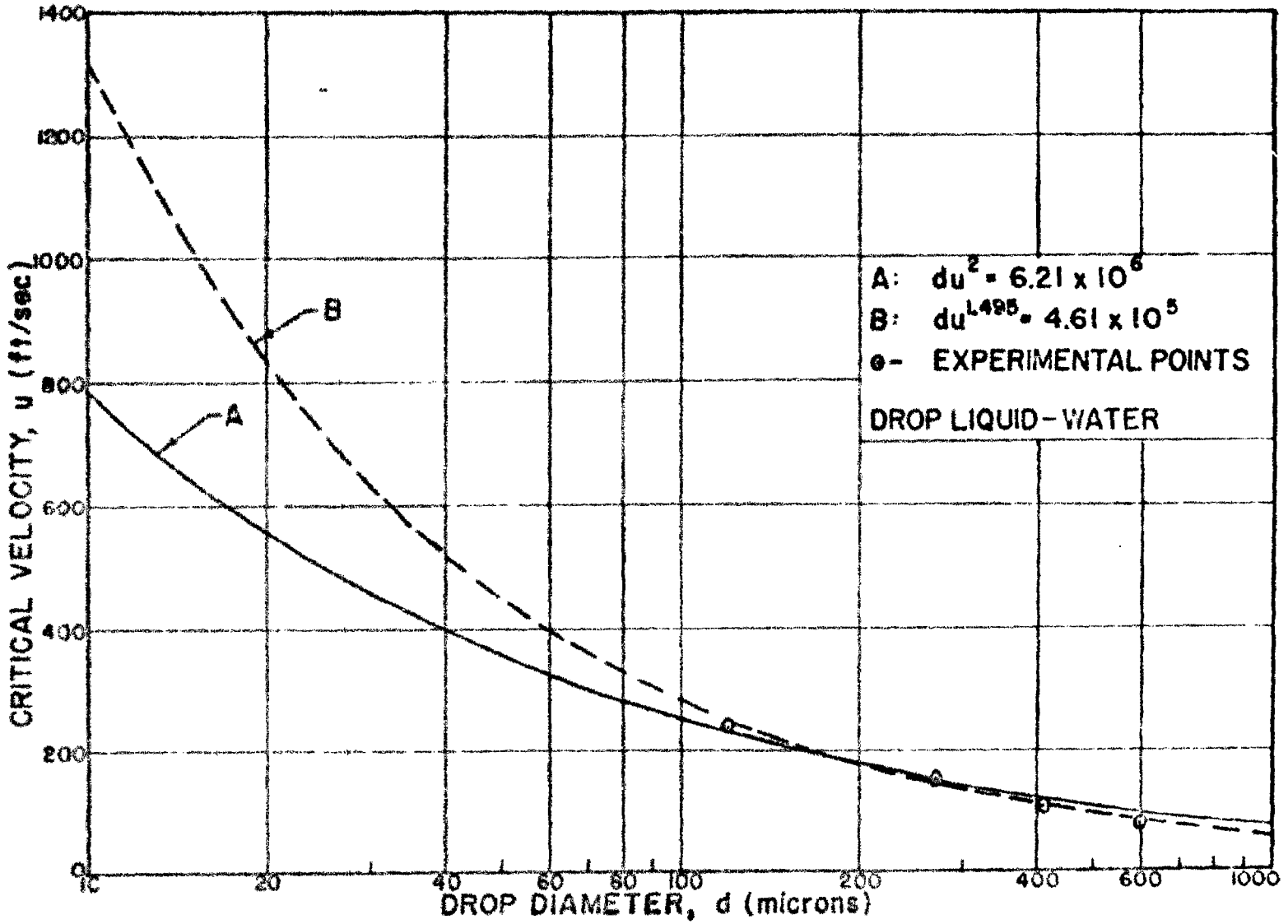

FIGURE 43. EMPIRICAL CURVES OF CRITICAL VELOCITY VS DROP DIAMETER FOR WATER

.12 .16 .20 .24 .28 .32 .36

FIGURE 50. DIAPHRAGM PRESSURE RATIO VS. SHOCK WAVE PRESSURE RATIO AND SHOCK WAVE DENSITY RATIO

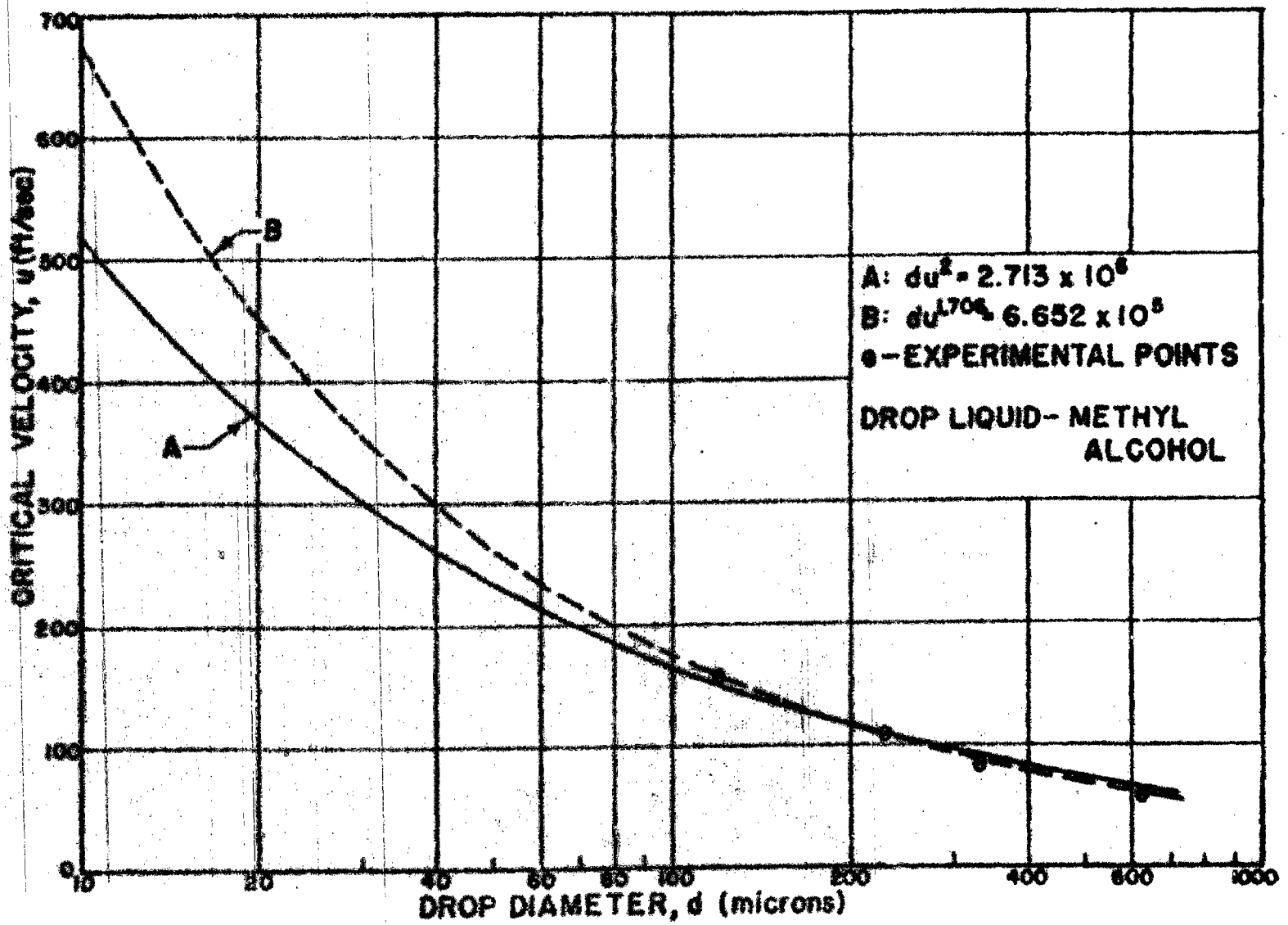

FIGURE 49. EMPIRICAL CURVES OF CRITICAL VELOCITY VS DROP DIAMETER FOR METHYL ALCOHOL

W_1 & U_{21} vs P_{41}
W_1
U_{21}
P_{41}
2.0
3.0

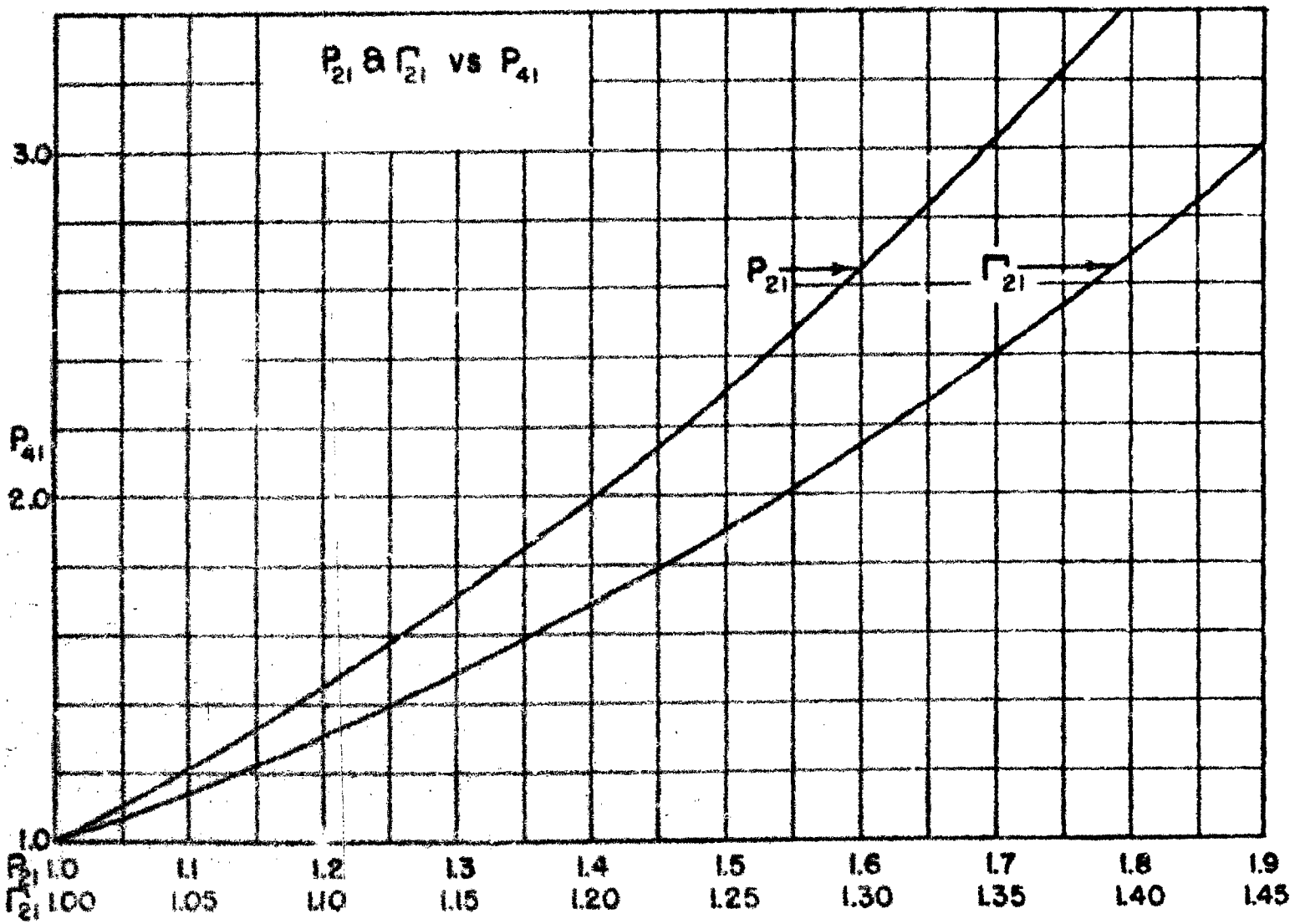

FIGURE 51. DIAPHRAGM PRESSURE RATIO VS. SHOCK WAVE PRESSURE RATIO AND SHOCK WAVE DENSITY RATIO

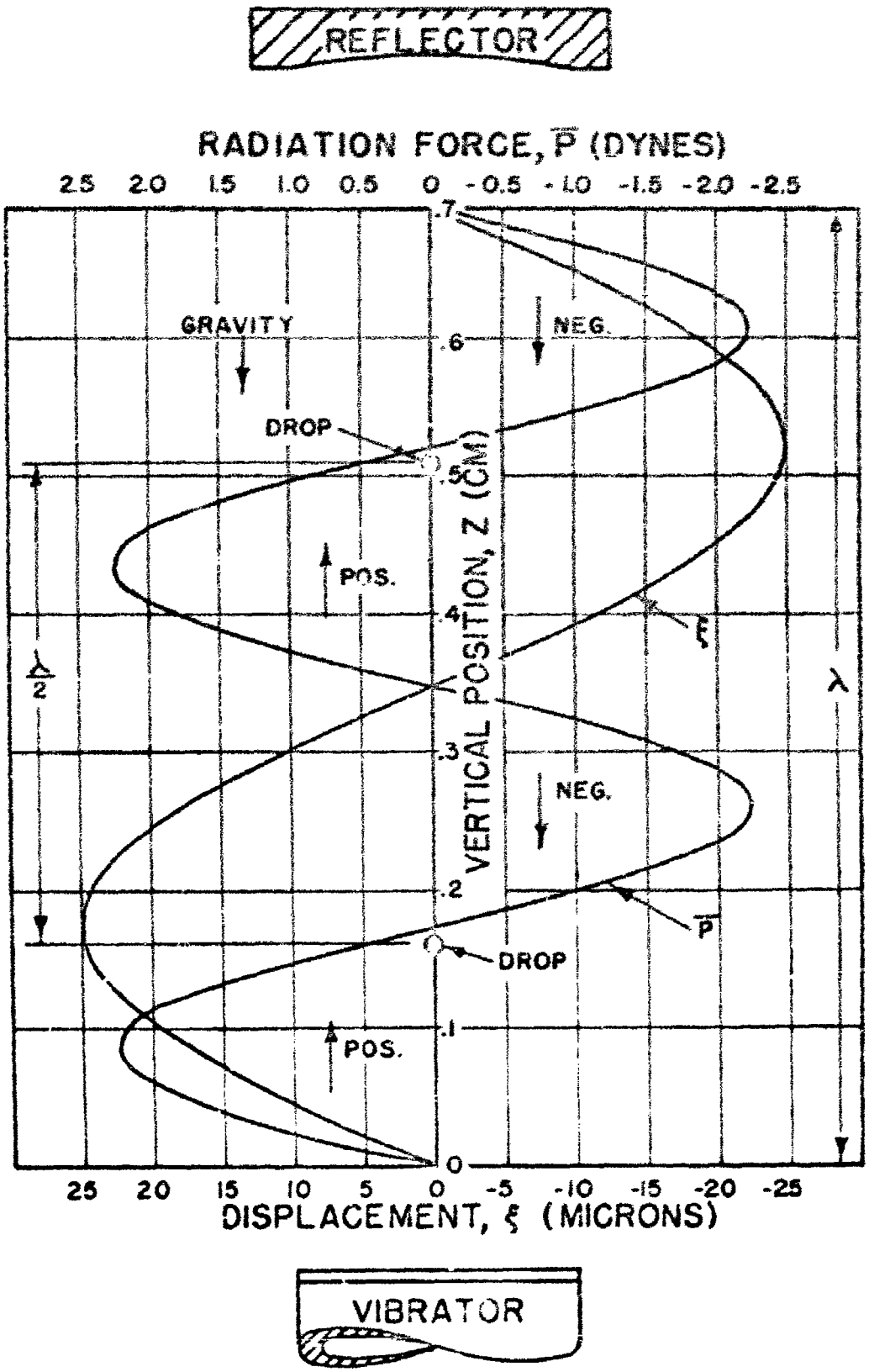

FIGURE 52. RADIATION PRESSURE ON A SMALL SPHERE

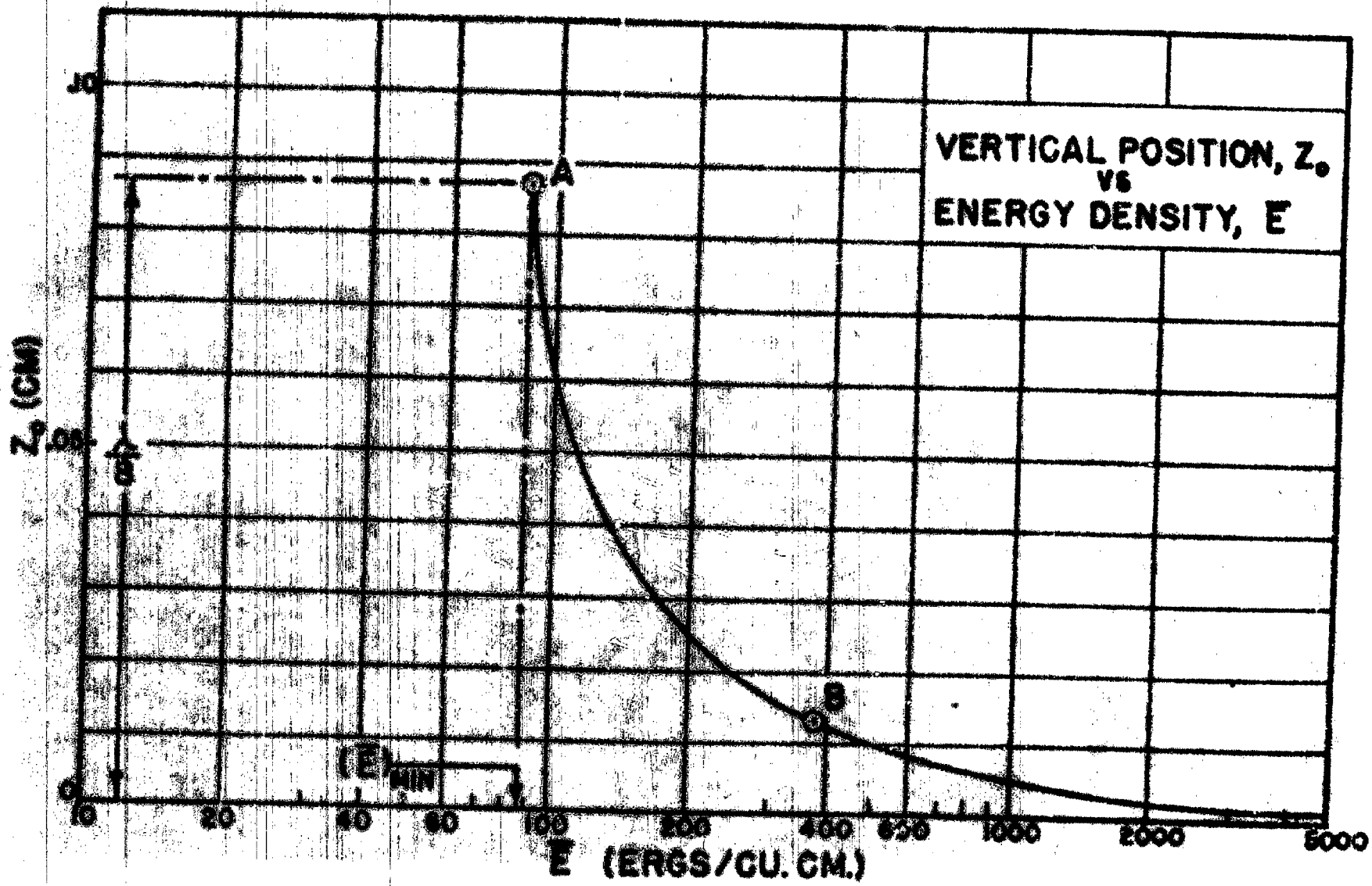

FIGURE 53. VERTICAL POSITION VS. ENERGY DENSITY OF SOUND FIELD

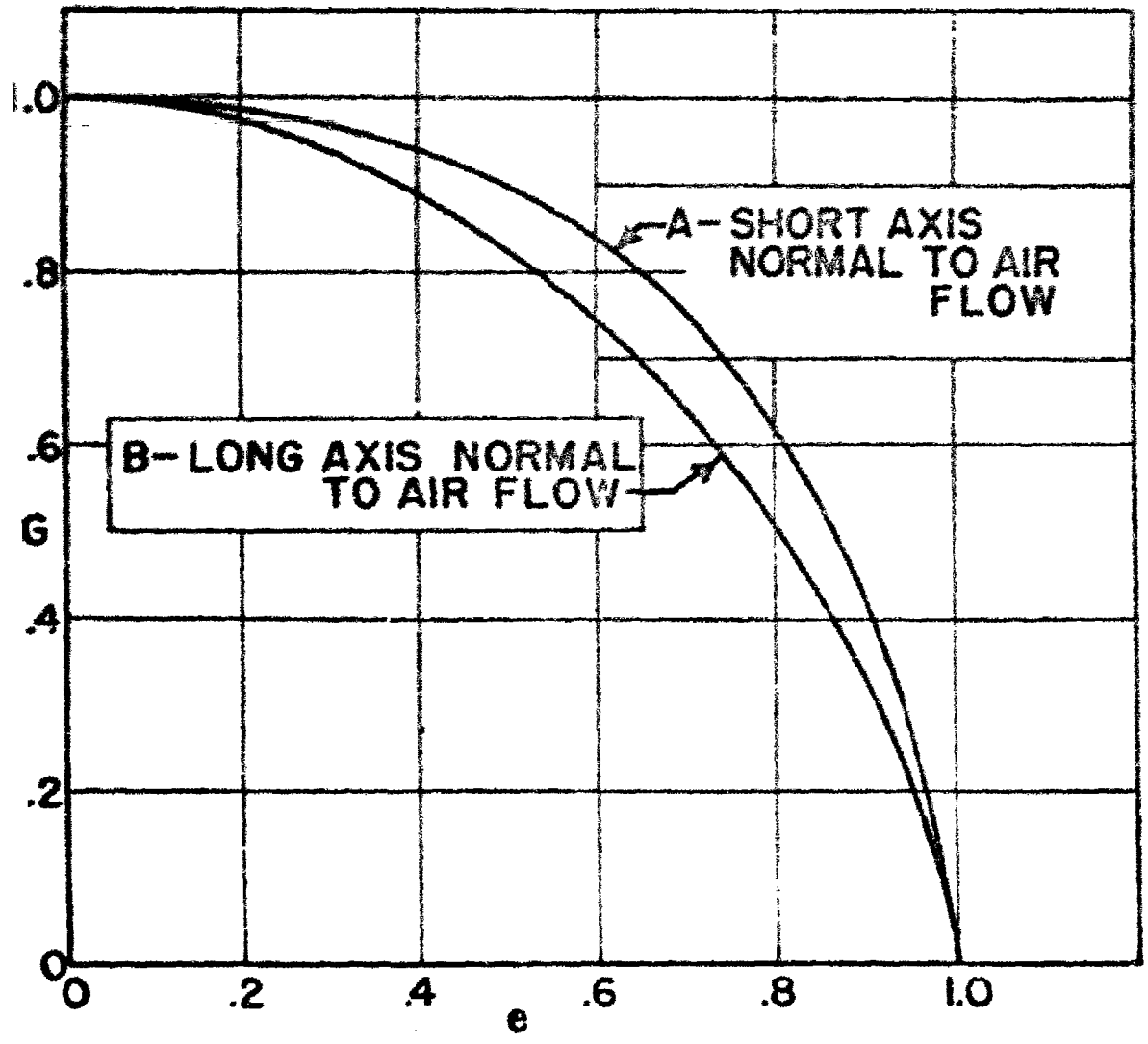

FIGURE 54. CURVATURE FUNCTION, G, VS. ECCENTRICITY, e, FOR AN OBLATE SPHEROID